SYNTHESIS AND APPLICATIONS OF DNA-BASED MATERIALS AT THE MESO AND MACROSCALE

A Dissertation

Presented to the Faculty of the Graduate School

of Cornell University

In Partial Fulfillment of the Requirements for the Degree of

Doctor of Philosophy

by

Kenneth Gene Yancey

August 2017

SYNTHESIS AND APPLICATIONS OF DNA-BASED MATERIALS AT THE MESO AND MACROSCALE

Kenneth Gene Yancey, Ph. D.

Cornell University 2017

DNA has commonly been viewed as a genetic material as opposed to a generic one. This is despite DNA's potential to create new paradigms in materials using its unique properties which can't be found in any other material. These properties are many but include the ability to code, store and replicate information in the form of proteins, self-modify by acting as a substrate for proteins, and create hybrid materials by binding proteins without degrading their activity. Traditionally, DNA's use as a generic material has been barred from most applications because many require scales larger than the nanoscale. In order to address this, our goal involved the scale up of DNA from a traditionally nanoscale material to a meso and macroscale material. Towards this pursuit, a platform for the mesoscale synthesis of DNA was created, the DASH platform, as well as a platform for macroscale DNA synthesis, the metagel platform. The hope was to demonstrate that not only can these larger scale DNA materials be synthesized in a simple and practical manner, but that DNA has the potential to open new paradigms in functional materials because of the ability to utilize DNA's useful nanoscale properties for meso and macroscale applications. Towards this goal, we demonstrated that our meso and macroscale platforms for DNA synthesis have potential in a wide array of applications including self-regenerating materials, cell-free protein expression, and protein immobilization and activity. We also included in depth studies in the area of detection of pathogens and diagnostic targets in the hopes of this work having real-world impact. By doing so, we demonstrated the ability of larger scale DNA materials to enable naked eye readout

for low picomolar concentrations of targets and even for the detection of single nucleotide polymorphisms. It is our hope that this work will pave the foundation for future studies which will help realize DNA's potential as a generic material rather than just a genetic one.

BIOGRAPHICAL SKETCH

Kenneth Yancey was born and raised in Lowville New York, a small town of ~3,000 people and ~30,000 cows. As the son of a farmer and a high school teacher, Ken learned the importance of hard work and academics. After graduating Lowville Academy high school, he chose to attend Clarkson University in 2008 as a chemistry major where he became interested in a career in research and development. This began the summer before freshman year when he was extended an offer to spend the summer developing antibody-based biosensors for the detection of peanut protein allergens. He continued in this area until Spring semester of freshman year when he was extended an offer to conduct research in the field of cervical cancer for Dr. Craig Woodworth. Ken continued in this area for the next two years after becoming interested in the mechanisms behind the carcinogenesis of cervical tissue as a result of Human Papilloma Virus infection. So began an obsession with research as Ken began to spend more time in laboratories than he did in classes by taking directed research credit during the semesters and working as a research assistant during the summer and winter breaks. Following this, Ken became interested in biomaterials and began to work with Dr. Sergiy Minko on stimuli-responsive tissue engineering scaffolds. He continued this for two years while completing his B.S. in chemistry in 2011 and his M.S. in chemistry in 2012. Ken then transition to Cornell in order to do his Ph.D. in biological and environmental engineering. Over the course of

his Ph.D. Ken has worked on a diverse number of areas including point-of-care diagnostics for resource poor settings and cell-free protein expression for the cost-effective production of biopharmaceuticals. Also during his Ph.D., Ken became involved in several organizations as a member of the Cornell Graduate and Professional Student Assembly, vice president of the Biological and Environmental Engineering Graduate Student Association and Advisory Board for Cornell's Broadening Experiences in Scientific Training Program (BEST).

To my family and friends

ACKNOWLEDGMENTS

I would first like to express my special appreciation to my Ph.D. advisor and committee chair, Dr. Dan Luo. Despite having many demands on his time, Dan has always gone above and beyond to provide both professional and personal mentorship. It has always been clear to me that Dan has made this a priority and I am lucky to have received it. I am better professionally for having learned to conduct research with both rigor and enthusiasm and I am better personally for having seen how a good mentor behaves. I would also like to thank my two committee members, Dr. Minglin Ma and Dr. David Putnam. I am deeply indebted to them for their willingness to provide personal mentorship as well as constructive advice on my projects. Without this example, It would not have been possible to finish this thesis.

In addition, I would like to acknowledge and thank my lab mates Tom Derrien, Duo An, Yue Hu and Dong Wang for their help and advice over the years. I would particularly like to thank Dr. Shogo Hamada and Yehudah Pardo who have worked with me on many of my projects. The discussions we have had over the years has provided some of the best training I have received during my Ph.D. and without them, I certainly would not have completed this dissertation.

Last but not least, I would like to thank my significant other and true friend, Marissa Smatlak. No one lives in a vacuum. Your love and support has aided me in a million subtle ways.

TABLE OF CONTENTS

LIST OF FIGURES

1 CHAPTER 1: INTRODUCTION

1.1 Chapter 1.1: DNA Properties at the nanoscale

1.1.1 DNA central dogma and biological importance

DNA has become a useful material for engineering in a wide range of applications because of its unique biological role. For instance, in virtually all high-level organisms, DNA acts as a template for RNA which acts as a template for proteins. This concept is so fundamental to the field of molecular biology, that it is called the central dogma [1]. In essence, DNA provides the genetic blueprint which differentiates human from plant from bacterium. It does this by providing a universal genetic code which is shared among all organisms. This genetic code codes for information such as proteins, can store information for hundreds of thousands of years [2], and replicates information so that it can be passed down instead of being lost.

The ability to store, read and propagate information using DNA comes from the molecule's ability to act as a template which can be modified by thousands of enzymes. These enzymes have evolved by necessity so that life as we know it can exist. Because nature has already gone through the hard work of developing the tools needed to engineer DNA, scientists can use these DNA-modifying enzymes in order to tailor the molecule for useful applications[3-5]. Specifically, these enzymes have proven powerful tools because of their extremely specific interactions with DNA which allow scientists to perform reactions such as selectively cutting DNA at specific locations using endonucleases, splicing DNA together with specific orientations using ligases, or even amplifying the amount of DNA using polymerases (Figure 1). To date, over one thousand enzymes have been identified which can allow scientists to selectively

manipulate DNA at the angstrom level [4, 6, 7]. These enzymes have thus become a toolbox for the engineering of DNA for specific applications.

1.1.2 DNA's chemistry.

DNA is also an excellent material for engineering from a chemistry perspective. DNA has a predictable and unique chemistry, termed Watson-Crick base pairing [1], and allows DNA-DNA interactions to be predicted or precisely tailored. Specifically, DNA is composed of four deoxy-nucleoside monomers: Thymine (T), Adenine (A), Guanine (G) and Cytosine (C) (Figure 2). The order of these four nucleotides make up the so called "sequence" of DNA and serve to govern DNA-DNA interactions. These interactions can be predicted from the DNA sequence because it is known that two DNA strands can only come together in an antiparallel fashion and thymine can only hybridize to adenine and guanine only to cytosine. The orientation and specific pairing of nucleotides allows for stable hydrogen bonds to form between the nucleotides. Specifically, only two hydrogen bonds can form between T and A and three hydrogen bonds between G and C. The end result of this simple chemistry is that the behavior of DNA can be easily predicted. This allows for the engineering of DNA into complex designs for desired applications.

This ability to predict DNA-DNA base pairing is a powerful tool when coupled with the ease at which scientists can synthesize and manipulate DNA. Any sequence can now be reliably synthesized with perfect monodispersity using solid-state synthesis techniques [8, 9]. This technique has an error rate as low as 1 per 10,000 nucleotides [9, 10] and even allows for chemical modification with functional groups such as alkynes, thiols, amines or biotin. The location of these groups on the DNA sequence can even be tailored [4] with base pair

resolution allowing scientists to selectively create hybrid materials with other materials such as proteins [11-18], nanoparticles [19-26] or polymers [27-32]. The synthesis of DNA with a given structure has become so routine that even whole chromosomes can now be synthesized [33] and sequenced [34]. This has transformed DNA engineering applications such as those involving recombinant DNA technology. Previously, lengthy molecular cloning techniques were used in order to insert gene sequences into plasmids. Now though, whole plasmids with any sequence can be routinely synthesized in-house or ordered commercially. Nearly any DNA structure can be synthesized with precise control thus allowing scientists to tailor DNA as needed for a desired application.

1.1.3 Dissertation goal.

Thus, DNA is an extremely promising material from an engineering perspective. DNA is of real-world relevance because it encodes vital biological information, it is easily manipulated and customized using DNA-modifying enzymes, its chemistry is simple and programmable allowing interactions to be design or predicted, and nearly any DNA sequence can be precisely synthesized. The result of this is that DNA has become an important class of materials for a wide array of applications such as expression profiling, genotyping, genetic prognostics, expression prognostics and the detection of infectious disease [35-39]. It is unfortunately still primarily used as a nanoscale material for nanoscale applications**. The goal of this thesis is to investigate the scale up of DNA materials from nanoscale to meso/macroscale so that we can utilize DNA's unique and useful properties for new real-world applications.**

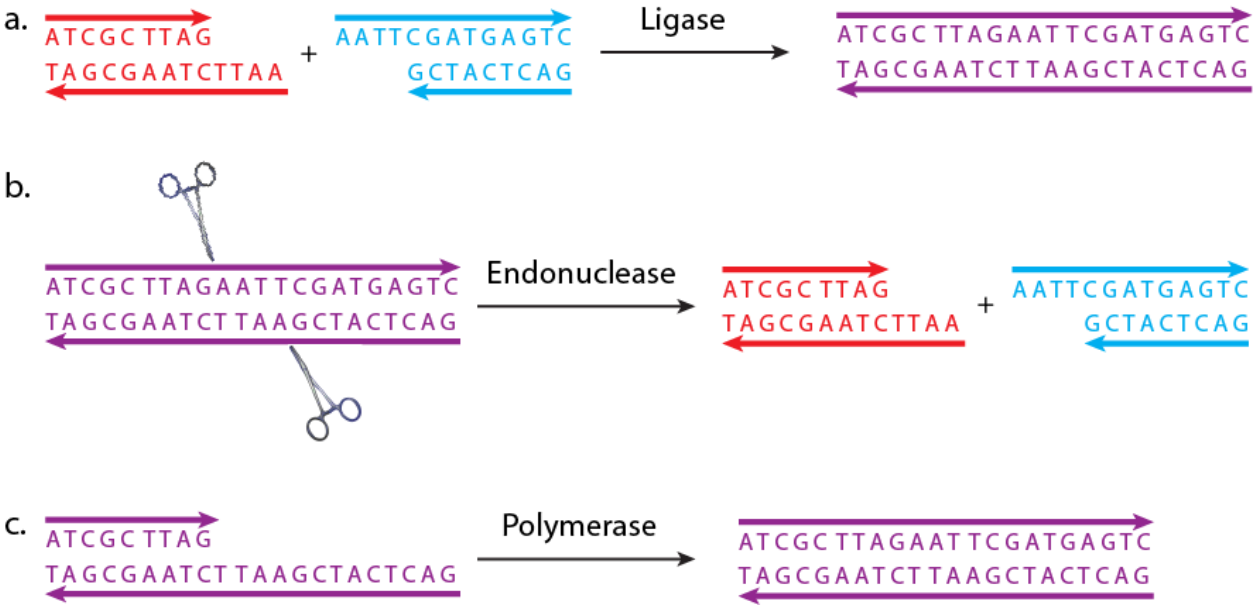

Figure 1. DNA as a substrate for enzymes [40]. Ligase can connect free ends of DNA (a) while endonucleases can cleave DNA at specific or nonspecific locations (b). Polymerases replicate DNA by using a DNA as a template and elongating a complementary strand.

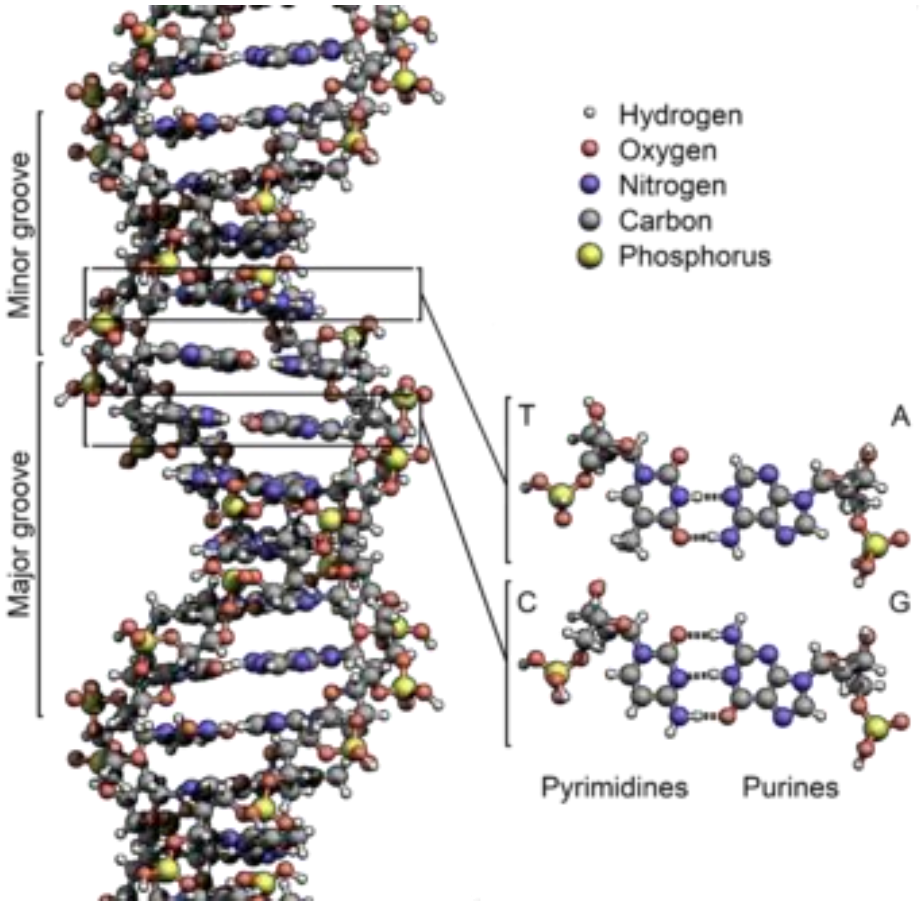

Figure 2. Structure and composition of DNA [41]. DNA is composed 4 different bases: Thymine, Adenine, Guanine and Cytosine. These bases are similar to monomers in a polymer backbone and have a particular sequence which encodes information determines DNA-DNA interactions due to Watson-Crick base pairing rules. These rules state that two DNA polymers hybridize in an antiparallel fashion by binding Thymine only to Adenine and Guanine only to cytosine through hydrogen bond formation.

1.2 Chapter 1.2: Methods to convert DNA from nanoscale to the meso/macroscale

1.2.1 Introduction to bulk DNA materials by enzymatic means

In order to scale up DNA from the nanoscale to the meso/macro scale, two main techniques are typically used. The first is to produce large structures of DNA by amplifying the low concentration of low molecular weight DNA into large amounts of high molecular weight DNA. The second is to crosslink existing DNA into larger structures. Both methods rely on DNA templated enzymes to accomplish this.

1.2.2 RCA-based materials

The first method to produce bulk DNA gels, producing high molecular weight structures by amplifying DNA, is typically done using variations of isothermal amplification. Some examples include loop-mediated isothermal amplification (LAMP) [42-44], nucleic acid sequence based amplification (NASBA) [45] and rolling chain amplification (RCA). Unlike RCA, LAMP and NASBA are typically adept and making large amounts of low molecular weight DNA. This is not ideal for our goal of producing large amounts of high molecular weight DNA. RCA on the other hand, is ideal. RCA has been shown to yield up to a billion-fold amplification level in less than an hour and is designed to produce extremely high molecular weight DNA [46]. In RCA, a single stranded circular DNA template is used. This template is annealed with a short single stranded DNA primer which contains a complementary DNA sequence. By binding to the template, the DNA primer allows a Phi29 DNA polymerase to bind and begin elongating the DNA primer strand by incorporating new nucleotides. Because the template is circular and has no end to stop the polymerase, the enzyme continues around the DNA template indefinitely. This produces a long DNA strand with high molecular which is extends into solution. The end

result is a large amount of extremely high molecular weight DNA which is ideal for making bulk DNA hydrogels. We will discuss examples of these bulk gels later in Chapter 1.3.

1.2.3 Mechanisms behind RCA-based materials

Rolling chain amplification (RCA) produces long single stranded strands of DNA with high molecular weights but how does this translate into bulk DNA hydrogels? The short answer to this is physical entanglement of the immensely long DNA strands. RCA has been reported to create DNA strands of over 46 million daltons [47]. Considering that the average molecular weight of single stranded DNA in ~330 Daltons per nucleotide, this equates to a DNA length of ~140,000 base pairs [48]. Double helix DNA, like that in cells, is ~3.4nm per base pair. If we use this approximation, RCA can produce strands exceeding ~42um. This is an interesting value considering that the human eye can theoretically distinguish these DNA strands. This is based on the diffraction limit formula $\Theta = 1.22 \times (\lambda/D)$ (Θ: angular size of the object, λ: wavelength of visible light, D: diameter of the pupil) which puts the distinguishable limit at ~40um [49]. Thus, RCA creates massive molecular weight structures but typically this is not enough to create bulk DNA hydrogels on its own. You also need some sort of crosslinking in order to give the large DNA stands cohesiveness so that they don't simply fall apart when some force is exerted on them. In RCA-based gels, these crosslinking forces are provided by two mechanisms, physical entanglement and partial hybridization along the DNA backbone. Physical entanglement is the literal tangling of DNA strands into a large interwoven mass of DNA. Because of the large molecular weight of DNA which can include hundreds of thousands of base pairs, a given DNA strand cannot simply disentangle itself by diffusion. This provides cohesion to the bulk DNA

hydrogel. Physical entanglement on its own is typically not enough to offset effects such as gravity and surface tension.

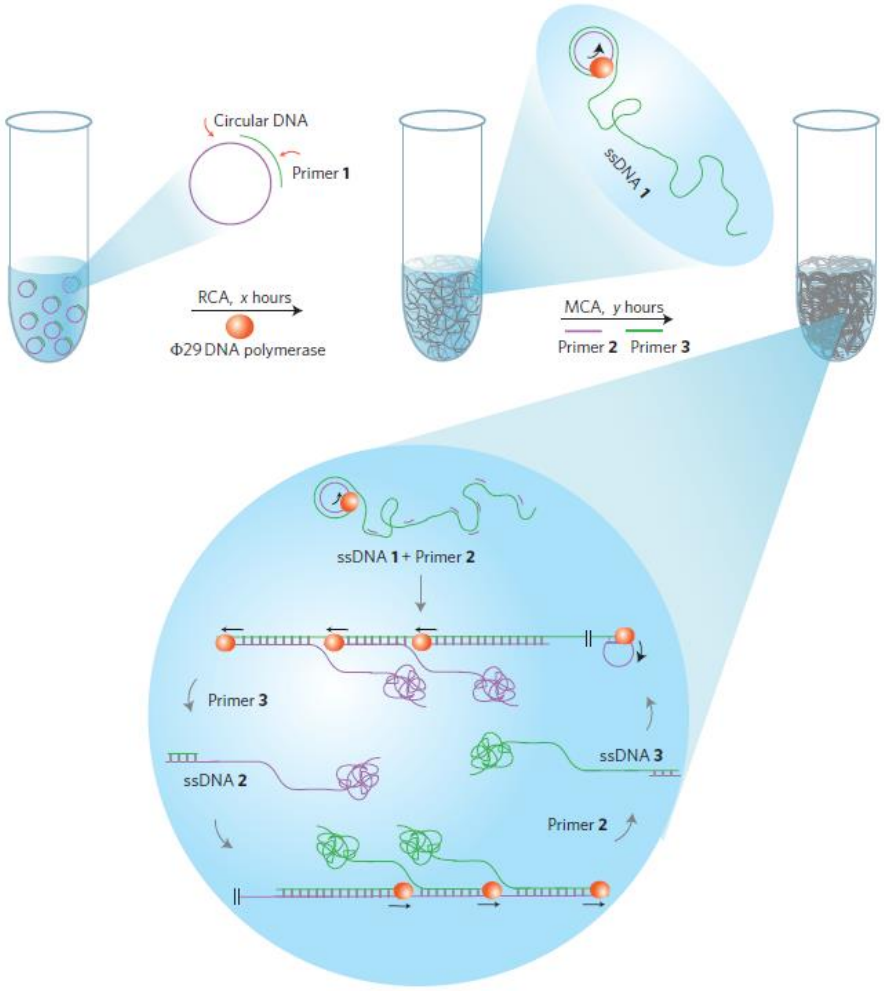

Figure 3. Schematic of Metagel synthesis [50]. RCA is performed in order to make high molecular weight single stranded DNA from a primed circular template. Following this reaction, two additional primers are added in order to exponentially amplify the long single stranded DNA using a process called multi-primed chain amplification.

Often additional crosslinking is needed which is provided by partial hybridization along the DNA backbone. This partial hybridization occurs because RCA produces long single stranded

DNA which is available for base pairing. Even without perfectly complementary DNA present in solution, complex DNA structures can be still be formed. The end result is DNA strands being linked together by hydrogen bonding which provides an additional cohesive force for the hydrogel. Without it, an RCA-based DNA hydrogel will often fall apart. This was shown by Lee et al. who showed that heating to 85°C would cause RCA-based gels to dissociate due to heat denaturing of the partially hybridized strands [50].

1.2.4 Ligation-based materials

The second main method for scaling DNA up from a nanoscale material to a macroscale material is by ligation of existing DNA into macro-sized structures. First of all, ligation is the joining of two free ends of DNA using a class of enzymes called DNA ligases. In order for these enzymes to function, two single stranded DNA strands must typically be aligned by hybridization with a complementary DNA strand. Alternatively, two double stranded DNA strands can by ligated if they can be oriented properly using hybridization of a single stranded complementary overlap (Figure 1A). During the process of ligation, the two strands are joined to form a covalent linkage. The energy for this reaction is provided by a phosphorylation on the end of the 3' end of the DNA. By joining free DNA ends in solution, the existing DNA is linked together to form high molecular weight structures.

1.2.5 Mechanisms Behind Ligation-based materials

As was previously discussed in a section on bulk DNA gels via physical entanglement, The production and physical entanglement of long DNA is typically not enough to create a bulk DNA hydrogel. Additional cohesive force needs to be provided by some form of crosslinking. In the case of ligation-based gels, this crosslinking is provided by branched DNA subunits (Figure 4).

These subunits are typically Y or X-shaped DNA which is formed by multiple partially complementary strands coming together to formed a branched structure. These branches provide multiple attachment points for a given subunit to crosslink and thus creates a highly branched network with a large amount of crosslinking holding it together.

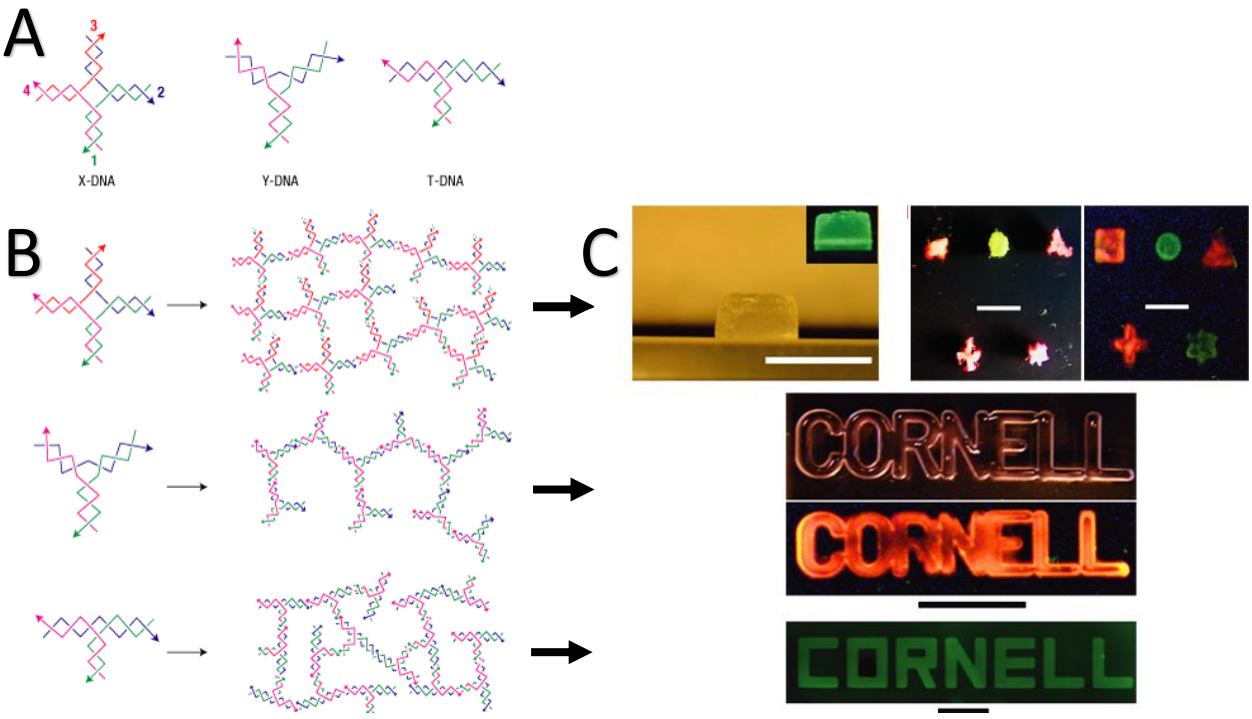

Figure 4. Schematic illustration of ligation-based bulk gel formation. Figure was adapted from Um et al. [51]. Partially complementary ssDNA strands hybridize with each other to form branched x, Y or T-shaped DNA. By designing complementary sticky ends on each arm, branched DNA can hybridize to form bulk DNA hydrogels. Branched structures are ligated to covalently link the branched DNA structures together.

1.2.6 Introduction to bulk DNA materials by non-enzymatic means

So far, we have discussed two methods for forming bulk DNA hydrogels using enzymatic reactions. These are RCA, via a DNA polymerase, and ligation via a DNA ligase. There are

however many examples of DNA hydrogels which do not need these enzymatic reactions to form. These examples do however form by similar mechanisms and physical entanglement and crosslinking via hybridization are still essential to maintaining gel cohesiveness.

1.2.7 Non-enzyme based bulk DNA materials (hybridization-based gels)

Previously, we discussed ligation reactions where two DNA strands can be linked together. This can occur when the strands hybridize due to overlapping complementary DNA (Figure 1) or when they are "stapled" together by hybridization with a third complementary strand. Ligation can covalently link the strands of subunits together to form ligation-based bulk gels but covalent links are not always necessary. This is seen in the case of hybridization-based gels [52]. If the overlapping single stranded regions on each of the subunit's arms are long enough, there is enough hydrogen bonds that the DNA strands will remain bound. This results in a given bulk gel maintaining cohesion under ambient conditions. Fortunately, the chemistry of DNA is predictable as was discussed earlier in Chapter 1.1. It is trivial to calculate the temperature at which two strands will associate or dissociate based on their length, sequence and salt conditions. This means that these types of gels are easily designed.

1.2.8 Non-enzyme based bulk DNA materials (Other meso/macroscale materials)

Another example of a nonenzyme-based class of meso/macroscale materials was demonstrated by the Luo Lab and were termed DNAsomes[53]. Though not DNA hydrogels as we've been primarily discussing, these micelles made of DNA deserve mentioning because of their similar mechanism of synthesis to hybridization-based gels. Specifically, several partially complementary strands are designed so that they hybridize x or y-shaped structures. This structure is then covalently linked to a hydrophobic lipid in order to form an amphiphile. When

placed in water, this created large micelle-like structures due to the hydrophilic charged DNA head that orients outward and the hydrophobic tail that orients inward. Hybridization of the branched x or y-shaped structure serves to keep the structure intact by linking the lipid to the branched DNA.

1.3 Chapter 1.3: Examples of bulk DNA materials

So far, we have discussed several methods of creating bulk DNA materials. In this section, we will give some examples of ligation and RCA-based bulk materials as well as some examples from materials that do not need enzymes for their synthesis. We will also be discussing applications of these materials.

1.3.1 Examples of ligation-based bulk DNA materials

Another common class of bulk DNA materials is ligation-based bulk materials. The synthesis and mechanism of these materials were discussed in Chapter 1.2. Now we will discuss examples and past applications. One of the first examples of a DNA material made from branched DNA comes from Um et al. [54]. Um demonstrated ligation based synthesis (Figure 4) as well as the ability to encapsulate cells and small molecule drugs into the hydrogel during the ligation step. To demonstrate this, Um encapsulate live CHO cells and showed that there was low cytotoxicity. He also loaded the gels with insulin and a DNA binding protein, camtothecin, as a model and showed controlled release.

This work was followed up within the same lab by Nishikawa et al. Instead of delivering drugs by encapsulating them in a ligation-based hydrogel, Nishikawa used the gel itself as both a nucleic-acid based drug and delivery mechanism in one. He did this by synthesizing x-shaped

DNA containing repeats of the immune-stimulatory sequence CpG in the DNA backbone. This x-shaped DNA was then ligated into a bulk hydrogel. Nishikawa found that these DNA gels could be made to degrade over time thereby releasing the immune-stimulatory DNA into solution. When the DNA gel was placed in the presence of immune cells, the cells were activated due to very high concentrations of CpG.

With Luo labs as well Park et al. used the same synthesis method to make bulk DNA hydrogels for cell-free protein expression (CFPE). In CFPE, cells are lysed and the content extracted so that proteins can be produced entirely in-vitro. By adding linearized plasmid with ends that were complementary to the arms of x-shaped DNA, Park successfully ligated plasmid into a bulk DNA material (Figure 5) [55]. He also showed that macroscale "pads" could be formed for ease of handling by molding the gel shape during ligation with a pdms mold. By placing these "pgels" into a cell extract containing supplemental atp and amino acids, pgel showed a 300-fold amplification over a convention plasmid only system. The system proved to be a dramatic step forward for the cell-free field by producing up to 5mg/ml of functional protein.

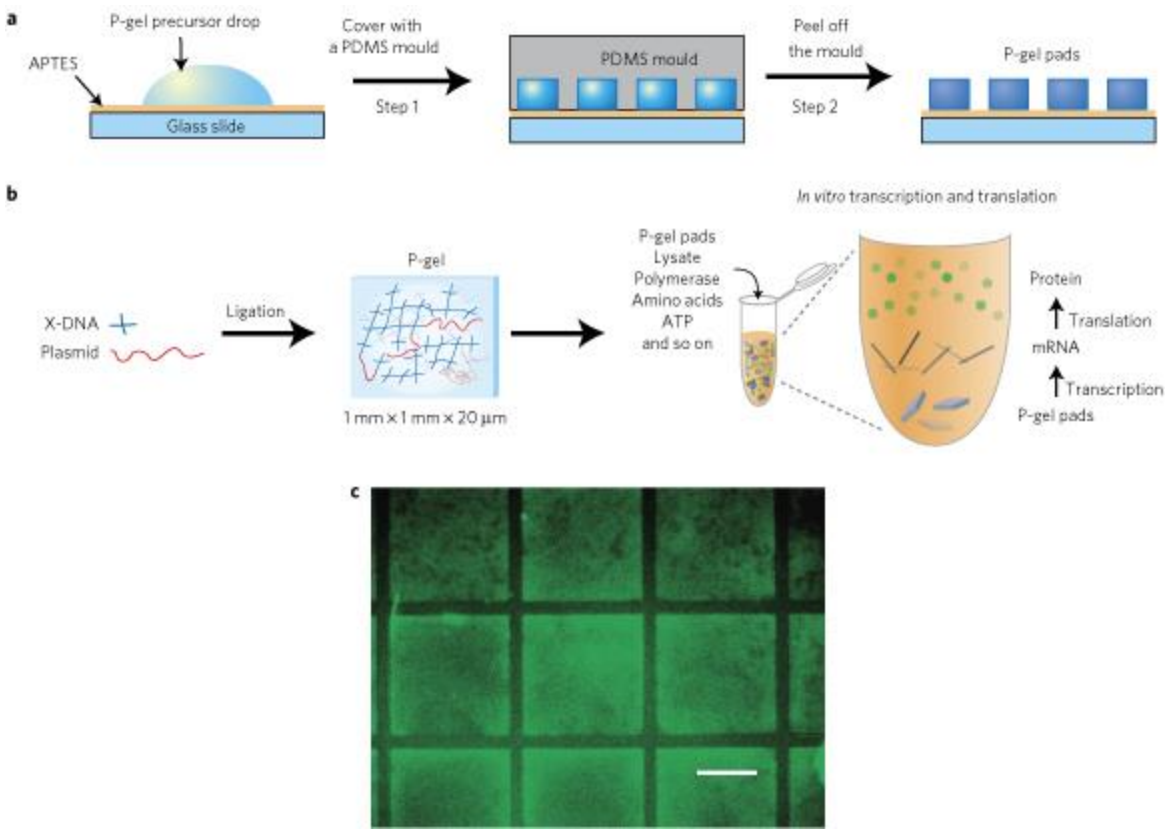

Figure 5. Schematic of a ligation-based bulk DNA hydrogel. This figure was adapted from Park et al. [56]. In A, the gel precursor solution was stamped into macro scale “pads” for ease of use using a PDMS mold. B shows a schematic of the ligation-based synthesis which ligates branched x DNA with a gene coding plasmid into a bulk DNA material. This material is then placed in a protein expression solution where it can produce a variety of proteins such as the green fluorescent protein shown in C. The scale bar shows 500um.

There have also been several examples of applications of these ligation-based materials outside of Luo labs. One example which I will mention briefly is by Hur et al. [57]. Hur showed that these ligation-based DNA materials could be used to make supercapacitors by doing layer by layer synthesis of DNA gel and deposited polyelectrolyte multilayers. These supercapacitors

showed low cytoxicity and had greater charge-discharge cycling in cell culture medium than conventional methods. This makes the device ideal for biological applications.

1.3.2 Examples of nonenzyme-based methods for bulk DNA materials

The next group of bulk DNA materials that we will discuss are synthesized using a similar method to the ligation-based materials discussed earlier but do not require a ligase enzyme to covalent ligate the material together. I will term these materials, hybridization based-materials. In order to make a ligation-based material, complementary DNA on the ends of branched DNA subunits are used to bind those subunits together via hybridization. Generally, ligation is then used to covalently link these structures but this is not necessary if the complementary regions holding the subunits together are sufficiently strong. These loosely bound DNA subunits make an ideal material for stimuli-responsive materials because subunits can controllably hybridize or dehybridize. Xing et al demonstrated this by using temperature to selectively form or dissolve a bulk DNA material [58]. Xing also showed that these materials will respond to DNA altering enzymes like restriction enzymes. Cheng et al. demonstrated that these materials will respond to other stimuli like pH [52]. By changing pH, one can controllably allow or prevent the DNA-DNA hybridization holding a bulk DNA material together. Lastly, Liedl et al. demonstrated that these materials can be controllably formed or dissolved by adding other sacrificial DNA to the hydrogel [59]. These DNA strands control bulk material formation by controlling the amount of crosslinking that occur between subunits. They do this by having an increased hybridization affinity for the branched subunits so that subunits will preferentially bind to sacrificial DNA over crosslinking with each-other.

1.3.3 Examples of RCA-based DNA materials

Despite the progress made by ligation and hybridization-based bulk DNA materials for many applications, these types of material suffer from one large downside. Both materials convert DNA from the nanoscale to a meso/macroscale material by linking existing DNA into large structures. This means that large amounts of DNA need to be initially present. This can be a cost-related issue because the initial DNA needs to be purchased as purified oligos which can cost hundreds of dollars per ml of bulk DNA material produced. Thus, RCA-based materials are promising because of their ability to enzymatically amplify existing DNA into meso/macroscale materials.

To date, there has been much less work done with RCA-based materials than ligation or hybridization-based materials. One example which is particularly interesting is by Lee et al. who showed that RCA could be used to synthesize DNA hydrogels in milliliter quantities [50]. What was most interesting about this work was some of the mechanical properties which emerged from the bulk DNA material. The bulk DNA hydrogels were found to have metamaterial-like properties in that they behaved like a liquid when dry and solid-like when hydrated (Figure 6). Furthermore, Lee showed that these gels can be casted in a variety of shapes and that once casted, the DNA hydrogels exhibit a memory effect. When water is removed, the casted gel will exhibit liquid-like properties but once rehydrated, the gel will return to its original casted shape. This moisture responsive conversion between a liquid and a pre-formed gel shape occurred on the order of seconds and was found to be repeatable without any ill effects to the gel. To demonstrate an application of this effect, Lee created a moisture-responsive electrode by casting a DNA hydrogel in the shape of a wire connecting two electrodes. When hydrated,

the DNA wire connected a circuit. When water was removed, gravity and surface tension resulted in the DNA wire flowing away from the two electrodes.

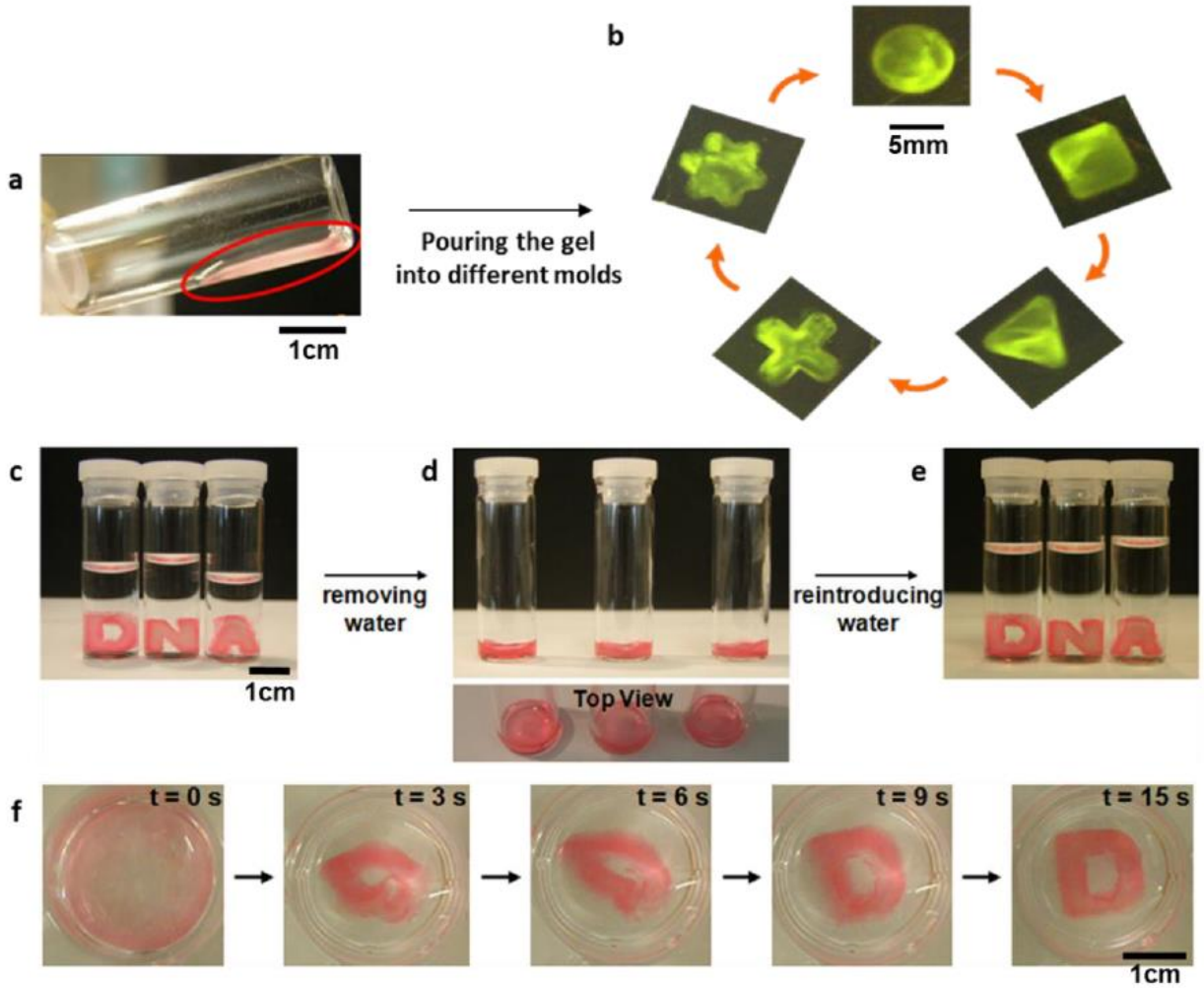

Figure 6. Metamaterial properties of an RCA-based hydrogel. This figure was adapted from Lee et al. [60] and demonstrates the metamaterial properties of a RCA-based bulk hydrogel which exhibits both liquid-like and solid-like properties. When the hydrogel is out of water, the material flows freely like a liquid (A) and can conform to any shape it is placed in (B). When the hydrogel is placed in water, the gel exhibits solid-like properties. This conversion between liquid and solid-like properties can be repeated without any noticeable effect (C, D, F). Furthermore, it

was found that metagel will maintain the shape of whatever shape the gel was casted in despite behaving as a liquid when dried. The original shape is reconstituted within 15 seconds whenever the hydrogel is placed back in water (F).

1.4 Chapter 1.4: Our approach to meso/macroscale materials for real world applications

1.4.1 Introduction to the format of this dissertation

The goal of this dissertation is to further develop bulk scale DNA materials for real world applications. Towards this goal, we have developed two forms of RCA-based materials (Figure 7). The first that we will discuss is the DASH platform, a DNA material that is designed primarily for mesoscale applications. Chapter two of this dissertation will discuss this material in general before touching on several applications that we are currently developing. Chapter three will zoom in on our efforts to apply the platform to the specific application of detection. The second RCA-based material that we will discuss is the metagel platform, a RCA bulk material which we have designed for macroscale applications. We will introduce this material in chapter four followed by a discussion of our efforts to apply it to the specific application of detection. We chose to focus our initial efforts on detection because of the field's potential for real world impact and the potential for the DNA materials that we are developing to fit well with this application. The overall format of this dissertation can be seen below in Figure 8.

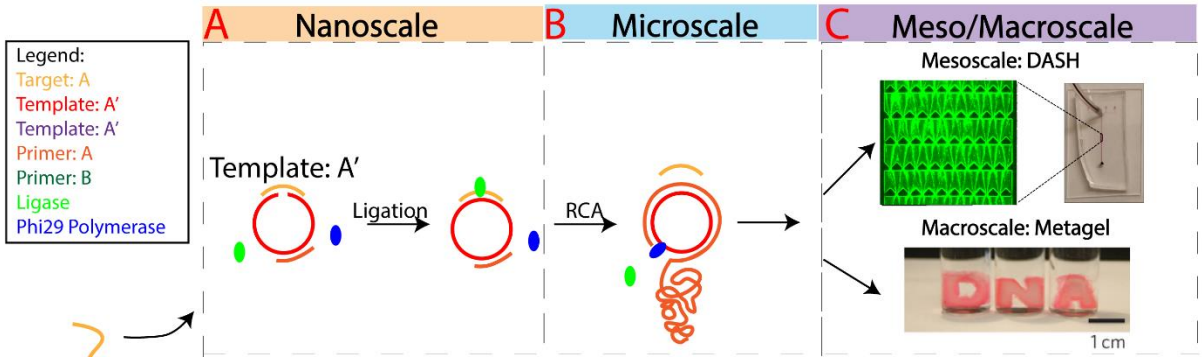

Figure 7. RCA-based approach to meso and macroscale DNA materials. A: Template preparation. B: Amplification via RCA. C: Resulting mesoscale DASH and macroscale Metagel.

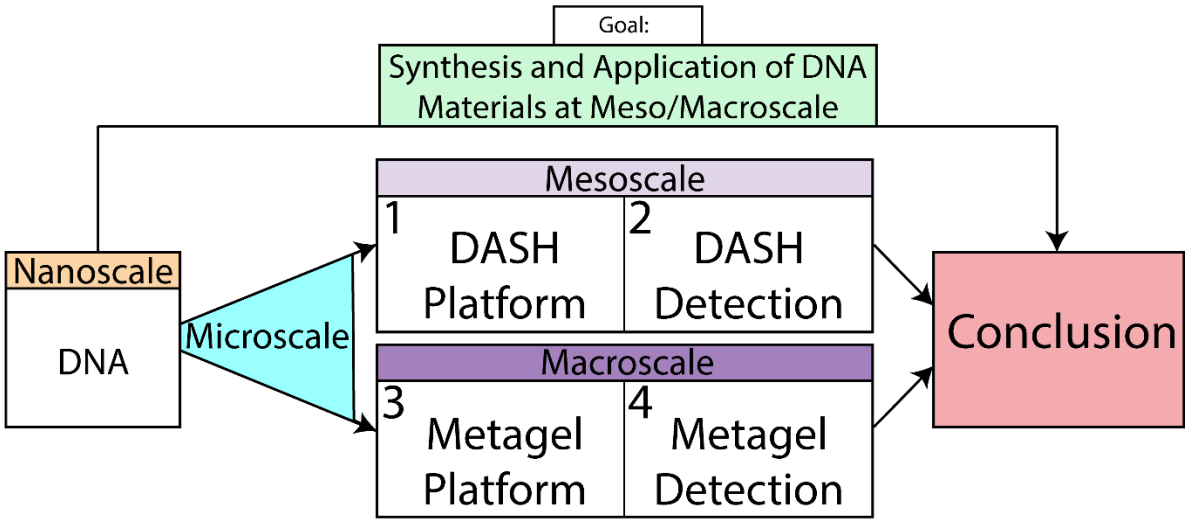

Figure 8. Schematic of the format of this dissertation. Chapter one discusses the conversion of nanoscale DNA to bulk DNA materials with an emphasis on RCA-based materials. Chapter two describes our general efforts to develop an RCA-based DNA material, the "DASH" platform (DNA-based Directed Assembly and Synthesis), for general mesoscale applications. Chapter 3 describes the application of the DASH platform to the specific application of detection. Chapter

4 describes the development of a “metagel platform for application of DNA materials to macroscale applications such as detection.

1.4.2 Why focus on RCA-based bulk DNA materials?

Previously in section 1.2, we discussed several methods for converting nanoscale DNA to meso/macroscale bulk materials. This dissertation focuses on RCA-based materials because we believe that RCA is an efficient means for producing bulk DNA materials for real world applications. We believe this because of RCA’s demonstrated ability to make large scale DNA materials at low cost. For example, Luo Lab has demonstrated the millileter level synthesis of pure DNA hydrogels [50]. Based on the cost of synthesis, bulk hydrogels can be synthesized for as low as $.31/ml if phi29 is produced and purified in-house. This is much cheaper than alternative methods such as ligation-based DNA materials where enzymatic amplification of DNA does not occur. In contrast, all DNA in ligation-based materials needs to be purchased as oligos which can be many times more expensive. The end result is that RCA is well suited for real-world applications which may require that a material be cheap or easily synthesized at large scale. These RCA-based materials are also especially well-suited for applications involving detection. For example, ligation-based materials function by linking existing DNA together. This is not an option in applications like detection where enzymatic amplification is not present and the initial target DNA is present at very low concentration. RCA on the other hand does provide enzymatic amplification of initial DNA with reaction conditions close to room temperature. This means that expensive equipment is not required nor is extreme heating or cooling. This is ideal for low resource environments, such as developing countries, where electricity may not be available.

1.4.3 Why detection: Potential for real world impact

As mentioned above, this dissertation will discuss the application of several meso and macroscale materials for the specific application of detection. We chose this application as a demonstration because we believe that DNA materials have a strong potential in this area and that point of care (POC) detection using materials has a strong potential to have real world impact. Before moving on, what is POC detection and why do we care about it. Recently, POC detection has become a hot topic because of the field's potential to increase access to sensing applications outside of traditional hospital or laboratory environments [61-64]. By enabling testing in areas like the home or developing countries, POC greatly expands the access to diagnostic tests [65-67]. The transformative nature of this technology can easily be seen by considering the home pregnancy test which has become a household name. POC devices have shown promise in numerous areas including agriculture for testing of crops and food supply, veterinary medicine such as the health of pets and livestock, public health and security such as for the monitoring of pandemics and bioterrorism, and environmental testing for air, water and soil contamination [63, 68, 69].

1.4.4 The DASH and Metagel platforms

Much of point-of-care's impact comes from the ability to bring a device to the application of interest. With the DASH platform, our goal was to produce a mobile device which can use mesoscale DNA materials for applications where needed. In Chapter 2, we will discuss the development of the platform as well as its demonstrate its potential for several applications such as cell-free protein expression, protein immobilization and activity, and unique metabolic properties of the system. This will segue into Chapter 3 where will discuss a specific application

in greater depth, detection. With the metagel platform, our goal was to synthesized bulk scale materials for real-world applications.

2 CHAPTER 2: THE DASH PLATFORM

2.1 Introduction to the DASH platform

2.1.1 Metabolic-like materials

Metabolism refers to the chemical processes which occur in living organisms in order sustain life. Specifically, anabolic reactions occur to build up higher order structures from base ingredients while catabolic reactions break down those higher-order structures once their usefulness has ended. What's unique about these reactions is that they are programmed by some template to make and maintain predefined structures. Furthermore, anabolism and catabolism occur simultaneously in order to continuously build and maintain a desired structure such as our body over the course of a lifetime. These autonomous functions have never been exhibited in synthetic materials. If they could be, it would represent a paradigm shift in the engineering of materials. Instead of using static "dead" materials, new applications could be opened by using materials which mimic our living bodies by being programmed to autonomously build a desired structure and maintain that shape over long periods of time. This could also lead to self-sustainable materials and structures that generate, and regenerate in order to adapt and function autonomously. Self-sustainable materials that exhibit artificial metabolism are the holy grail of the synthetic materials field, but have yet to be achieved. We believe that we have developed a system that exhibits some of these properties though by using the unique genetic and generic properties of DNA to bridge traditional living and synthetic materials.

2.1.2 What is the DASH Platform?

One possible solution which has proven promising for artificial metabolism is the DASH platform which is currently in development in Luo Labs. DASH (DNA-based Directed Assembly and Synthesis of Hierarchical material platform), is a unique system that represents a new class of materials with properties that have not been seen before in a synthetic material. Unlike synthesizing DNA in a tube using RCA until the reaction stops and then using that static material for some application, DASH is a living system which uses microfluidics to guide the RCA-based synthesis of DNA materials in an autonomous fashion (Figure 9). The end result is that mesoscale DNA structures are synthesized in such a way that they can be programmed into complex geometries that are determined by simple design rules. This autonomous and programmed synthesis of higher order structures from base ingredients is analogous to the anabolic reactions. These higher order structures can then be maintained by continuously generating and degenerating the DNA material according to the programmed pattern.

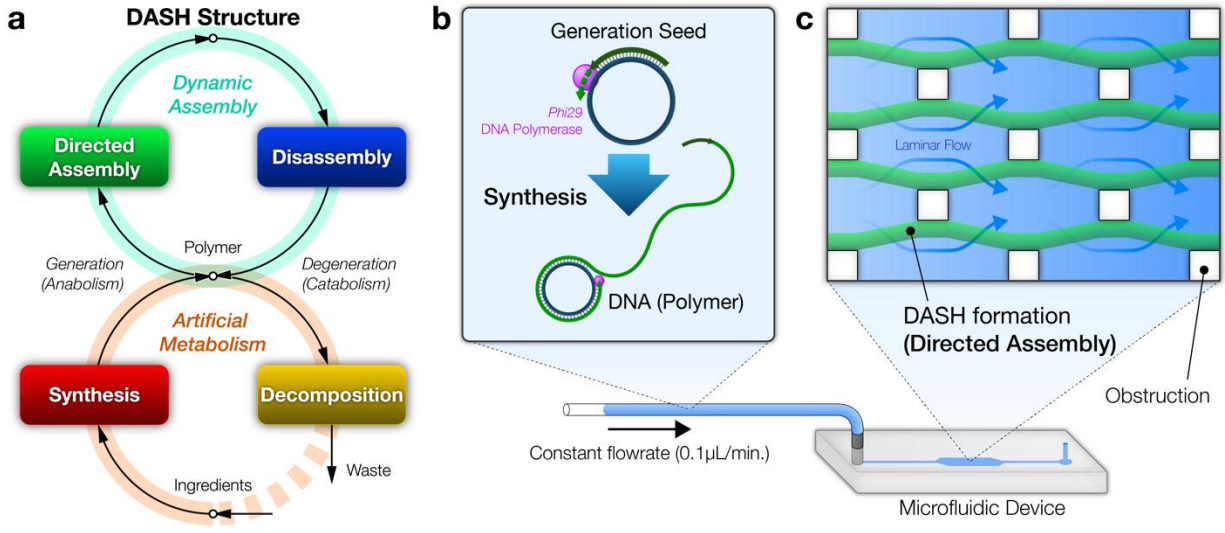

Figure 9. Schematic of the DASH platform. In A, a rolling chain amplification reaction is started by adding a circular DNA template, a primer and a Phi29 polymerase. The primer allows Phi29 to bind to the DNA template and synthesize long strands of single stranded DNA. Once this reaction is started, the solution is immediately pumped into a microfluidic device at .1ul per minute. By flowing the solution through a series of PDMS pillars that guide DNA by obstructing laminar flow, DNA fibers with predefined geometries are formed.

2.1.3 Autonomous generation of DASH

Similar to anabolism, DASH directs DNA into forming complex structures autonomously based on programming from some template. We will discuss the mechanism of how this works in the next section but the end result is that we can program the morphology of the DNA material produced and this synthesis occurs in an autonomous manner. For example, DNA synthesis was guided into producing well-defined mesoscale materials of any desired shape by following two main design criteria. These criteria were that 1: DASH fibers will form by following the direction of flow inside the device and 2: that fibers will take the shortest route inside the channel while connecting between PDMS pillars. Using these design rules allows for the autonomous mesoscale synthesis of DNA in virtually any shape (Figure 10). But what are DASH DNA fibers, how do they form, and how are we able to program them?

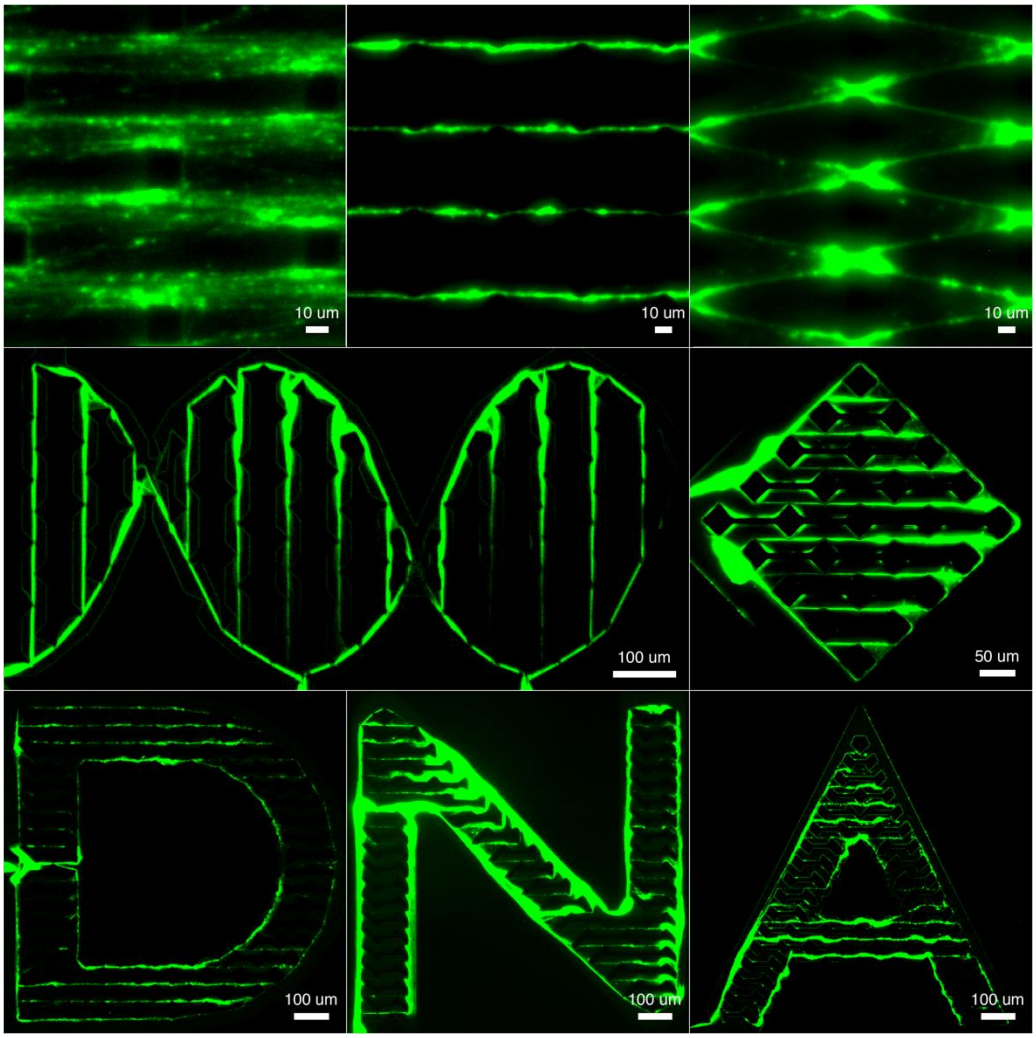

Figure 10: Examples of mesoscale DNA shapes that were autonomously generated by the DASH platform.

2.1.4 Mechanism of Autonomous Generation of DASH

But what is the mechanism behind how DASH generates these complex DNA materials autonomously and how is it programmed. The generation of DASH fibers relies upon rolling chain amplification to massively amplify a low molecular weight template into many copies of high molecular weight ssDNA. Unlike previous RCA-based materials, formation of DASH fibers does not occur due to simple physical entanglement in a tube during RCA. Instead, the RCA

reaction is started and immediately flowed into a microfluidic device that autonomously guides the RCA-based synthesis of DNA in real-time to create a programmed pattern of DNA fibers. The device does this using various geometries of PDMS pillars that direct DNA growth by obstructing and directing laminar flow. Laminar flow between PDMs pillars causes a constriction of flow which then causes a weaving like effect of large DNA fibers. The weaving effect serves to physically entangle the long strands of DNA and orient them in a lengthwise manner so that partial hybridization can occur. This mechanism is supported by the fact that DASH DNA fibers can be several millimeters long. The length is too long to be accounted for by a single DNA fiber even when we take into account the extremely high molecular weight DNA which RCA can produce. Thus, we conclude that the fibers must be due to many long DNA strands woven together and bound by physical entanglement and partial hybridization.

As mentioned, the location of where DASH fibers occur depends on the placement of pillars in the microfluidic device. Pillars obstruct the flow through the device and determine where laminar flow occurs. Because DASH fibers appear to occur where laminar flow is present, the pillar placement also controls where DASH fibers form. Thus, we have two design rules which allow for the programming of DASH fiber synthesis: 1: DASH fibers will form by following the direction of flow inside the device and 2: that fibers will take the shortest route inside the channel while connecting between PDMS pillars.

2.1.5 Microscopy of DASH fibers

The proposed mechanism for DASH formation is supported by direct observation of the DASH fiber using scanning electron (SEM) and confocal microscopy (Figure 11). This work was done via collaboration with Duo An of Luo labs at Cornell University. Using SEM, we can see

that the DASH is made up of many anisotropic, fibrous bundles of DNA networks which are oriented in the direction of flow. These fibrous bundles were multiple microns in diameter confirming that DASH fibers are made up of many DNA strands which are physically entangled and partially hybridized. DASH fibers were also found to be present in the gaps between PDMS pillars instead of wrapped around them. This seems to indicate that DASH is indeed formed by interweaving in the gaps of PDMS pillars due to the constriction of laminar flow and not due to simple impedance from tangling with PDMS structures. Many of these observations regarding DASH fiber morphology were also supported by confocal microscopy. Confocal microscopy was used to directly observe the formation of DASH fibers as they were formed in solution. Confocal confirmed that DASH fibers are on the order of micrometers and that they form from the side of pillars as opposed to wrapping around them.

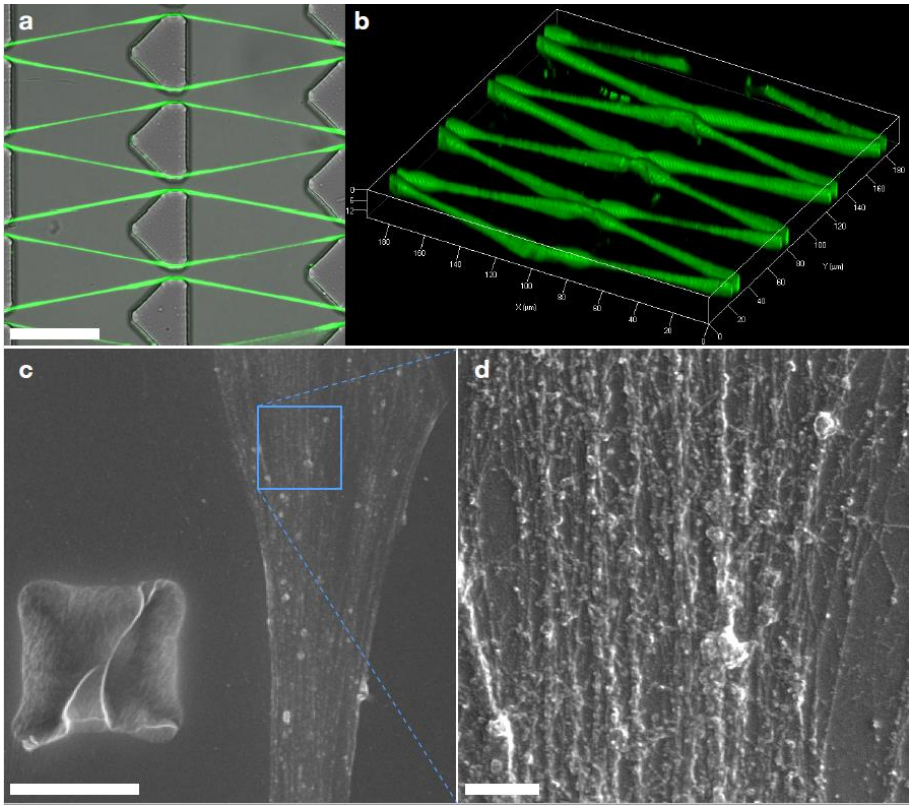

Figure 11. Microscopy analysis of DASH. A/B: Confocal Microscopy of DASH formation showing the location and Morphology of DNA fibers. C/D: Scanning electron microscopy showing the detailed morphology of DASH fibers.

2.1.6 Simulation of DASH fiber formation

The proposed mechanism for DASH fiber formation was also supported by computational fluid dynamics (CFD) simulation. This was done via a collaboration with the Sabin Group at Cornell University and is incorporated in this dissertation with their permission. CFD was used to determine the areas with highest vorticity and the location of laminar flow by measuring flow velocity. This was done theoretically using simulation as well as experimentally by observing the flow of nanoparticles through a DASH device (Figure 12). Figure 12 shows a CFD simulation of the flow direction and velocity using arrows and a heat map. The arrows direction and color indicate that the flow is constricted by the PDMS pillars causing the flow rate and vorticity to increase in the gap between pillars. This increase in the vorticity and the speed of the flow can be seen using a simple heat map in B and C and is confirmed by experimental observation of the flow rate of nanoparticles in D. What is interesting about this is that DASH fibers grow along the paths of highest flow rate and laminar flow. The result is that we can place PDMS pillars to direct this flow and therefore DASH fiber growth.

We believe though that the relationship between flow rate and DASH fiber growth may not be as simple as it appears though. The interesting relationship between DASH fiber growth and flow velocity can be seen experimentally in Figure 13. By Increasing flow rate, we found that we increase a parameter called vorticity. While the shape of DNA is determined by flow velocity and laminar flow, we found that vorticity determines the starting point of the DASH fibers. By

comparing Figure 11a and Figure 12c, we found that the highest vorticity is found on the side of pillars. This is interesting because direct observation using SEM and confocal microscopy agreed that this is the starting point for DASH formation. As a result, we believe that vorticity plays a crucial role in where DASH fibers start to form by dynamically triggering physical entanglement of DNA in solution. Thus, we believe that flow rate may affect the DASH formation kinetics due its influence on vorticity. Now that we know how and where DASH fibers are generated, how can the DASH platform mimic catabolism by degenerating DASH.

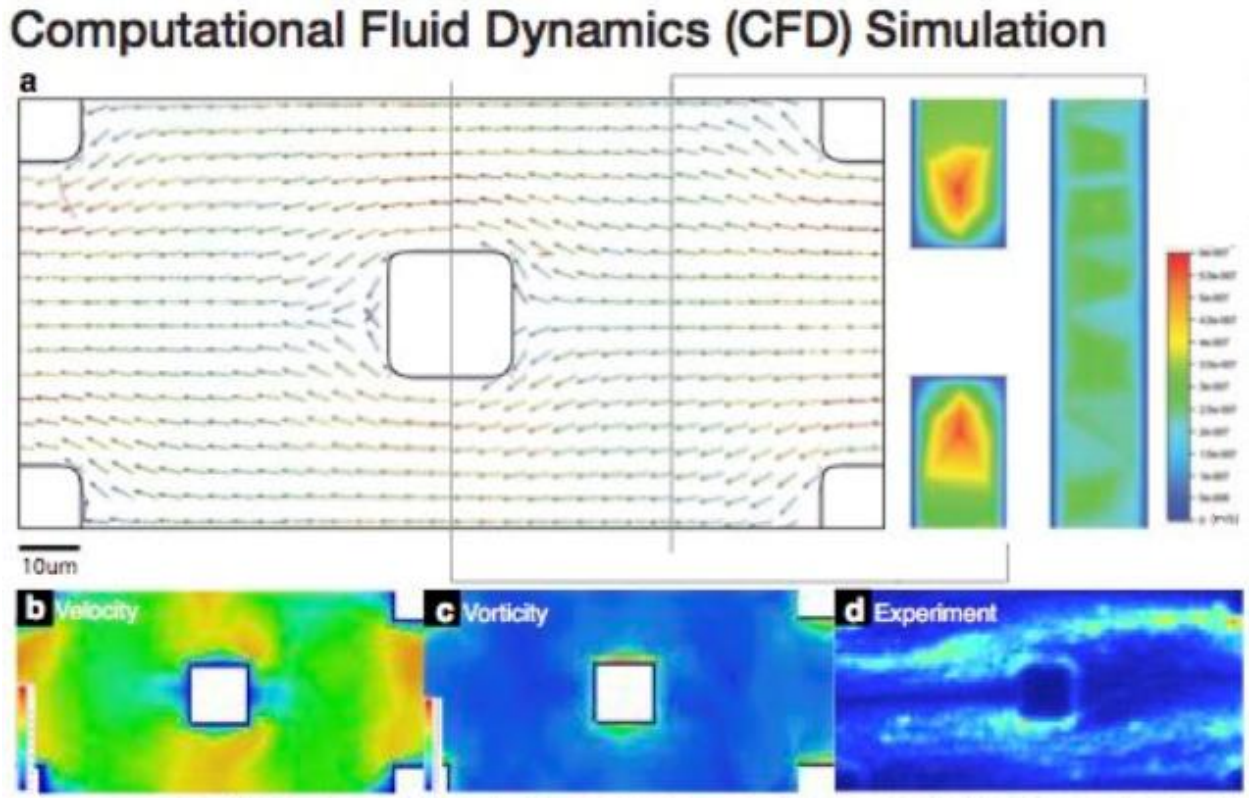

Figure 12. Computation fluid dynamics (CFD simulation of a DASH device and comparison with experimental data. A: Flow vector and velocity heat map of a DASH device using CFD. B Velocity simulation. C: Vorticity simulation. D: Experimental comparison by tracking the speed and direction of nanoparticles through a DASH device.

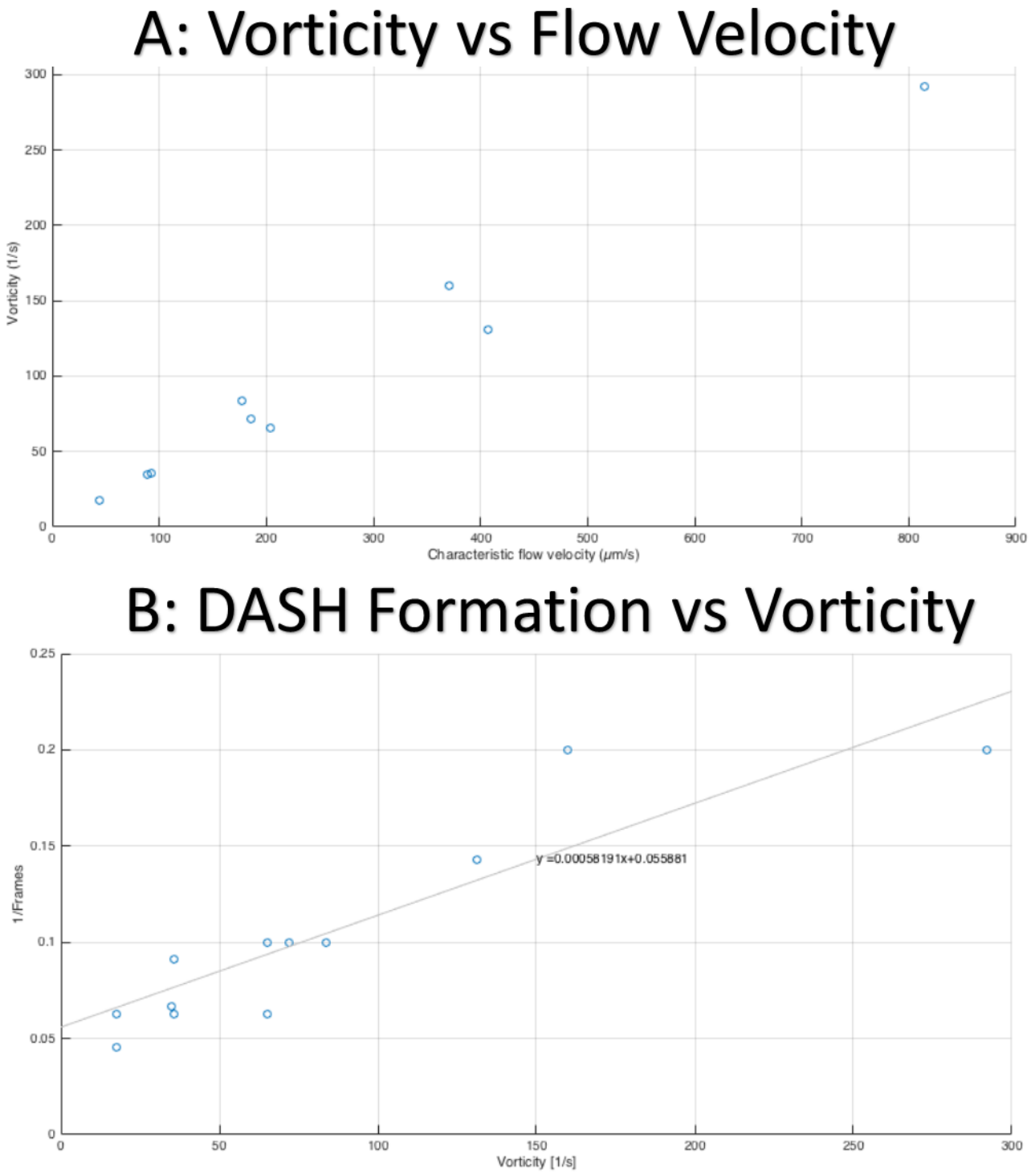

Figure 13. Analysis of DASH formation in relation to flow rate and vorticity. A: Vorticity vs flow velocity in a DASH device. B: DASH starting time vs vorticity.

2.1.7 Autonomous Generation and Degeneration of DASH

What is unique about DASH is not its ability to mimic anabolism by creating higher order structures, but rather its ability to simultaneously and autonomously mimic both anabolism and catabolism. For example, Figure 14 shows autonomous generation and degeneration of DASH by simultaneously flowing an RCA solution and a DNASE solution through a microfluidic device. The RCA solution serves to generate DASH fibers while the DNASE solution simultaneously degrades DASH. The result can be seen in Figure 14a. Specifically, no DASH is formed within the first 2 hours because the rate of DNA degradation by DNASE is faster or equal to the rate of DNA synthesis by RCA. We find that synthesis begins to outpace degradation by the third hour (B) as DASH begins to form and then reaches its max amount by the fourth hour (C). By the fifth hour, the rate of degradation exceeds the rate of synthesis again and DASH begins to degrade (D). We found that this cycle of generation and degeneration is continuous with several cycles occurring over the course of several hours. The end result is that by continuous flowing in ingredients, DASH exhibits some potential as a self-sustaining material. It is able to maintain its complex structure by continuously and autonomously generating and degenerating. We believe that this is the first time that a synthetic material has been able exhibit this kind of artificial metabolism.

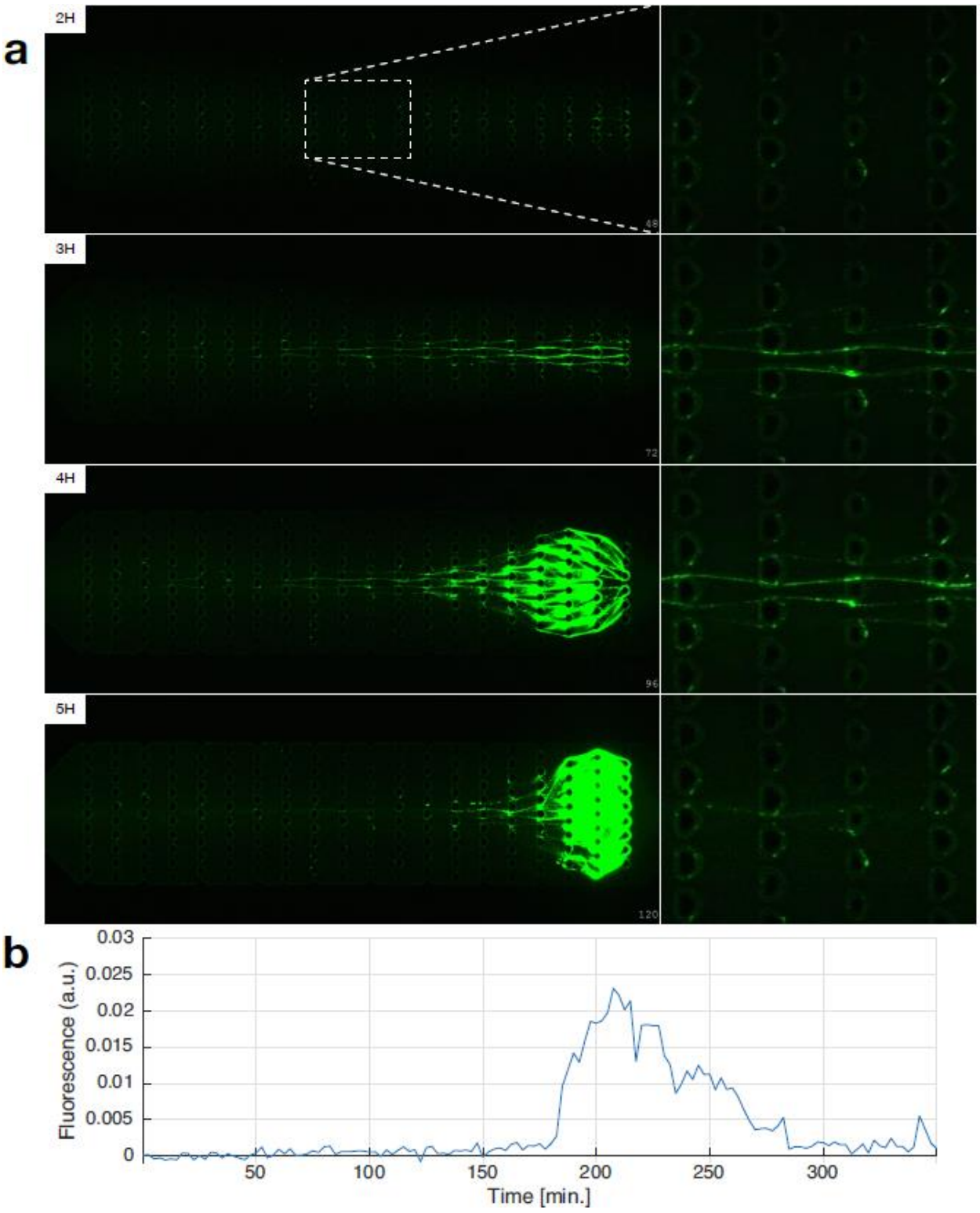

Figure 14. Simultaneous and autonomous generation and degeneration of DASH. An RCA reaction solution for generating DNA fibers was flowed into a microfluidic device at the same

time as a DNASE solution for degrading the DNA fibers. (A) 0-2 hours: the degradation rate equals or exceeds the generation rate. (B) 3 hours: the generation rate exceeds the degeneration rate. (C) 4 hours: DASH reaches its max amount of DNA. (D) 5 hours: the degeneration rate starts to exceed the generation rate.

2.1.8 Mechanism of DASH generation and degeneration

DASH exhibits artificial metabolism due to a complex mechanism that results from the interplay of DASH generation from the RCA-based solution and DASH degeneration from a DNASE-based solution. Previously in this chapter, we discussed how DASH fibers form in the area of greatest vorticity in the microfluidic device, the sides of the PDMS pillars, then grow along the areas of great flow velocity. When a generating and degenerating solution is simultaneously flowed through the device, an interesting series of events occur. First, DASH takes several hours longer to form than normal which we can see from Figure 14A and B in which there is no presence of DASH until the third hour. This is due to the fact that less DNA is available to weave into the start of DASH fibers at the sides of pillars. Instead, free DNA in solution is being degraded before the vorticity can cause physical entanglement and fiber growth. Once DASH fibers begin to grow, the rate of formation greatly increases as can be seen by large amount of growth that occurs from hour 3 in B and hour 4 in C. This would indicate that once DNA is physically entangled into a DASH fiber, it is provided some protection from DNASE that is flowing through the device. Eventually, DASH reaches a maximum density which we can see at hour 4. DASH growth slows because fibers begin to fill the junctions between pillars and therefore obstruct the flow. As we know from our discussion of Figure 12 and Figure 13, DASH fiber formation and flow rate appear to be closely linked. A slower flow rate means

slower DASH growth. By slowing the flow rate though, DNASE activity may be increased. Instead of the enzyme being quickly pumped out of the device, its residence time increases giving it more time to bind to, and degrade, DNA. The end result is that DASH is degraded until fibers no long obstruct the flow and the process can start all over again.

A second possible mechanism for the autonomous generation and degeneration of DASH involves mixing. During normal flow through A DASH device, computation fluid dynamics predicts that multiple inlets and laminar flow will result in discrete streams of each solution being pumped in with minimal mixing occurring (Figure 15). This effect was also confirmed experimentally in Figure 16 which will be discussed later on. When a blockage in the center of the DASH device occurs, such as what is shown in Figure 14c when DASH reaches its max amount, the streams of different liquids are interrupted and forced to mix in order to bypass the blockage. By mixing the DNASE and RCA solutions, the kinetics of DNA degradation should be much faster due to increased molecular collision.

Low Mixing:

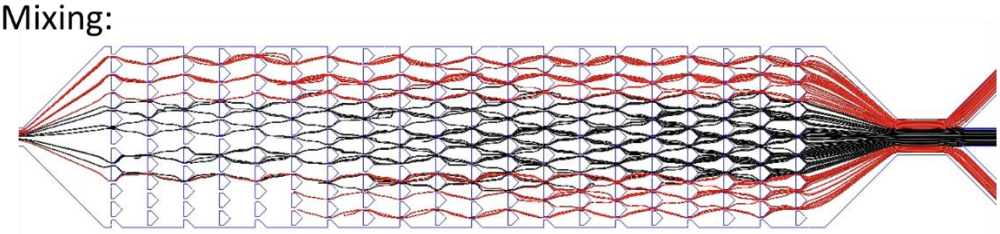

High Mixing:

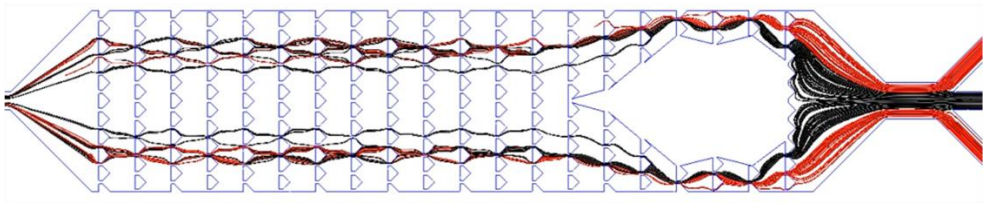

Courtesy of Max Vanatta and Jenny Sabin of the Sabin Group. Cornell University

Figure 15. Computational fluid dynamics simulation of DASH generation and degeneration.

2.2 General Applications of DASH

2.2.1 Introduction

Once we demonstrated that DASH can exhibit artificial metabolism by generating and degenerating complex DNA materials based on a program, our goal was to demonstrate its broad applicability as a platform by demonstrating its usefulness in a wide range of areas. We did this by showing that the DASH platform has utility to applications such as protein immobilization and biocatalysis, cell-free protein expression, and detection.

2.2.2 Protein Immobilization and Biocatalysis

The DASH platform has great potential in the area of protein immobilization and biocatalysis. Part of this is due to DNA's unique well defined chemistry and role in biology which allows many enzymes to interact with DNA. This was discussed at length in Chapter 1 of this thesis. One protein which reacts strongly with DNA is avidin. Avidin is a highly positively charged protein which is known to bind strongly to negatively charged DNA. By flowing yellow and red fluorescently labelled avidin through DASH, we found that avidin is patterned by DNA as a result of strong avidin-DNA binding. What's interesting about this is that now not only can the DASH platform pattern both DNA and any proteins which bind DNA, but we can pattern and bind virtually any protein by creating avidin-protein conjugates. An avidin-protein conjugate is a complex of avidin and any other protein which are bound together covalently. This greatly expands the utility of the DASH platform because virtually any protein can be linked to avidin and patterned by the DASH platform by either chemical coupling or co-expression from a plasmid. What's even more interesting is that proteins can also be immobilized in a spatial

manner. In Figure 16, DASH fibers which are stained by either red fluorescently labelled avidin or red and green fluorescently labelled avidin. These proteins were able to be immobilized in a yellow to red to yellow pattern from top to down by controlling the position of the inlet in which the protein was injected into the DASH device. The spatial control over protein location is extremely useful for applications such as biocatalysis.

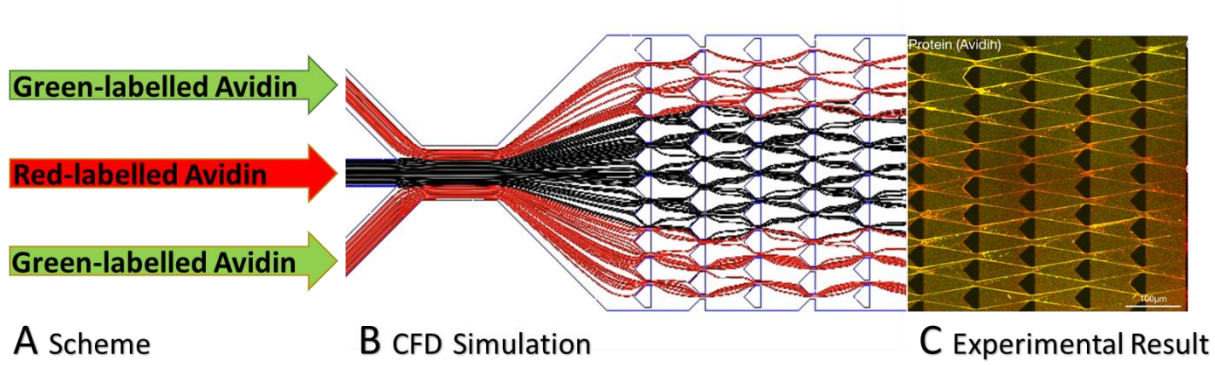

Figure 16. Fluorescently labelled avidin binding on Dash fibers. (A) Avidin with different fluorescent tags was injected into a three-inlet microfluidic device according to the arrows shown. Green-labelled avidin was injected in the top and bottom inlets while red was injected in the center inlet. (C) A red strip corresponding to the center inlet of the device occurred because of bound red-labelled avidin. A yellow top and bottom band occurred due to binding of both red and green-labelled avidin. (B) A computational fluid dynamics simulation of the laminar flow is also shown and describes why the banding pattern occurs. Avidin binding data was kindly provided by Yudi Pardo of Cornell University.

In order to demonstrate the usefulness of the DASH platform for applications such as biocatalysis, we used the immobilization of an avidin-HRP (horseradish peroxidase) conjugate as a model. We then tested the activity of HRP using several methods in order to confirm that

immobilized enzymes are still active. As shown in

Figure 17, HRP was clearly still active following immobilization in the DASH device. Specifically, we can see the activity of HRP in real time within the device using fluorescent microscopy. The red fluorescent product which results from DASH activity can be seen to be originating from the DASH fibers. We also tested the activity using TMB (3,3',5,5'-Tetramethylbenzidine). What's interesting about TMB is that not only was the correct colored product of HRP activity observed but an intermediate product was found to be coating the DASH fibers allowing them to be seen with the naked eye Figure 18. It is likely that this is due to the charge of the intermediate blue product and the final yellow product. The intermediate blue product is highly positively charged causing it to bind strongly to negatively charged DNA whereas the final yellow product is neutral and can flow through DNA unimpeded.

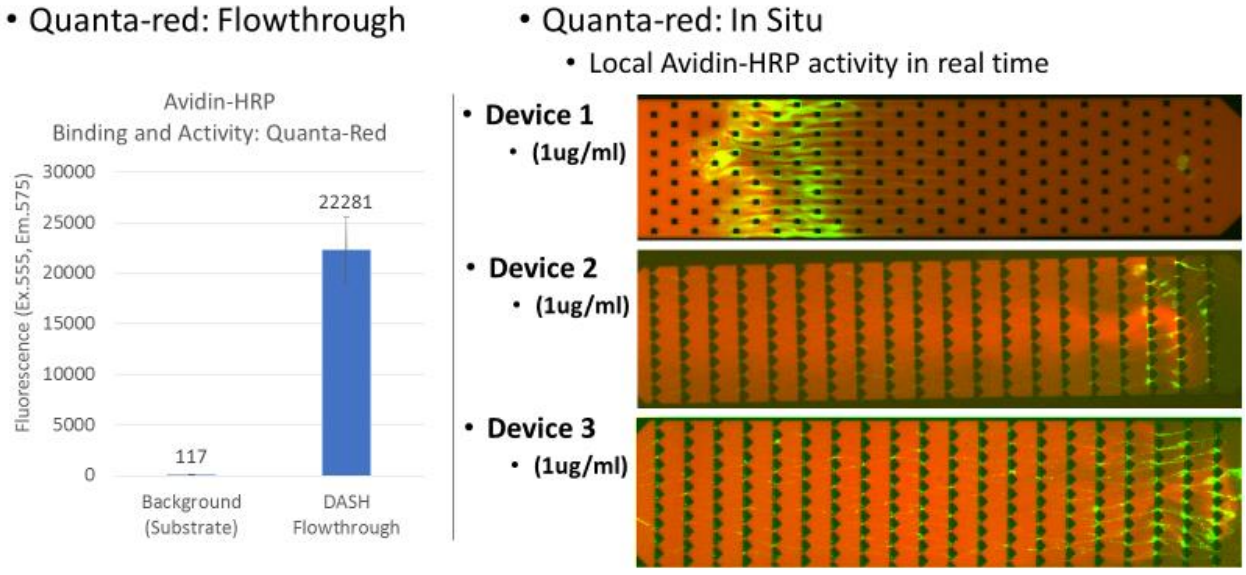

Figure 17. Avidin-HRP binding and activity. Samples were prepared by forming DASH and flowing through avidin-HRP through for one hour. The sample was then washed with buffer and a quanta red

HRP substrate flowed through. Right shows the in-situ red fluorescence due to the HRP activity. Left shows the red fluorescence of the collected solution.

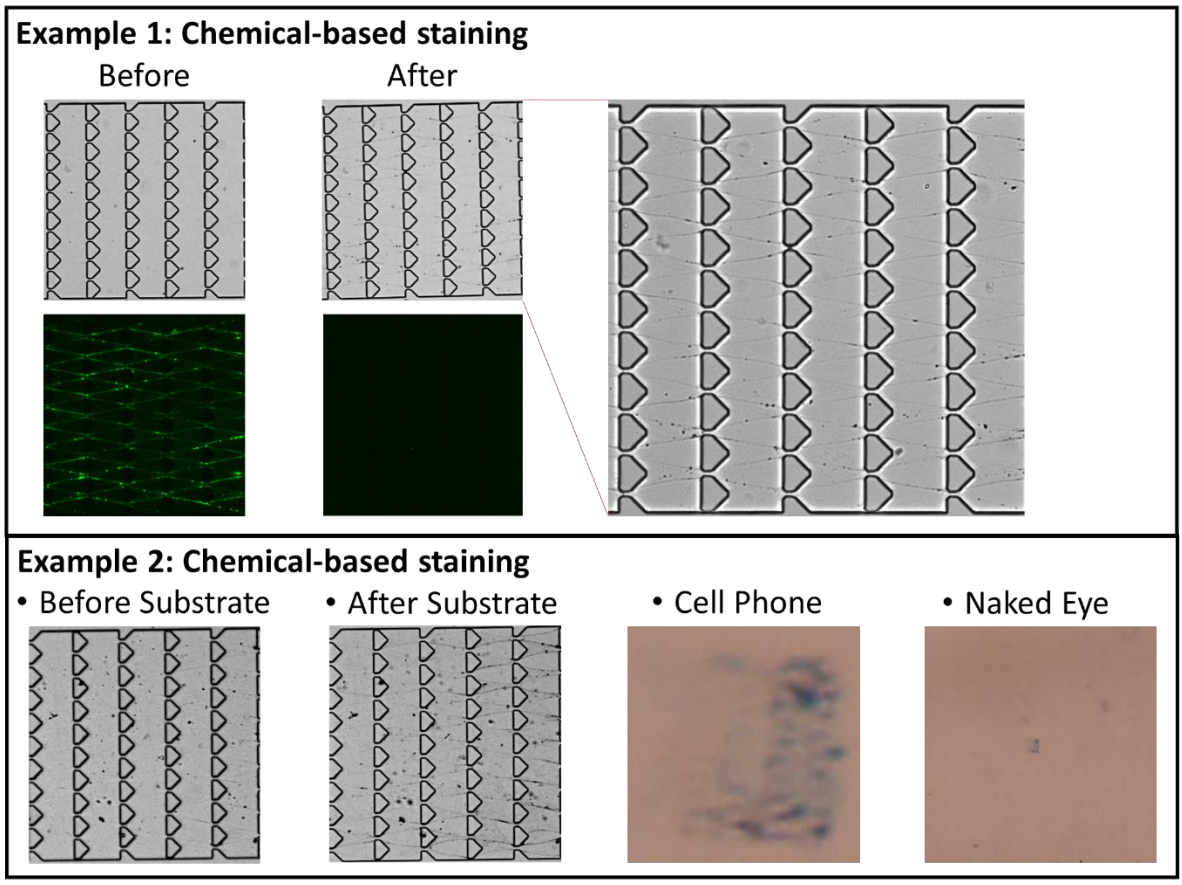

Figure 18. DASH staining due to conversion of TMB to TMB-diamine by DASH immobilized avidin-HRP.

2.2.3 Cell-free Protein Expression

A logical application for DNA materials in general, and DASH in particular, is cell-free protein expression (CFPE). In conventional protein expression, an expression plasmid is transfected into a cell which then carries out several dozen reactions to transcribe RNA from

the DNA and then protein from the RNA. In contrast, CFPE is a cell-free method in which cells are lysed so that protein expression can occur in vitro. By adding an expression plasmid to the lysate, proteins are produced in a simple open system which is ideal for real-time manipulation of the synthesis or monitoring to ensure product quality. Furthermore, proteins are produced in a matter of hours instead of days or weeks. This ability to rapidly produce a protein of interest could be potentially invaluable to point of care (POC) applications by quickly producing therapeutics close to where they are needed without the need for complex cell-based manufacturing facilities. Being able to produce therapeutics in low resource environments like the home or in developing countries would increase patient access to medications and ease the logistical burden of transporting frozen protein-based medications with limit shelf-life.

CFPE for the POC production of proteins is a logical application for the DASH platform because of the device's ability to manipulate DNA and the format of the device. For example, DASH can amplify DNA of interest to produce complex DNA materials which are self-sustaining. If an expression plasmid is used as a template, the DASH platform can amplify the DNA gene by many orders of magnitude in order to produce large amounts of protein and potentially maintain the production by regenerating the plasmid-based DNA material. Furthermore, it is an ideal format for POC. DASH DNA is generated using an isothermal process and room temperature which reduces the equipment needs. It also confines the protein production to a microfluidic device making it highly portable compared to the large facilities needed for cell-based protein production.

2.2.4 DASH from Plasmid DNA

In order to demonstrate CFPE using the DASH platform, it was first necessary to convert an expression plasmid into a template for RCA-based DASH (Figure 19). RCA requires that a template be single stranded, circular DNA so that a primer can hybridize, the polymerase can bind, and a new DNA chain elongated. Expression plasmids on the other hand are double stranded circular DNA. In order to convert the plasmid from double stranded to single stranded, the scheme in Figure 19 was used. Firstly, a nicking endonuclease was used to cut the coding strand of the plasmid. This nick provides a free end of DNA which allows the strand to be completely digested by adding exonuclease 1 and 3. In order to confirm that the plasmid was successfully converted from double to single stranded, gel electrophoresis was used and the resulting gel imaged in Figure 20. Lane 2 showed a large dark band at the ~3000bp ladder marker which corresponded perfectly to the size of the expression double stranded expression plasmid. Following nicking with an endonuclease and digestion with an exonuclease, the band shifted downward to the ~1250bp ladder marker. The shift downward is confirmation that the reactions were successful because single stranded circular DNA will migrate faster during gel electrophoresis than double stranded DNA because of the double stranded DNA's increased rigidity. This was confirmed by placing the template in an RCA solution containing primer and phi29 and injecting the solution into a DASH device where DASH DNA fibers were successfully generated.

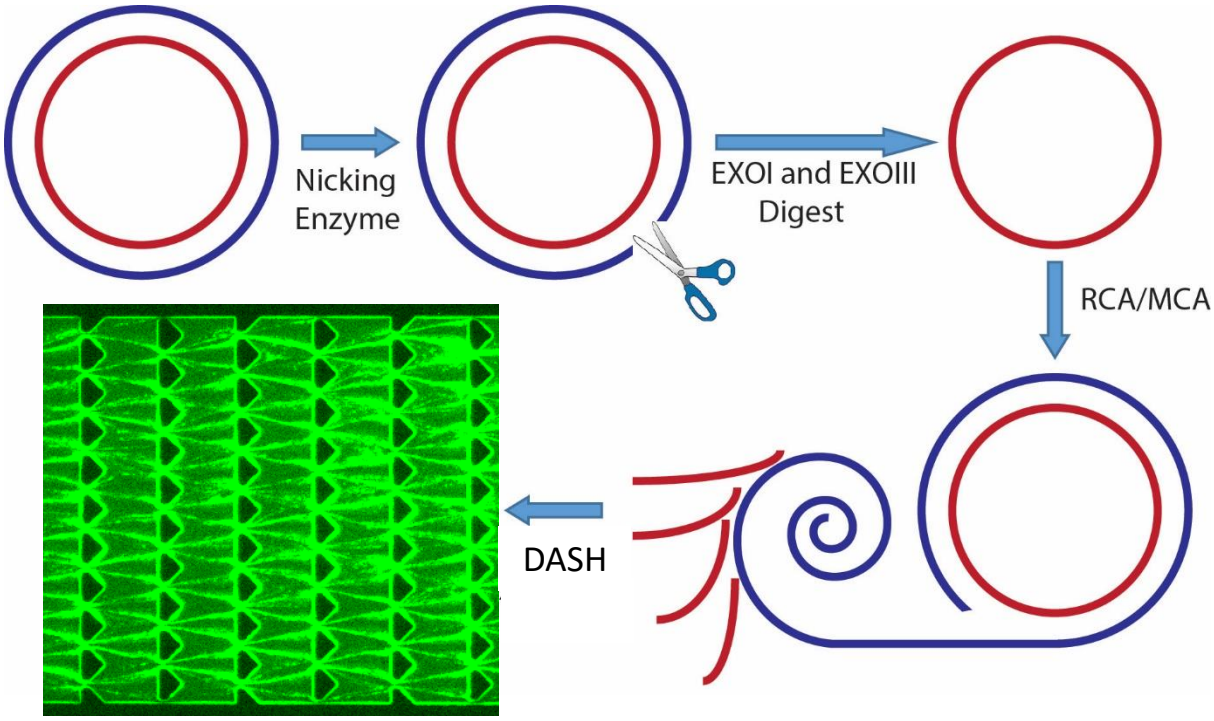

Figure 19. Schematic of template preparation and DASH formation from an expression plasmid.

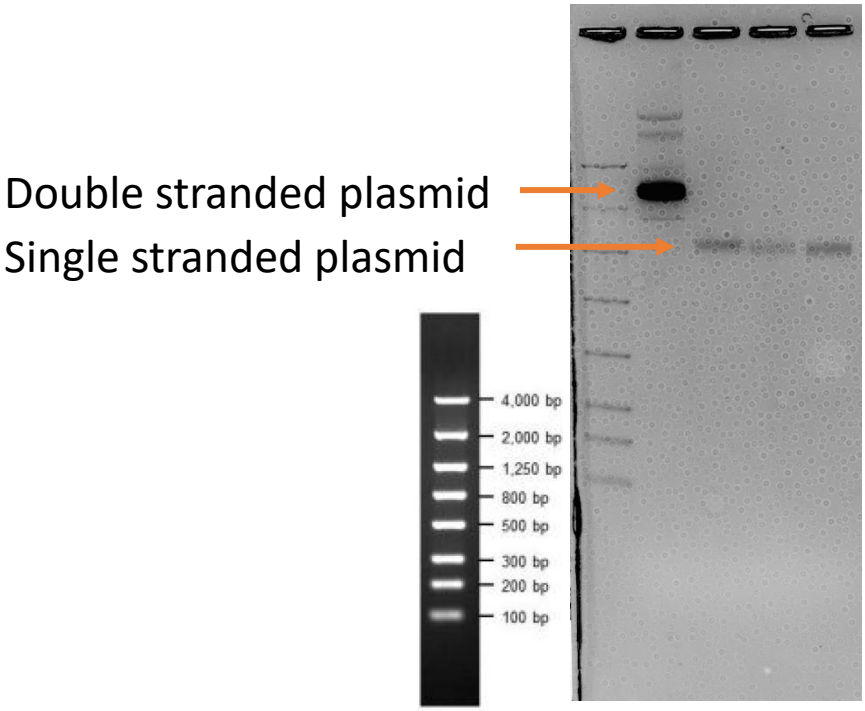

Figure 20. Confirmation of the preparation of a plasmid template for RCA using gel electrophoresis. Lane 1: 100bp+ ladder. Lane 2: Untreated double stranded circular plasmid. Lanes 3, 4 and 5: replicates of a treated plasmid. The band shift from ~3000bp according to the ladder markers to ~1500bp is conducive with the conversion of the plasmid from double stranded circular to single stranded circular.

2.2.5 Cell-free Protein Production Using DASH

Once DASH was able to be formed using an expression plasmid, the ability of the DASH platform to produce protein was evaluated using the s30 T7 high yield protein expression kit from Promega. Specifically, a solution containing everything needed for CFPE was flowed through two DASH devices, one with DASH made from a green fluorescent protein (GFP) coding plasmid and one without DASH (Figure 21). Within two hours, significant amounts of green fluorescence could be seen within the DASH-containing device due to the production of GFP. In order to confirm that the fluorescence came from GFP, the flowthrough solutions from the DASH and no DASH devices were collected and analyzed using a fluorescent plate reader (Figure 22). Using a spectral scan, the plate reader found that excitation and emission wavelength of the solution corresponded well with that of GFP and that there was significantly more fluorescent protein present in the DASH containing device than the no DASH device.

The effectiveness of the DASH platform for producing proteins for POC depends on the yield of a protein of interest and the dose needed for a patient. These experiments showed that large amounts of GFP can be produced. If a more difficult to produce protein is needed for an application, such as monoclonal or domain antibodies, yields will be lower. Thus the yield and dose response needs to be evaluated. That said, CFPE has improved yields by orders of

magnitude over the past two decades. We envision that at some point, tens of milligrams of virtually any protein could be produced cell-free. These high yields could be coupled with the DASH platform to produce lifesaving therapeutics where and when they are needed.

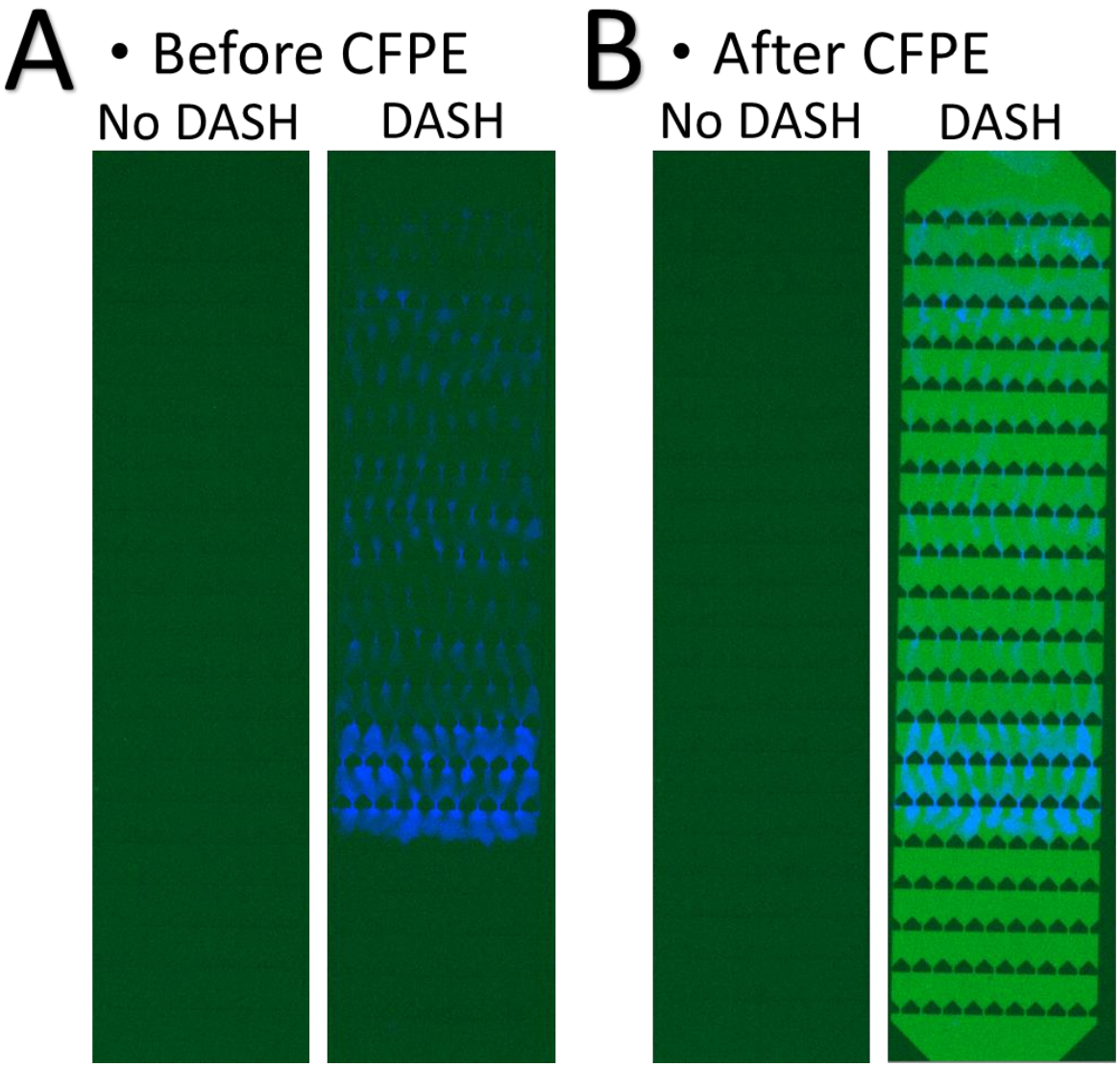

Figure 21. In-situ DASH-based cell-free protein expression (CFPE). A: A DASH device with and without plasmid-based DASH. These photos were taken before a CFPE solution was flowed through. DASH fiber are shown in blue due to their staining with a Hoecst 33342 dye. B: A DASH device with and without plasmid-based DASH following the cell-free protein production of

green fluorescent protein. The high green fluorescence present in the sample with DASH shows the successful production of GFP compared to the blank device. The DASH, which is stained in blue, is still present after CFPE.

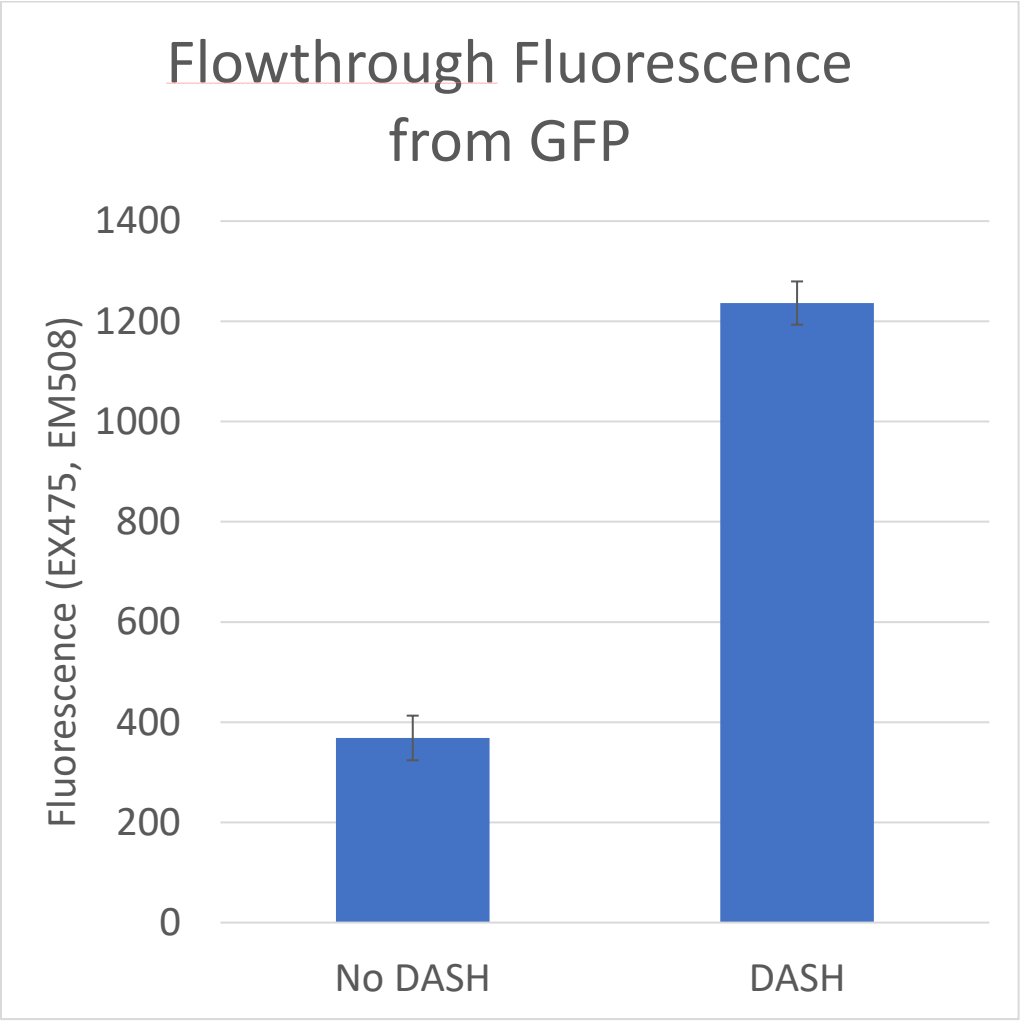

Figure 22. Resulting fluorescence of Green fluorescent protein from DASH using cell-free protein expression. A solution for the cell-free production of proteins was flowed through a blank DASH device and a DASH device containing DNA fibers which were made from a GFP-encoding plasmid. The solutions were then collected and the fluorescence measured in order to

compare the amount of GFP produced to the background fluorescence of the cell-free expression kit.

2.2.6 Concluding Remarks

Earlier in this chapter, we've seen that the DASH platform is a unique system because of its ability to exhibit artificial anabolism and catabolism. Dash can be easily programmed by a microfluidic device to make intricate patterns of mesoscale DNA materials. Furthermore, it can self-sustain these materials by degenerating and regenerating autonomously. In the future, we hope to directly utilize artificial metabolism to demonstrate new applications but for now, we wanted to simply demonstrate the broad applicability of the DASH platform. Thus, we used the latter half of this chapter to show that the DASH platform is broadly applicable to a number of applications such as protein immobilization and cell-free protein expression. In the next chapter of this dissertation, we will be discussing one application in greater depth to show that the DASH platform has enormous potential for having real-world impact.

3 CHAPTER 3: THE DASH PLATFORM FOR DETECTION

3.1 Introduction

In the previous chapter, we discussed the DASH platform's ability to produce complex patterned shapes by guiding RCA-based DNA growth using microfluidic-based control of laminar flow and vorticity. In this chapter, we want to discuss our efforts in integrating a detection mechanism into DASH synthesis that allows for detection with high sensitivity and specificity. Furthermore, our goal with this project was to demonstrate that the DASH platform can have

real-world impact in the area of detection. Thus, we our goal was to demonstrate DASH's usefulness in a promising area of detection which have the potentially to revolutionize access to diagnostics, point-of-care detection using naked eye readout.

Towards these goals, we modified the original DASH synthesis scheme in order to utilize ligation for the specific recognition of targets. This can be seen schematically in Figure 23a. Specifically, a single stranded linear DNA template can only be amplified by RCA if the correct target is present to span the ends of the template and allow it to be ligated into a circle. If an incorrectly match target is present, the template cannot ligated and cannot act as a template for RCA. Ligation provides the specificity but RCA provides the sensitivity by allowing for a billion-fold amplification of the initial DNA [46]. This makes our RCA-based scheme ideal for detection-based applications because of the massive amplification of signal that it provides.

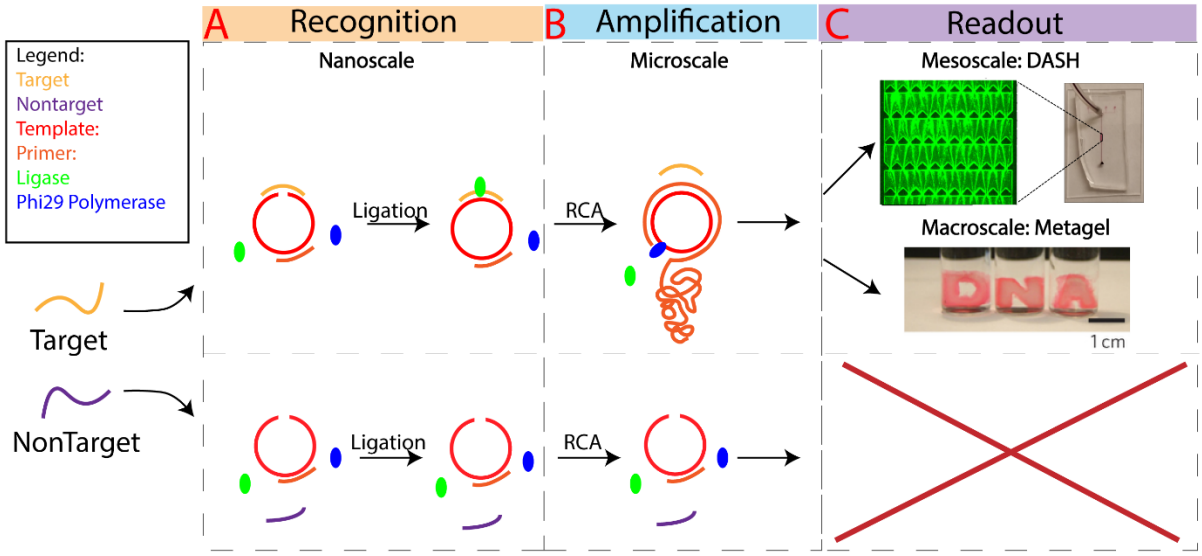

Figure 23. Schematic of our RCA-based approach to detection for the DASH and metagel platforms.

By utilizing DASH for detection, we are able to demonstrate a concept which we believe has never been applied to detection-based systems, Pattern-based detection. In previous systems, particularly those utilizing RCA, signal intensity over noise has been used as the readout. This can be problematic because when noise is high, the signal can be difficult to interpret. For example, when using fluorescence as a detection output, there is inevitably some level of background fluorescence present due to autofluorescence. In order to address this issue, we attempted to use the DASH platform to circumvent this issue by using both signal intensity and pattern as our readout. Unlike signal intensity, the human brain is geared to easily interpret patterns. For example, even if a stop sign if damaged, obscured, faded or peeling, we can still interpret the meaning.

DASH is unique for its ability to produce virtually any structure desired via simple microfluidics design and so it is an ideal platform to test the principle of pattern-based recognition. By being able to optically stain DASH fibers using nanoparticles, we are also able to see the fibers with the naked eye allowing us to test the use of the DASH platform for naked eye detection.

3.2 Results and discussion

3.2.1 Ligation efficiency using polyacrylamide gel electrophoresis for CMV and mtDNA specificity

The specificity of our ligation reaction was tested using polyacrylamide gel electrophoresis (PAGE). Two model DNA targets were chosen, a cucumber mosaic virus (CMV) pathogen and a mtDNA diagnostic target, and compared to a two base pair mismatched version of each target. We attempted to quantify the ligation efficiency by digesting the sample with

exonuclease I and III to degrade any non-ligated DNA according to the scheme shown in supplementary Figure 27. The results for cmv and mtDNA showed that only the correct target had significant ligation (Figure 24a and b). Following digestion, the correct target had a band present which matched the location and intensity of the original template (lane 5). The nontarget however, had no band present (Lane 9). When the band intensity in lanes 5 and 9 were quantified and compared to their theoretical intensity, it appeared that nearly all template was ligated by the correct target (Figure 24c). A mismatched target however had no detectable signal. This would indicate that our system is highly discriminating for the correct target even over slightly mismatched versions like a two base pair mismatch.

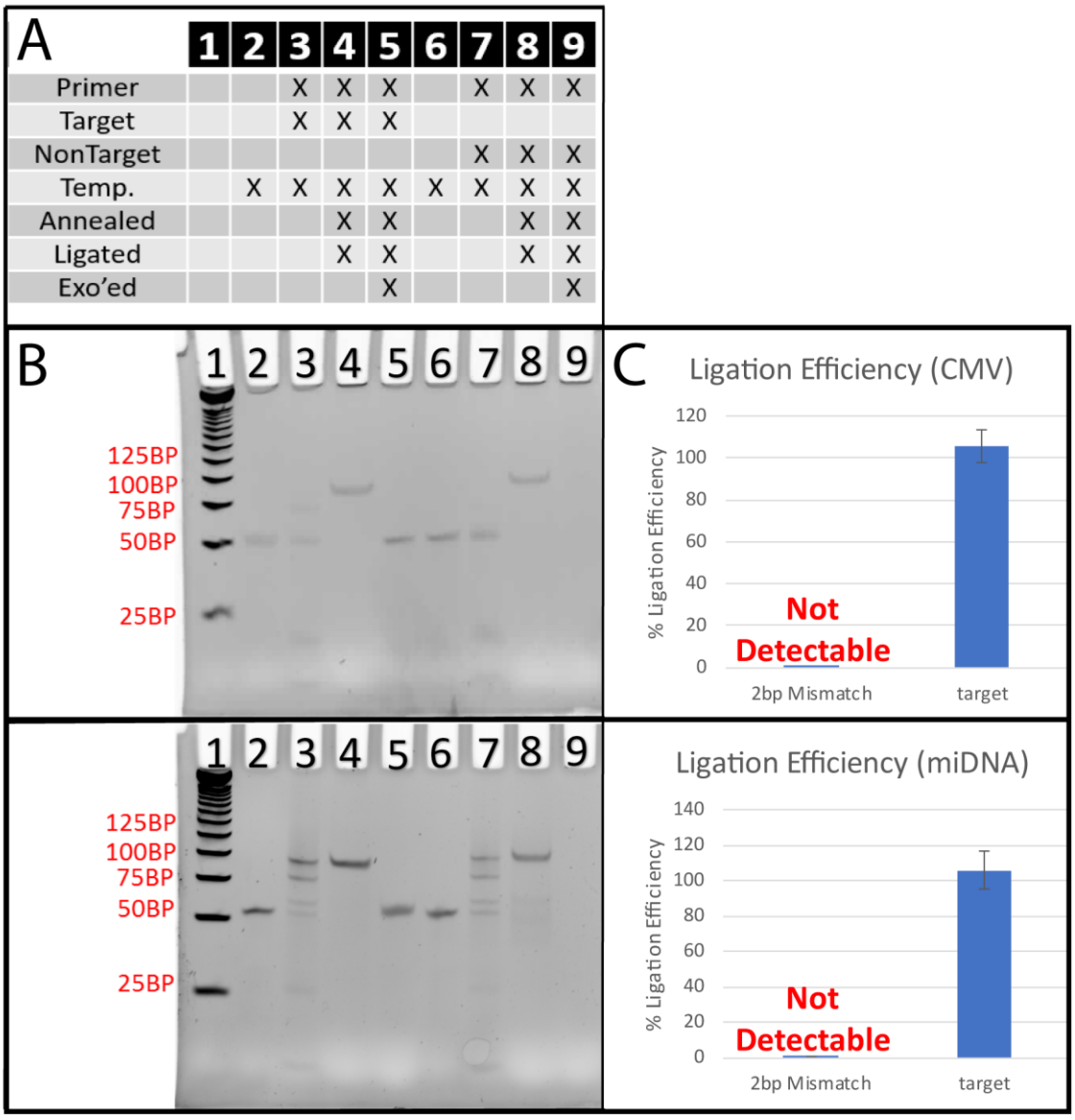

Figure 24. Ligation efficiency results for CMV and mtDNA specificity. A: Sample treatment info for polyacrylamide gel electrophoresis (PAGE). Gel results for PAGE showing Ligation efficiency for specificity. Lane 1: Ladder, Lane 2: Template, Lane 3: Primer, target, template, Lane 4: Primer, target, template (annealed and ligated), Lane 5: Primer, target, template (annealed, ligated, EXO digested), Lane 6: Template, Lane 7: Primer, 2BP mismatched target, template, Lane 8: Primer, 2BP mismatched target, template (annealed and ligated), Lane 9: Primer, 2BP

mismatched target, template (annealed, ligated, EXO digested). C: Quantitative band analysis of ligation efficiency for specificity.

3.2.2 Sensitivity and specificity results for the DASH platform-based detection of CMV and mtDNA

In order to determine the sensitivity and linear dynamic range of the DASH platform for detection, CMV and mtDNA targets were tested from 500pM to 5pM. The resulting DASH formation can be seen in the microscopy images in Figure 25a. Using the STR method described in supplementary Figure 28, the signal to noise ratio was calculated for each concentration and plotted in Figure 25b. To summarize, both the CMV and mtDNA target could be detected down to 5pM and the signal from 500pM to 5pM appeared to be linear. This would indicate that DASH could be used to detect a wide range of nucleic acid targets with high sensitivity which still allowing quantification because of the linear dynamic range reaching several orders of magnitude.

In order to confirm the usability of DASH as a detection system, the specificity was also tested from 500pM to 5pM for both CMV and mtDNA. For all concentrations and targets, it was found that no DASH forms for nontargets that are even highly similar to the correct target sequence. In order to simulate this, a two base pair mismatched target was tested and the microscopy images shown in Figure 30. The signal to noise ratio of these samples were also quantified using the STR method and the resulting data shown in Figure 25b. The signal from the mismatched target was lower than the true target as expected and was found to not interfere with the assay. However, the signal level from the target and nontarget seemed to converge at

just below 5pM indicated that the limit of detection is likely just around the femtomolar detection level.

As an ultimate test of specificity, a one base pair mismatched target for CMV and mtDNA was also tested and the data shown in supplementary Figure 29. To summarize, we found that the mismatch could easily be distinguished for CMV and but was not distinguished for mtDNA. As a result, we concluded that the ability of the DASH platform seems to robustly distinguish all two base pair mismatched targets but distinguishing single nucleotide polymorphisms is on a case-by-case basis depending on the location and identity of the mismatch. This is supported by the literature which concludes that the specificity of the ligation reaction using T4 DNA ligase is highly dependent on the location and identity of a mismatch [70].

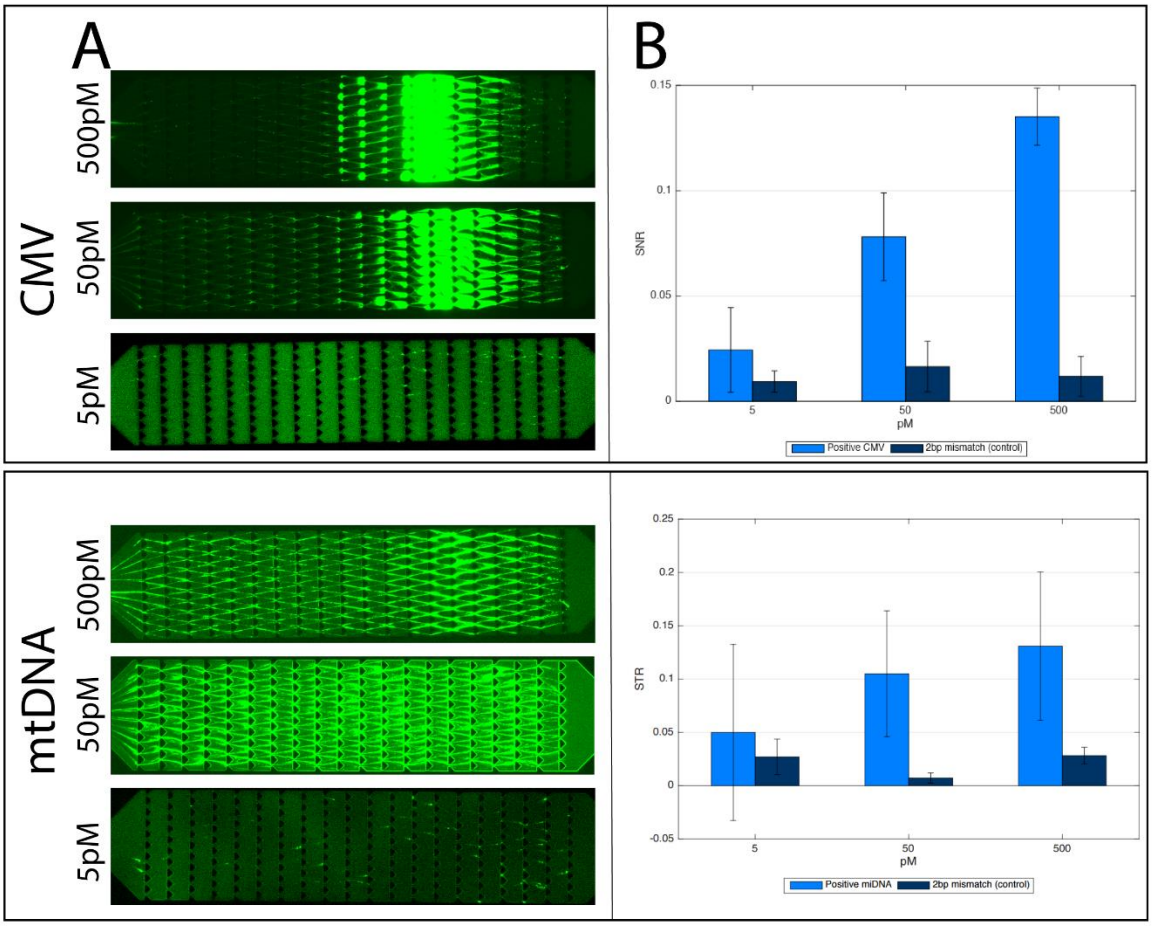

Figure 25. Sensitivity and specificity results for CMV and mtDNA. Column A shows microscopy images of CMV and mtDNA at 500pM to 5pM. This data was quantified using the STR method described in the supplementary Figure 28 and the data displayed in column B. No DASH could be seen for the 2BP mismatched target (supplementary Figure 30) but images were quantified using the STR method and also displayed in column B for comparison.

3.2.3 Naked eye detection using the DASH platform

One unique property of DNA is the ease at which it can be stained with optical or fluorescent dyes. Dozens of dyes are commercially available and bind to DNA either by

electrostatic interactions or binding within DNA's major or minor grooves. In order to translate our mesoscale DASH formation to a macroscale signal for detection, we found that DASH could be optically stained using 40nm gold nanoparticles (Figure 26). By flowing through DASH, nanoparticles bound to DNA via electrostatic interaction in order to form structures mimicking the pattern of DASH formation. This pattern was clearly visible using either a cell phone to detect the result or even with the naked eye. The end result was that a 50pM pathogen could be clearly detected with the naked eye making the DASH platform ideal for point-of-care applications.

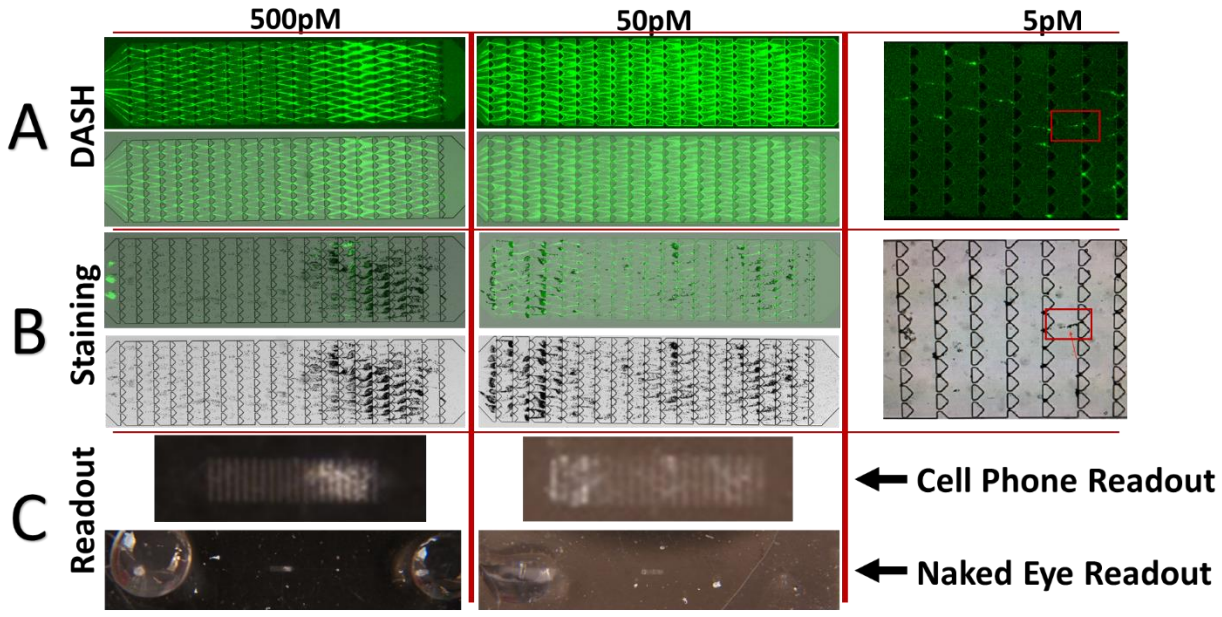

Figure 26. Proof of principle of naked eye detection using DASH staining. A: Typical DASH results for a 500pM, 50pM and 5pM target. B: A solution of 40nm gold nanoparticles was flowed through the DASH devices at .1ul per min post DASH formation in order to stain the DASH for cell phone and naked eye readouts. C: The resulting images are shown using a cell phone to magnify the image and the naked eye.

3.3 Chapter 3: Supplement

In order to quantify the ligation efficiency and compare a correct target to a slightly mismatched target, a correct target and a two base pair mismatched target were incubated for several hours in a solution of buffer, detection template and T4 DNA ligase. Following this, the sample was split and exonuclease I and III added to half the sample. The reaction was then incubated for several hours and analyzed using polyacrylamide gel electrophoresis (PAGE). Specifically, all samples were run out on a PAGE gel and the band pattern compared in order to analyze the effect of exonuclease digestion on the target-ligated template and the nontarget-ligated template. The correct target resulted in a band which was shifted downward due to digestion of the target and primer which were hybridized to the template pre-exo. In the case of the nontarget, there was no band present because the template was degraded due to the lack of any nontarget induced ligation. This would indicate that our system has high specificity for a correct target versus even a slightly mismatched version of the target.

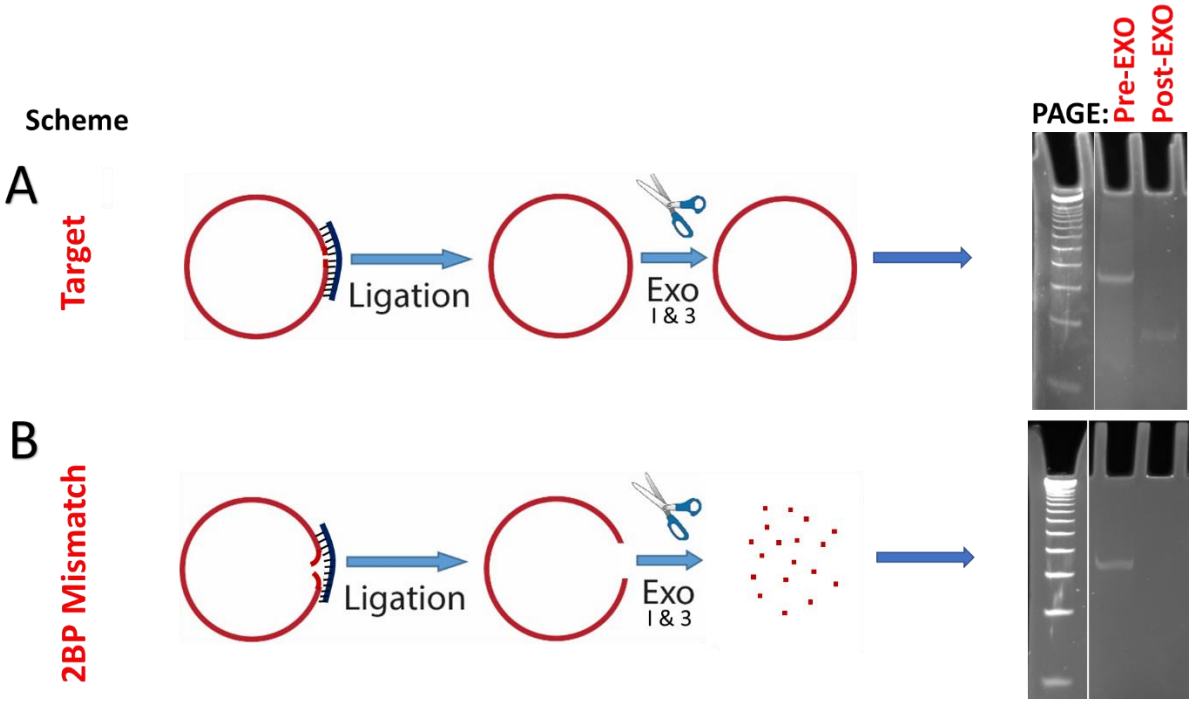

Figure 27. Scheme for quantifying ligation efficiency of a target versus nontarget.

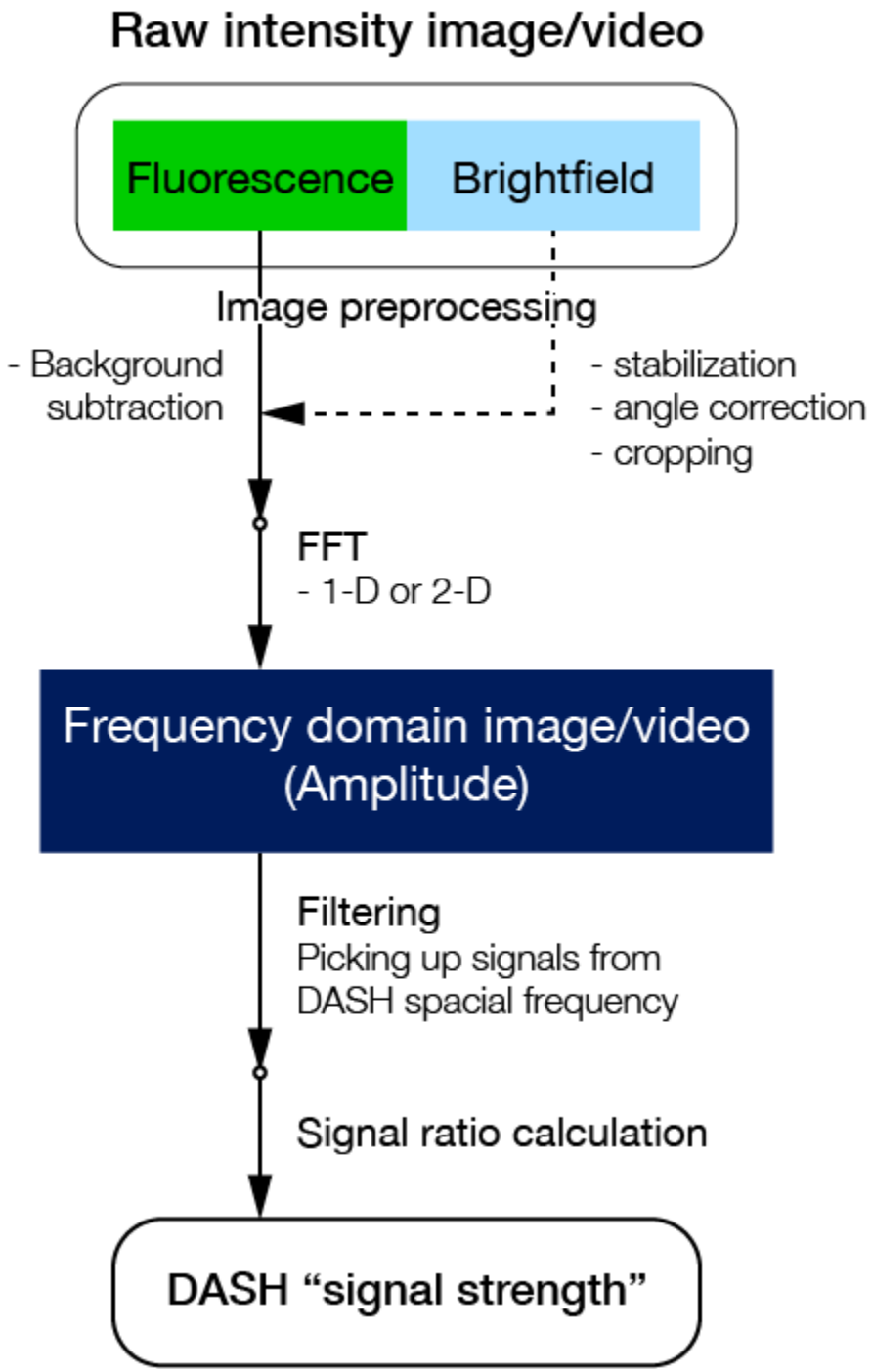

Figure 28. Quantitative analysis of DASH patterns and signal intensity.

In order to determine the absolute specificity limit of detection using the DASH platform, targets with a single base pair mismatch were studied for CMV and mtDNA (Figure 29).

For CMV, it was found that this detection method can reliably distinguish between the true target and even a single base mismatch. Unlike CMV though, a 1bp mismatched mtDNA target couldn't be as precisely distinguished. Of three samples, two made DASH due to nonspecific ligation. Thus, it was decided to complete the specificity study using a two base pair mismatch because all targets were distinguished from a two base mismatch (supplementary Figure 30). Furthermore, the difficulty with distinguishing a single base pair mismatch using a ligation-based approach is well known. T4 DNA ligase is considered highly effective for these kinds of ligation-based assays but it is also known to be promiscuous. This refers to the enzymes tendency to not differentiate well between a properly matched target and template and a 1bp mismatched target and template [70]. The result is that some single base pair mismatches can be distinguished and some can't be depending on where they occur and the identity of the base pair that is mismatched. For example: T4 DNA ligase has poor specificity for mismatches on the 5' phosphorylated side of the nicked template and for non A:G or G:A mismatches.

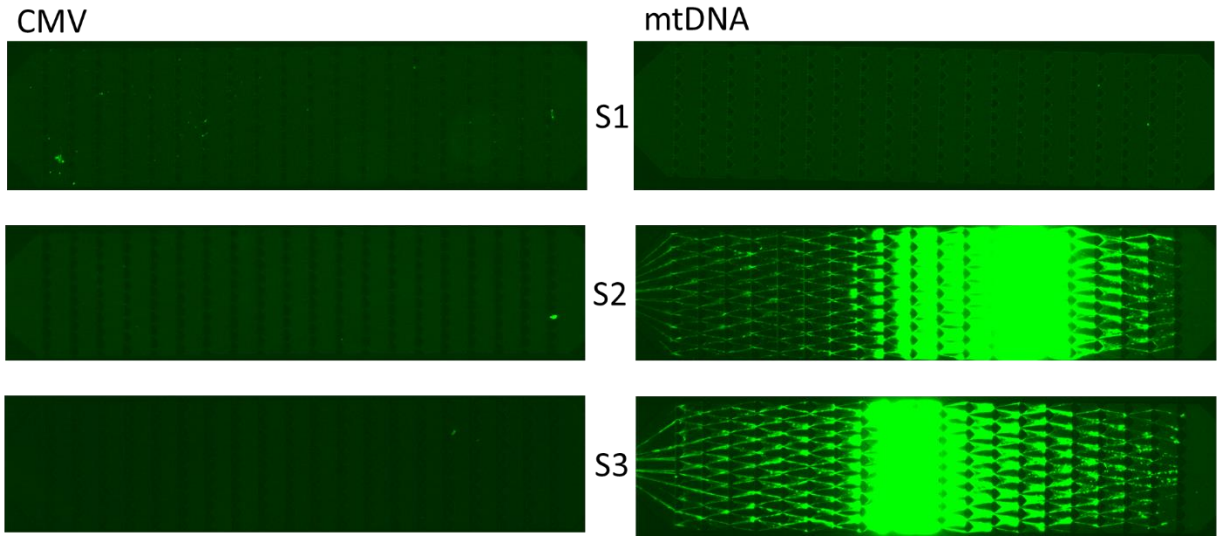

Figure 29. One base pair mismatched target results for CMV (A), and mtDNA (B).

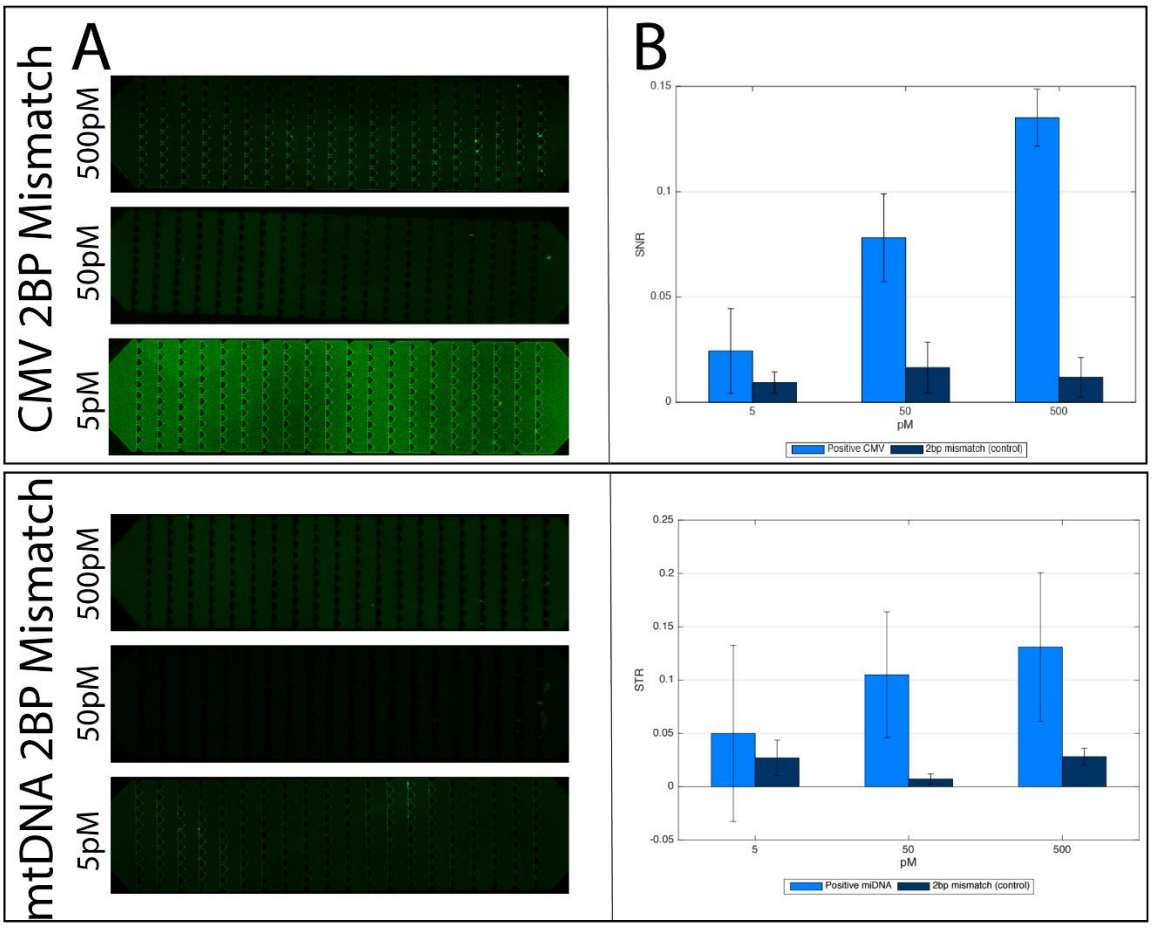

Figure 30. DASH results for two base pair mismatched targets of CMV and mtDNA (A). Signal to noise ratio calculated by the STR method (B). The data is of a triplicate data set for each concentration of the mismatched CMV and mtDNA targets. The resulting signal to noise data for the true targets are shown as a comparison.

As an alternative to staining by flowing through 40nm gold nanoparticles, we also investigated chemical-based staining of DASH for naked eye readout. Because DNA is highly negatively charged, there are a large number of optically colored chemicals which bind to DNA

through electrostatic interaction. One example which we discovered serendipitously was 3,3',5,5' tetramethylbenzidine diamine (TMB-diimine). TMB-diamine is a colored product which is used as a readout for detection HRP-activity using a TMB substrate. We found that TMB-diamine is highly charged and will bind to DNA electrostatically. Upon binding, it stains the DASH fibers blue allowing them to be seen with the naked eye as shown in Figure 31.

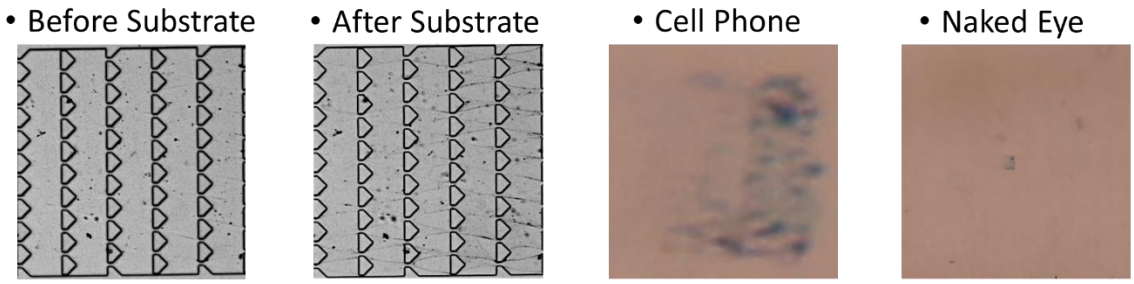

Figure 31. Proof-of-principle test for chemical staining of DASH using 3,3',5,5' tetramethylbenzidine diimine.

4 CHAPTER 4: BULK DNA METAMATERIAL HYDROGELS FOR THE NAKED EYE DETECTION OF PATHOGENS AND DIAGNOSTIC TARGETS

4.1 Introduction

DNA has become a useful material for a wide range of applications because of the molecule's unique biological role. Specifically, DNA plays a vital role as an information carrying molecule by encoding proteins and passing down protein-encoding information. This has resulted in the evolution of many enzymes that encode, retrieve or propagate this genetic information. These enzymes that act on DNA as a substrate have become essential tools for the engineering of DNA and have driven progress in applications such as expression profiling, genotyping, genetic prognostics, expression prognostics and the detection of infectious disease

[35-39]. For example, enzymes such as polymerases allow DNA to be amplified. This is essential to applications such as detection where the low signal associated with pathogens or diagnostic markers would otherwise be undetectable [71-73].

Despite the high fold amplification of these isothermal techniques, much of the prior literature has relied on some form of orthogonal signal amplification such as fluorescent staining in order to generate a sufficient output signal. It's only recently that the sophistication of DNA manipulation has reached the point where the degree of DNA amplification can directly produce bulk scale materials. For the first time, DNA can be treated as a generic material as well as a genetic one thus enabling new applications for DNA. For example, bulk DNA hydrogels have been used for applications such as supercapacitors[74], cell-free protein expression[56] and drug delivery[53, 75]. They have also been used to report or respond to physical stimuli such as pH[52], heat[76] and moisture[50]. Previously, our lab demonstrated the formation of a bulk DNA metamaterials which behave like a fluid when dry but like a hydrogel when hydrated [50]. This "Metagel" material was synthesized using isothermal RCA and exhibited unique properties not found in nature such as the ability to reassemble its original casted shape despite any deformation experienced.

Now that the synthesis and application of bulk DNA materials has become an attainable goal, we wish to investigate the material's potential for applications such as the Point-of-care (POC) detection. In recent years, POC detection has become a hot topic due to its potential to increase the access to, and efficiency of, sensing applications outside of traditional hospital and laboratory environments. This is important to resource limited settings such as the developing world [61-64] and to expanding access to diagnostic tests via enabling at-home testing [65-67].

The nature of limited resource settings dictates that POC detection methods be minimally complex, not rely on electricity-dependent conditions and utilize minimal or no equipment. Despite these strict constraints, POC devices have shown promise in numerous areas including agriculture for testing of crops and food supply, veterinary medicine such as the health of pets and livestock, public health and security such as for the monitoring of pandemics and bioterrorism, and environmental testing for air, water and soil contamination [63, 68, 69]. This is especially true in the case of POC methods utilizing naked eye detection. The use of naked eye readouts introduces trade-offs such as reduced quantitative capability or lower sensitivity but have near universal accessibility. A good example of this is the at-home pregnancy test and several approaches for the detection of nucleic acids. For example, sensitivity has been demonstrated to be as low as 10 attomolar in 30 minutes for an lateral flow assay [77] and zeptamole levels using directed particle aggregation [78].

In this chapter, we propose a method which utilizes advances in the formation of bulk DNA materials to allow for the naked eye detection of pathogens and diagnostic markers using direct and unambiguous observation of bulk DNA gel formation. We propose to do this by pathogen-triggered formation of bulk scale “Metagel” which can encode the identity of the pathogen by producing different shapes for different pathogens. This provides an unambiguous readout which can be read with the naked eye for POC applications. Though there has been some prior work by Lee et al. involving the formation of a microscale gel clog in a microfluidic device as a pathogen readout [79], we are not aware of anyone who has demonstrated sensitive pathogen detection using pathogen-triggered macro-scale gel formation as a readout.

4.2 Result and Discussion

4.2.1 Detection scheme

In order to synthesize macroscale DNA materials using a DNA target as a trigger, we used ligation to provide specificity, RCA to provide amplification and metagel's memory effect to provide a readout. Figure 32a shows our scheme. In it, a linear template for RCA can only be circularized if the correct target is present and hybridized to a template strand. Once circularized, the template can then be ligated and used for an RCA reaction. RCA provides the massive amplification needed to convert the DNA present from the nanoscale to the macroscale where the detection results can read with the naked eye. In order to multiplex this system, we used a unique property of the metagel platform which is its ability remember whatever it is casted in (Figure 32C).

4.2.2 Readout scheme

Specifically, the metagel platform produces macroscale DNA materials which can be grown or casted in a desired shape. This allows different targets of interest, such as pathogens, to produce different shaped DNA gels depending on their identity. This is done by adding templates which are specific for different pathogens into different shaped molds as shown in Figure 32b. By adding an aliquot of an unknown sample into each mold, only the DNA gel shape corresponding to the correct pathogen target will be synthesized. Metagel's unique metamaterial properties also allow the material to behave like a liquid when wet and a solid when placed in water. The liquid-like property allows the gel to be easily removed from the mold and placed into water. The water immediately-makes the gel behave like a solid and reassemble its casted shape so that the detection result can be read with the naked eye.

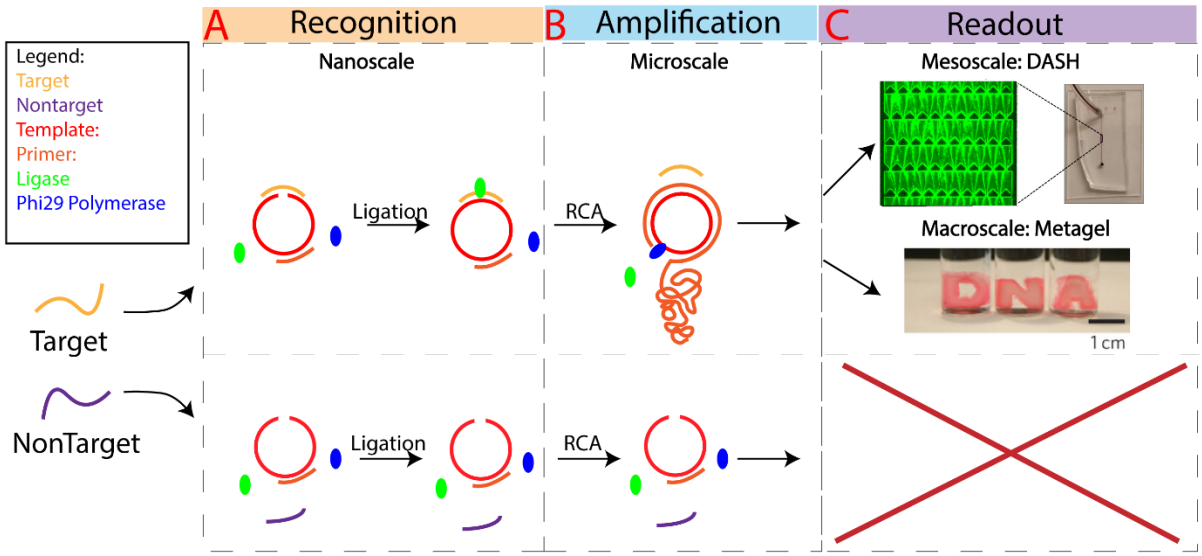

Figure 32. Schematic Illustration of Pathogen-induced macroscale DNA Formation. A: Recognition using ligation. B: Amplification using RCA. C: Naked eye/macroscale readout using a metamaterial that can remember its casted shape.

4.2.3 Detection Results

Ligation efficiency using polyacrylamide gel electrophoresis for CMV and mtDNA specificity

The specificity of our ligation reaction was tested using polyacrylamide gel electrophoresis (PAGE). Two model DNA targets, a cucumber mosaic virus (CMV) pathogen and a mtDNA diagnostic target, were tested and compared to a two base pair mismatched versions of each target. Successful ligation was confirmed by digesting the sample with exonuclease I and III to degrade any non-ligated DNA. The results for cmv and mtDNA showed that only the correct target had significant ligation (Figure 33a). Following digestion, the correct target had a band present which matched the location and intensity of the original template (lane 5). The nontarget however, had no band present (Lane 9).

4.2.4 Sensitivity and specificity results for macroscale DNA materials using CMV and mtDNA.

In order to determine sensitivity, target concentrations were tested from 500nM to 500pM. Specificity was tested at the same concentrations using a nontarget which was a two base pair mismatch of each target. The results for CMV and mtDNA can be seen in Figure 33b. To summarize, both model DNA targets could be clearly detected from 500nM to 500pM with the naked eye. The fluorescent images of the samples were shown in order to confirm the presence of the DNA gels using gelRed staining. The bright field images of all samples can be seen in the supplement. When a two base pair mismatch of each target was tested at the same concentrations, no macroscale DNA materials were produced and all samples were indistinguishable from water. In order to confirm that any macroscale DNA materials were a hydrogel by definition, rheology was performed on a representative sample and the results shown in supplementary Figure 40.

Because the naked eye readout of bulk DNA formation is a binary readout, similar to the pregnancy test, we did not ascertain any linear dynamic range. We expect that this platform will be most useful for applications in which detecting only a relevant threshold concentration is necessary. The high demonstrated sensitivity and specificity, combined with a naked eye readout make this metagel platform ideal for such applications which involve point of care.

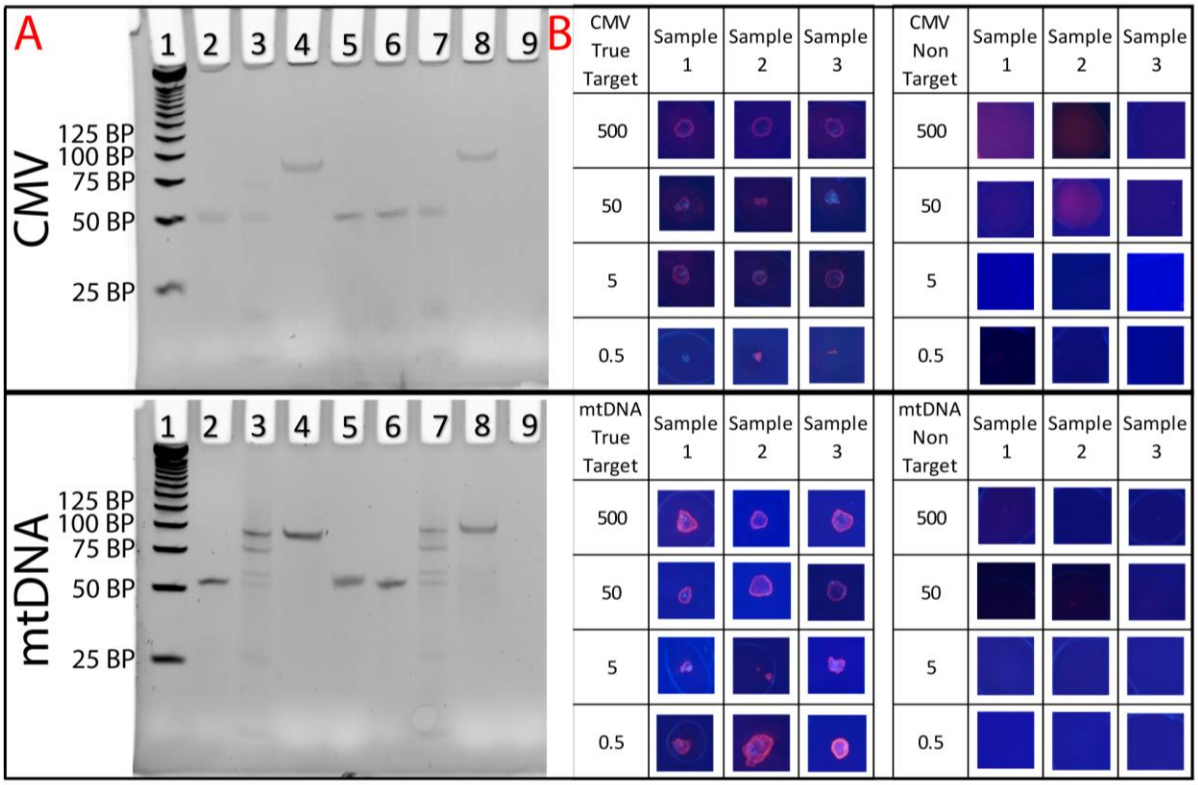

Figure 33. Detection results for two model targets, a cucumber mosaic virus (CMV) pathogen and a mtDNA diagnostic target. A: Ligation efficiency using polyacrylamide gel electrophoresis for CMV and mtDNA specificity. Lane 1: Ladder, Lane 2: Template, Lane 3: Primer, target, template, Lane 4: Primer, target, template (annealed and ligated), Lane 5: Primer, target, template (annealed, ligated, EXO digested), Lane 6: Template, Lane 7: Primer, 2BP mismatched target, template, Lane 8: Primer, 2BP mismatched target, template (annealed and ligated), Lane 9: Primer, 2BP mismatched target, template (annealed, ligated, EXO digested). B: Sensitivity and specificity results for CMV and mtDNA using the metagel platform to form macroscale DNA materials.

4.2.5 Feasibility of multiplexing: Combination results for macroscale DNA materials from CMV and mtDNA.

In order to evaluate the usefulness of this platform for multiplexing using shape-based encoding, a blind study was performed in which different or multiple targets were present in solution (Figure 34a). The result was that only the correct target matched with the correct template made a bulk DNA material. Furthermore, no interference or nonspecific response was detected from any pathogen being matched with the wrong template or multiple pathogens being matched with a single template. There was also no interference from any of the two base pair mismatched targets. Thus, the metagel platform performed well and seems promising for multiplexed detection due to its demonstrated specificity and robustness.

4.2.6 Feasibility of multiplexing: Shape based encoding

Two main strategies were discussed for integrating multiplexing into the metagel platform, shape-based encoding and position-based encoding of multiple targets. For shape-based encoding, metagels were either synthesized in a mold with a specific shape identifying the target being tested for, or synthesized and then placed in the same mold. If placed after being synthesized, metagels were frozen in order to program their shape to the shape of the mold according to scheme in Figure 43. The feasibility of shape-based encoding of different DNA targets was evaluated and the abbreviated results for all samples types shown in Figure 34b in order to demonstrate proof of principle.

Conceptually, shape-based encoding was successful though there was some variability in the gel shapes due to damage during the removal of the DNA material from the 3d printed cast in Figure 34b. Full results showing variability can be found in Figure 38 and Figure 39 of the

supplement. As a result of this variability a revised molding process was implemented by using smooth molds casted from pdms. The result was much cleaner shapes which demonstrated the potential for encoding large numbers of targets for multiplexed detection (Figure 35).

4.2.7 Feasibility of multiplexing: Position-based encoding for multiplexing

Positional-based encoding of different targets for multiplexing was also tested. Specifically, reaction wells were each assigned to test for a different target. This was done by adding the template specific to that target to the well so that macroscale DNA materials would be produced only if the assigned target was present. Correct and mismatched targets were then added in order to confirm proof of principle and the results shown in supplementary Figure 42. These results confirmed that the metagel platform can be multiplexed using position-based encoding for naked eye detection.

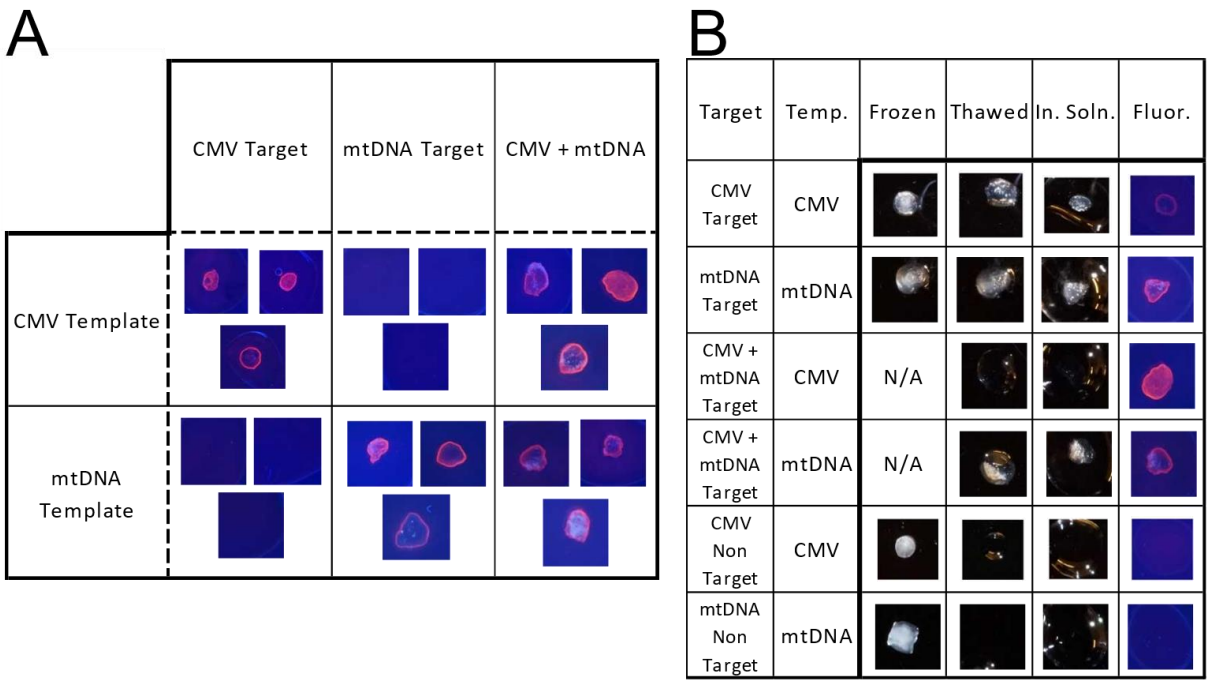

Figure 34. A: Combination sample results for proof of principle multiplexing using shape-based encoding. Macroscale DNA material results from CMV and mtDNA. B: Casting results using a 3d printed mold for proof-of-principle, multiplexed, shape-based encoding of detection. These are abbreviated results of the casting of macroscale DNA materials, photos of the full results can be found in the supplementary data.

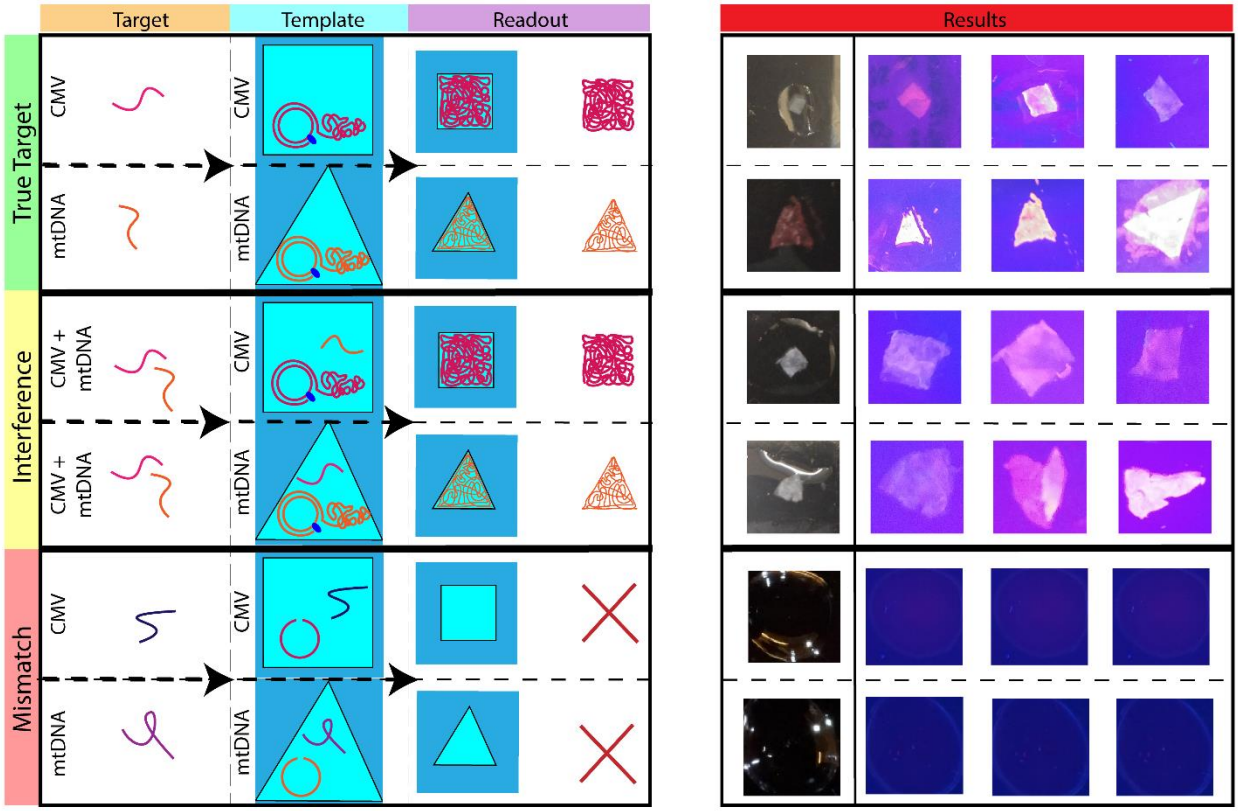

Figure 35. Proof-of-principle multiplexing using shape-based encoding with a smooth PDMS mold.

4.2.8 Properties of the Metagel

In a previous publication introducing the metagel platform, our group showed that metagels have a unique metamaterial-like property which causes them to behave like a liquid when dry and solid-like when in water. Figure 34b demonstrates this property. The third column

shows the gels frozen as soon as they are released from the mold. The fourth column shows the gels in a thawed state in air while the fifth and sixth columns shows the gels in a gelRed solution using bright field and fluorescence respectively. The metagels' liquid-like properties in air and solid-like properties in water were each confirmed using microaspiration testing (Figure 36). In it, metagels in water (shown in red) behaved like water (black) due to a lack of any asymmetric behavior during stretching. When the same metagels were placed in solution (blue), they showed highly asymmetric behavior and resisted stretching.

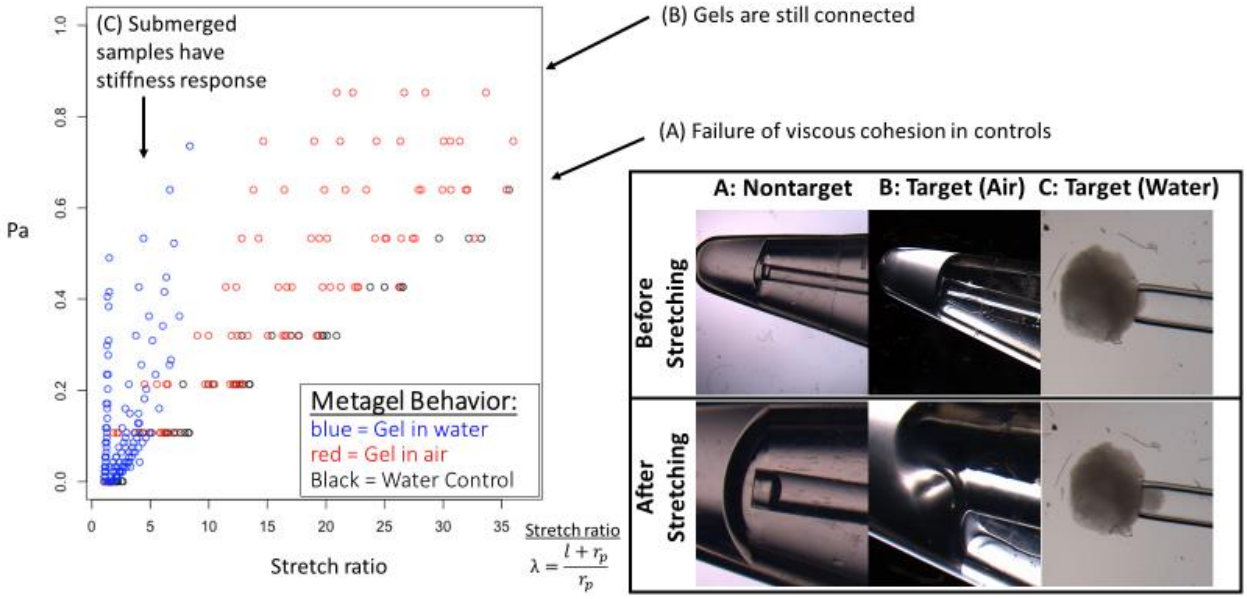

Figure 36. Metamaterial-like properties of metagels for detection. A: Target nontarget, water in air. B: target, nontarget, water in water.

4.3 Chapter 4 Supplement

In order to quantify the ligation efficiency and compare a correct target to a slightly mismatched target, a correct target and a two base pair mismatched target were incubated for several hours in a solution of buffer, detection template and T4 DNA ligase. Following this, the

sample was split and exonuclease I and III added to half the sample. The reaction was then incubated for several hours and analyzed using polyacrylamide gel electrophoresis (PAGE). Specifically, all samples were run out on a PAGE gel and the band pattern compared in order to analyze the effect of exonuclease digestion on the target-ligated template and the nontarget-ligated template. The correct target resulted in a band which was shifted downward due to digestion of the target and primer which were hybridized to the template pre-exo. In the case of the nontarget, there was no band present because the template was degraded due to the lack of any nontarget induced ligation. This would indicate that our system has high specificity for a correct target versus even a slightly mismatched version of the target.

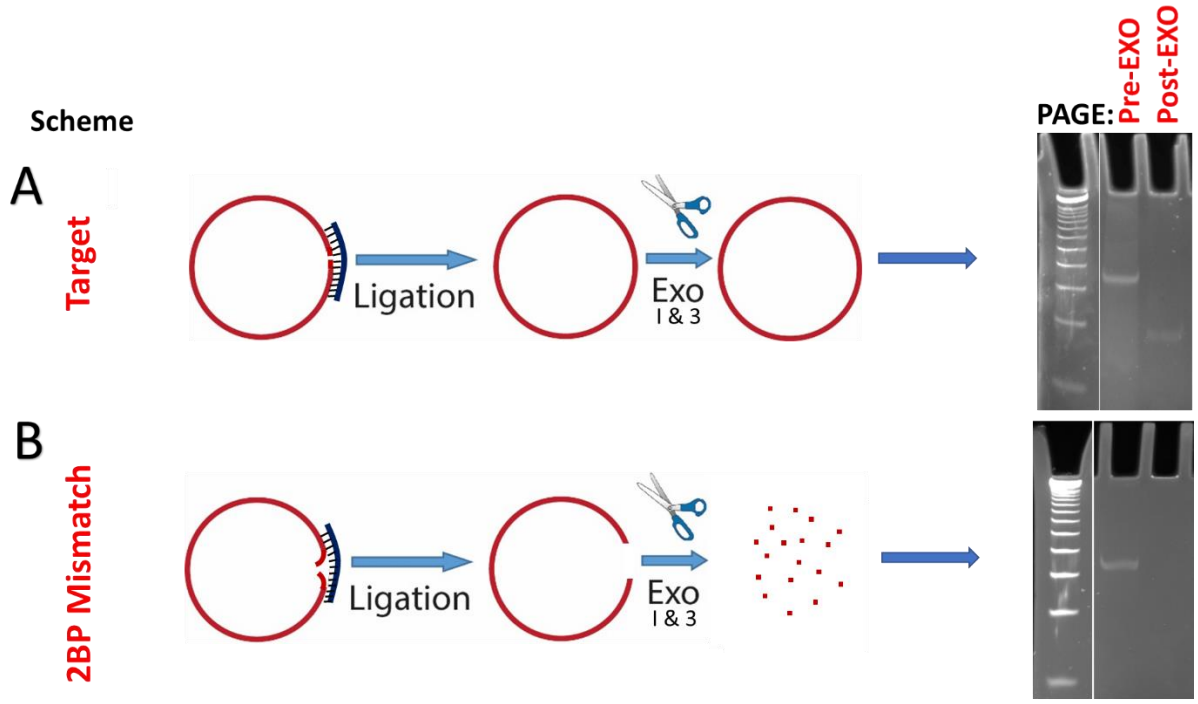

Figure 37. Scheme for quantifying ligation efficiency of a target versus nontarget.

CMV Target	Frozen	Thawed	In. Soln.	Fluor.
500				
500				
500				
50				
50				
50				
5				
5				
5				
0.5	N/A			
0.5				
0.5	N/A			

CMV Non Target	Frozen	Thawed	In. Soln.	Fluor.
500				
500				
500	N/A	N/A		
50				
50				
50				
5				
5				
5				
0.5				
0.5				
0.5				

mtDNA Target	Frozen	Thawed	In. Soln.	Fluor.
500				
500				
500				
50	N/A			
50	N/A			
50				
5	N/A			
5	N/A			
5				
0.5	N/A			
0.5	N/A			
0.5		N/A		

mtDNA Non Target	Frozen	Thawed	In. Soln.	Fluor.
500	N/A			
500				
500				
50				
50				
50	N/A			
5				
5				
5				
0.5				
0.5				
0.5				

Figure 38. Complete concentration range results for the detection of CMV and mtDNA using the metagel detection platform.

Target	Temp	Frozen	Thawed	In. Soln.	Fluor.
CMV	CMV				
CMV	CMV	N/A			
CMV	CMV				
mtDNA	mtDNA				
mtDNA	mtDNA	N/A			
mtDNA	mtDNA				

Target	Temp	Frozen	Thawed	In. Soln.	Fluor.
mtDNA	CMV				
mtDNA	CMV				
mtDNA	CMV				
CMV	mtDNA				
CMV	mtDNA	N/A			
CMV	mtDNA				

Target	Temp	Frozen	Thawed	In. Soln.	Fluor.
CMV + mtDNA	CMV				
CMV + mtDNA	CMV	N/A			
CMV + mtDNA	CMV				
CMV + mtDNA	mtDNA	N/A			
CMV + mtDNA	mtDNA				
CMV + mtDNA	mtDNA				

Figure 39. Complete combination results for the detection of CMV and mtDNA using the metagel platform.

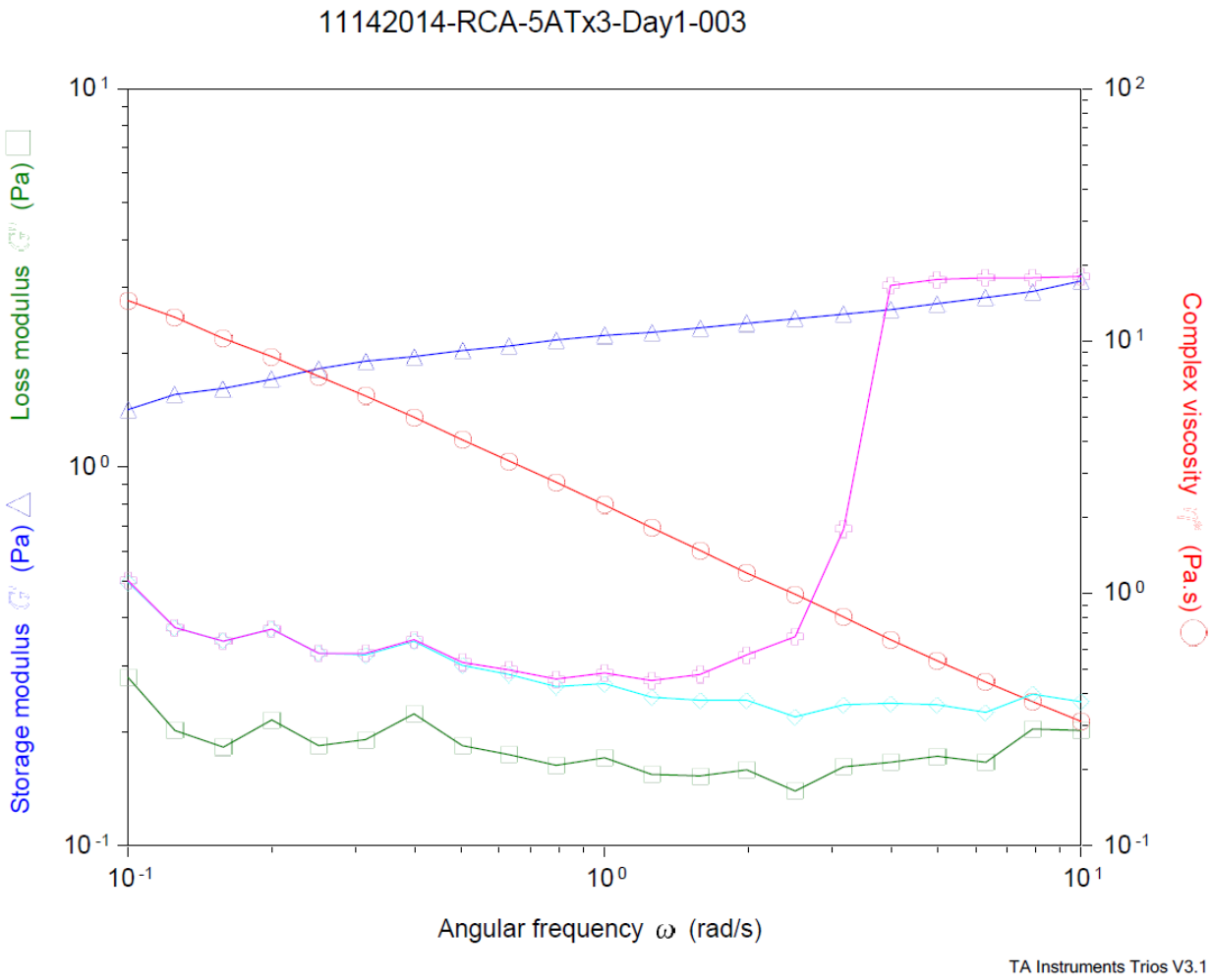

Figure 40. Rheology of macroscale DNA materials showing hydrogel-like behavior.

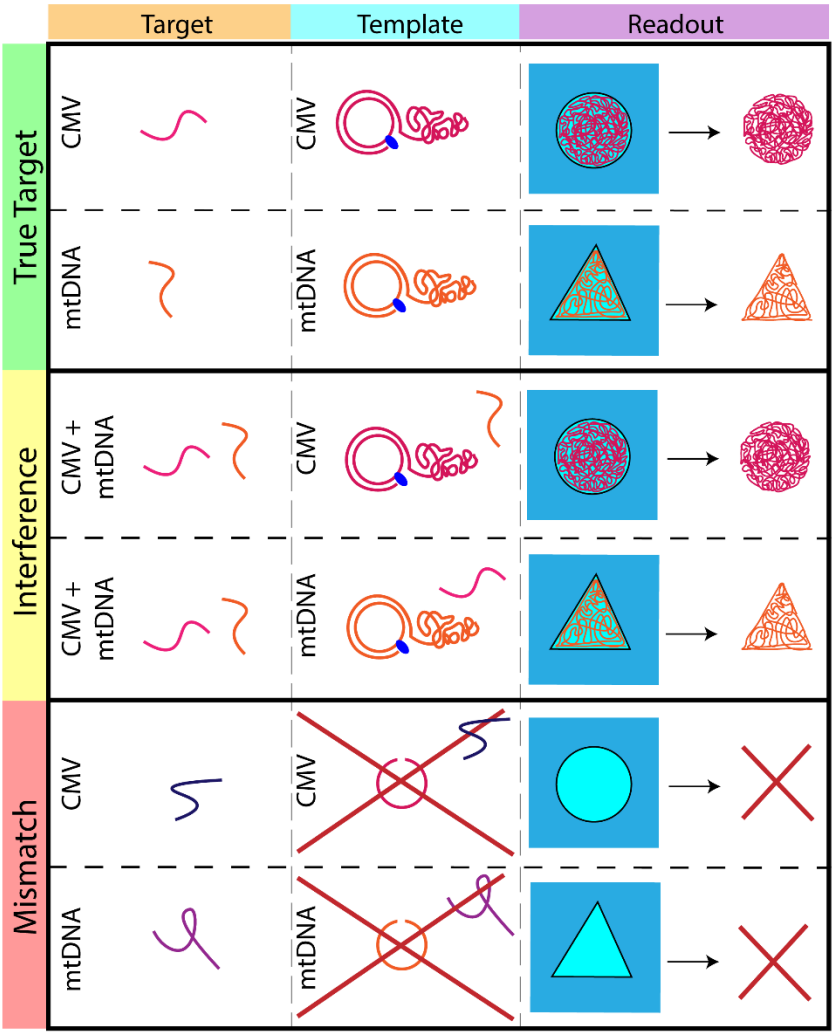

Figure 41. Schematic of shape-based encoding for metagel-based detection.

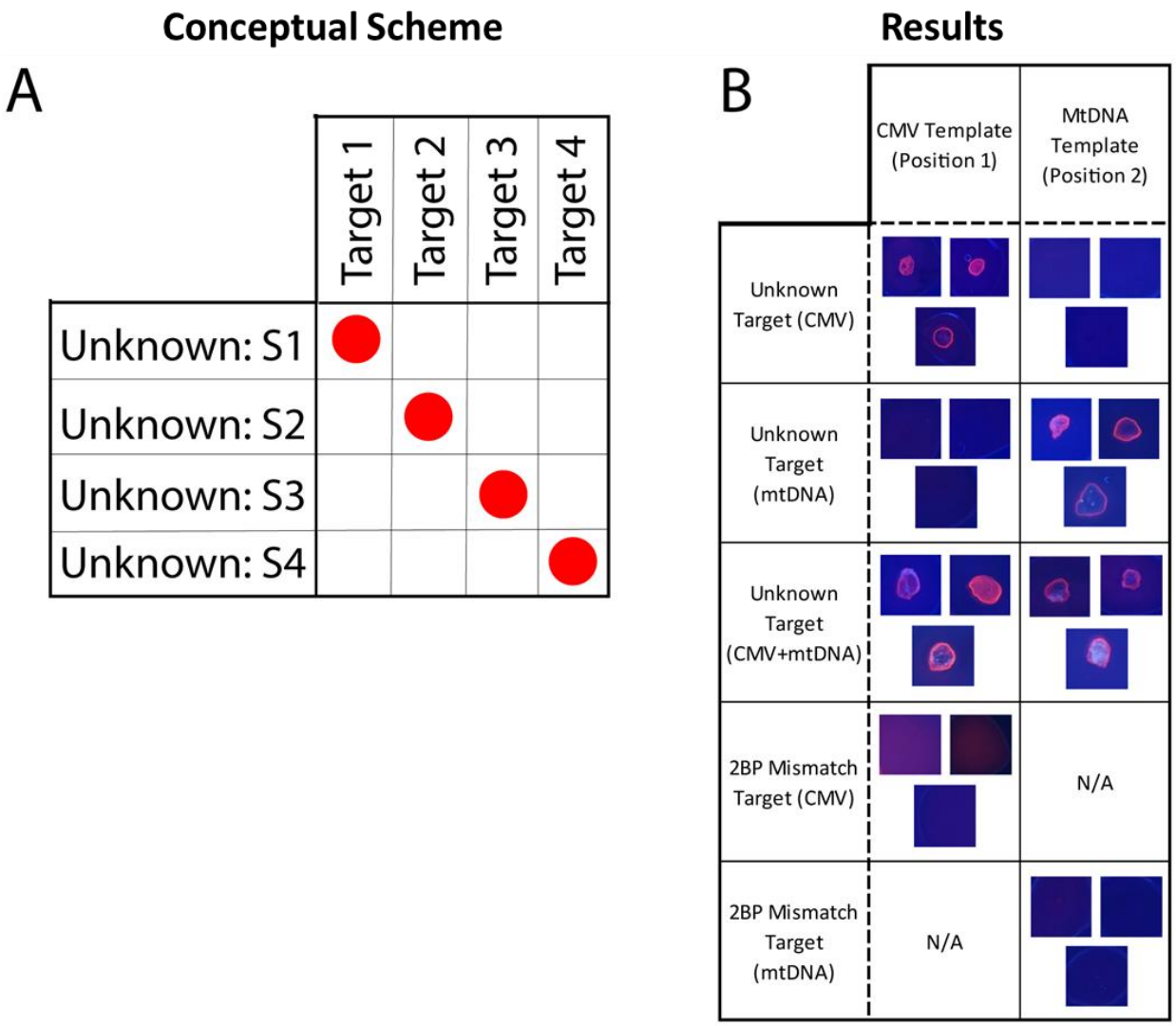

Figure 42. A: Conceptual scheme of shape-based encoding. B: Results for position-based encoding.

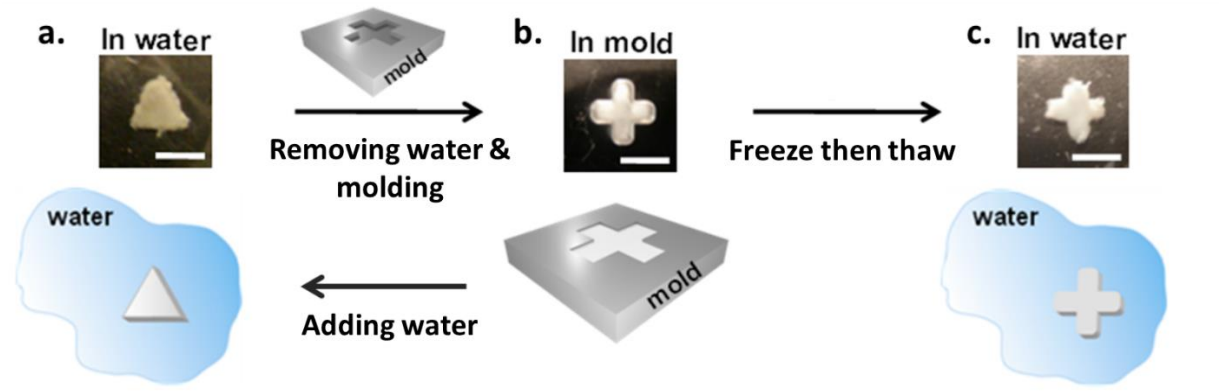

Figure 43. Conceptual scheme of cold-based casting of bulk DNA metagels. Gels are first synthesized in water (A), placed in a mold (B), then frozen (C). When removed from the mold, metagels will behave liquid-like when in air but will behave solid-like and assume their casted shape when placed in water.

5 CHAPTER 5: CONCLUSIONS AND FUTURE PERSPECTIVES

In the course of this dissertation, we have discussed the importance and potential of DNA as a generic material as opposed to a genetic one. We have also discussed existing ways of synthesizing meso and macroscale structures from DNA, examples in the literature of DNA materials which were synthesized by each method and which method appears to be the most feasible for creating DNA materials for real world applications.

We then discussed our work regarding the synthesis of DNA materials at the mesoscale using the DASH platform as well as demonstrated its applicability for applications including regenerating materials, cell-free protein expression, protein binding and activity and detection. In the course of this work, we showed that mesoscale materials can utilize the inherent properties of nanoscale DNA to create uniquely functional larger scale materials. By using DNA as a substrate for enzymes like phi29, we can synthesize large scale DNA materials cheaply, whether mesoscale DASH or macroscale metagel. For the first time, this makes DNA an affordable material for large scale applications. By using DNA as a subtrate for phi29 and dnase, we showed that we can generate and degenerate DASH in a cyclical and autonomous manner as a proof of concept experiment for regenerating materials. By using DNA as a template for the expression of proteins, we showed that we can produce proteins from larger scale materials.

This opens up a new class of materials which involve protein-producing materials, DNA-protein hybrid materials, or even self-modifying materials. In order to demonstrate the concept of hybrid materials with added functionality, we showed that proteins which could hypothetically be produced by DASH using cell-free protein expression, could be immobilized on DNA while preserving their activity.

Following this, we discussed the application of the DASH and metagel platforms for use in detection. We found that a ligation-based approach to target recognition was an effective way of distinguishing a true target from even highly similar targets such as a two base pair or one base pair mismatched target. It was also shown that this ligation reaction could easily be incorporated into our RCA-based approaches to making meso or macroscale materials so that these bulk materials would only be synthesized if the correct target was present. Because this effectively translates a nanoscale signal, the presence or absence of a target, to a macroscale readout, we found this method ideal for the naked eye-based detection of pathogens or diagnostic targets. This proved effective both at the mesoscale using nanoparticles to stain the DASH DNA fibers so that they could be seen with the naked eye and using macroscale bulk DNA hydrogels using the metagel platform. Lastly, we showed that the metagel platform in particular was ideal for multiplexed detection. We demonstrated successful implementation of both position-based encoding and shape based encoding using naked eye recognition.

So how do we expect this work to progress in the future? What is particularly important to keep in mind about this work is that all of the functionality we have demonstrated through various applications is not discrete. We have demonstrated that DASH at the mesoscale, and metagel at the macroscale, can utilize the unique properties of DNA whether for regeneration,

protein expression, hybrid materials or recognition of targets. All of these functionalities are not mutual exclusive thereby creating the potential for coupling these properties together to create new and interesting materials with emergent properties. It is our hope that we can continue this work to open new classes materials that can't be realized with any material other than DNA. Furthermore, we hope that we can continue to drive down the price of DNA so that bulk DNA materials can become widespread and open new large scale applications. With the development of RCA-based bulk DNA materials and their applications, we believe we have made substantial steps towards these goals.

6 METHODS

6.1 Chapter 2: DASH platform methods

6.1.1 Dash Generation and Degeneration.

Oligonucliotides and reagents. RepliPHI™ Phi29 DNA Polymerase, 10x Phi29 buffer (400mM Tris-HCl (pH 7.5), 500mM KCl, 100mM MgCl, 50mM $(NH_4)_sSO_4$ and 40mM DTT) and deoxynucleotides (dNTPs) were obtained from Epicenter. An alternative source of Phi29 DNA polymerase was also used from Thermo Scientific. If used, it was paired with its ideal 10x buffer which was 330mM, 100mM Mg-acetate, .1% Tween 20, and 10mM DTT. NEBuffer 3.1 (1M NaCl, 500mM Tris-HCl, 100mM $MgCl_2$, 1mg/ml bovine syrum albumin (pH 7.9)). DNASE I was obtained from New England Biolabs. Oligonucliotides were obtained from Integrated DNA Technologies (IDT) and purified using standard desalting. Polydimethylsiloxane (PDMS) was obtained from Sylgard/Elast kits which were manufactured by Krayden and purchased from Fisher. Nuclease free water was obtained from VWR.

Sequences. Primer T1C: GACCACCTTCGCGTCCAAAGC. Template T2: /5Phos/CGAAGGTGGTCTTTTTTTTTATATAGAATTCTATATATTTTTTTTGCTTTGGACG.

DASH Device Fabrication. All devices were designed using LayoutEditor and KLayout, and exported to GDSII format. (Data available upon request.) Chrome photomask fabrications were performed by an external vendor (Suzhou Mask-Fab Corp., China), except for the initial trials at Cornell NanoScale Science and Technology Facility (CNF) (Ithaca, NY) by following the standard protocols provided by the facility. In CNF, a Heidelberg DWL2000 was used for the mask writings and a Hamatech-Steag Mask Processor for the development and post treatment.

Glass wafers (diameter of 4 inches) were washed by water and then immersed into acetone with sonication for 5 min. They were then transferred into isopropanol for another 5 min with sonication. After that, the wafers were washed with deionized water and dried in a clean air flow. All glass wafers were then pretreated by hexamethyldisilazane before being treated by the photoresist coating AZ4620. The photoresist was dripped onto the wafer center and spun on spin-coater at 1000 rpm for 2 min to achieve a ~16 μm thickness. Following this, the wafers were baked on hot plate at 95 °C for 8 min and gradually cooled down to room temperature. The coated wafer was then exposed to UV light on a mask aligner (Karl Suss MA6) for 30s with a quartz mask and then placed into developer composed of az400K and deionized water with ratio of 1:3 for 2 min. The developed wafers were then rinsed with deionized water and dried by air blow. Finally, the wafers were baked on a hotplate at 100 °C for 30 min to improve photoresist adhesion.

Device casting. Glass wafers were placed on a petri dish (Greiner Bio-One, Austria), and secured to the dish by taping the four edges down. Microfluidic devices were then covered with a

polydimethylsiloxane (PDMS) silicone elastomer at Base : Curing Agent ratio of 10:1 (Sylgard 184, Dow Corning, Corning, NY). After baking at 70 °C for 1 hour, individual devices were cut out from the petri dish, and the inlet and outlet ports punched out using a press. Finally, devices were covalently bonded to PDMS-coated glass microscope slides (VWR, Radnor, PA) via oxygen plasma treatment.

Template preparation. Template was prepared mixing a 45uM solution of T2 template, and T1C primer in 1x Phi29 Buffer. The solution was then heated to 95°C and then cooled at 1°C per minute to anneal the template. 10 units of T4 DNA Ligase per ul of solution was then added along with 1.19mM ATP and the reaction left at 4°C overnight.

Amplification to generate DASH. Following ligation, 4mM of a mix of deoxynucleotides was added to the reaction along with a known concentration of ligated template, 5.7 units of Phi29 DNA polymerase per ul of solution and enough 100x Sybr Green 1 and Phi29 buffer for the solution to have a 1x concentration. The solution was then placed into a syringe and injected into a microfluidic device to form DASH at .1ul per min for 4 hours. While this occurred, the device was imaged using fluorescent microscopy with a 4x objective and an exposure of 100ms for bright field and 2000ms for the green fluorescent channel.

Amplification for autonomous DASH generation and degeneration.

In order to demonstrate the metabolic-like properties of DASH, three solutions were prepared. The first was a template + dNTP solution for DASH generation composed of a .47nM concentration of ligated T2 template, 2mM each of dNTPs, enough 100x SYBR Green 1 and 10x Phi29 buffer to reach a 1x solution concentration. The second solution was a template + Phi29

solution composed of .47nM T2 template, .18ug/ul of Phi29 DNA polymerase from Thermo Scientific and enough 100x SYBR Green 1 and 10x Phi29 buffer to reach a 1x solution concentration. The final solution for DASH generation was composed of a 1x solution of Phi29 buffer from Thermo Scientific and SYBR Green 1 as well as 2mM each of dNTPs and 1 unit/ul of DNASE I.

Once solutions were prepared, solution 1 and solution 2 were combined and flowed into the first inlet of a microfluidic DASH device at .1ul per minute. Solution 3 was flowed into a second inlet at the same rate. Alternatively, solutions 1 and 2 were each flowed into a microfluidic DASH device where they mixed and incubated for 2 hours before entering the DASH portion of the device. Once entering, they mixed with solution 3 which was injected into a third inlet. Regardless, the reaction was allowed to proceed for 12 hours.

6.1.2 Computational fluid dynamics (CFD) modeling

The Rhino model was exported as a STEP file in order to be imported in to the CFD software. For the fluid flowing through the DASH geometry, the default water profile was used for simplification. For the PDMS structures such as the channels and pillars, the following properties were used due to their similarity to the silicone rubber. Though these are approximate values and do not have exactly the same material properties as the experimental device, they were acceptable approximations. Water: Density 998.2 kg/m3, Viscosity 0.001003, Pa-s, Conductivity 0.6 W/m-K, Specific Heat 4182 J/kg-K, Bulk Modulus 2.18565e+09 Pa, Emissivity 1, Wall Roughness 0, b. Solid (Silicone Rubber), Density 1700 kg/m3, Transmissivity 0, Conductivity 0.7 W/m-K, Specific Heat 700 J/kg-K, Wall Roughness 0.

Simulations were run for a maximum of 500 iterations or until the result reached convergence. There were three methods of result visualization used for the simulations: heat maps, vector fields, and particle traces. Heat maps and vector fields were normalized between all results to maintain uniformity and were located at 8µm from the bottom of the volume (mid-point). The particle trace was done using particles of 13.8µm radius and a density of 1.34g/cm3. These particles were seeded at the inlet face of the geometry.

6.1.3 Confocal laser scanning microscopy

Confocal microscopy was performed using either a ZEISS LSM710 or an Olympus IX-81. Z-stacked videos were taken using a 10x objective due to the focal length using an excitation of 488nm and an emission of 520nm. The capture interval was set to 110 seconds and 30 layers were recorded. Each stack was composed of 30 layers.

6.1.4 Scanning Electron Microscopy (SEM)

SEM was performed after DASH formation. A 4% paraformaldehyde fixative (Electron Microscopy Science, Hatfield, PA) was flown into the device at 0.1 µL/min for 10 min. After performing fixation for 24 h at 4 ºC, the device was opened. DASH was found to be fixed on the PDMS substrate. After rinsing with nuclear-free water, DASH was dehydrated by immersing in a series of ethanol solutions (10%, 25%, 50%, 75%, 90% and 100%) followed by final immersion at 100% ethanol. DASH was then dried with critical point drying process (Baltec CPD 408) and examined with SEM (LEO 1550 FESEM).

6.1.5 Avidin-HRP Binding and Activity

Oligonucliotides and reagents. RepliPHI™ Phi29 DNA Polymerase, 10x Phi29 buffer (400mM Tris-HCl (pH 7.5), 500mM KCl, 100mM MgCl, 50mM $(NH_4)_sSO_4$ and 40mM DTT) and

deoxynucleotides (dNTPs) were obtained from Epicenter. NEBuffer 3.1 (1M NaCl, 500mM Tris-HCl, 100mM $MgCl_2$, 1mg/ml bovine syrum albumin (pH 7.9)), Nb.BsmI, Exonuclease I and III were obtained from New England Biolabs. Oligonucliotides were obtained from Integrated DNA Technologies (IDT) and purified using standard desalting. Polydimethylsiloxane (PDMS) was obtained from Sylgard/Elast kits which were manufactured by Krayden and purchased from Fisher. Nuclease free water was obtained from VWR. One-Step Ultra TMB-ELISA substrate, QuantaRed Enhanced Chemifluorescent HRP Substrate Kit and Hoechst 33342 were obtained from ThermoFisher.

Sequences. Primer T1C: GACCACCTTCGCGTCCAAAGC. Template T2: /5Phos/CGAAGGTGGTCTTTTTTTTTATATAGAATTCTATATATTTTTTTTGCTTTGGACG.

DASH Device Fabrication. See 6.1.1: DASH Device Fabrication.

Device casting. See 6.1.1: Device Casting.

Template preparation. Template was prepared mixing a 45uM solution of T2 template, and T1C primer in 1x Phi29 Buffer. The solution was then heated to 95°C and then cooled at 1°C per minute to anneal the template. 10 units of T4 DNA Ligase per ul of solution was then added along with 1.19mM ATP and the reaction left at 4°C overnight.

Amplification to form DASH. Following ligation, 4mM of a mix of deoxynucleotides was added to the reaction along with a known concentration of ligated template, 5.7 units of Phi29 DNA polymerase per ul of solution and enough 100x Sybr Green 1 and Phi29 buffer for the solution to have a 1x concentration. The solution was then placed into a syringe and injected into a microfluidic device to form DASH at .1ul per min for 4 hours. While this occurred, the device

was imaged using fluorescent microscopy with a 4x objective and an exposure of 100ms for bright field and 2000ms for the green fluorescent channel.

Binding of Avidin-HRP. Solutions of avidin-HRP were prepared in 1x phi29 buffer at concentrations ranging from 10ng/ml to 10ug/ml. 1x Sybr green was also added so that DASH DNA would be visible. The solution was then placed in a syringe and flowed through a DASH containing device at .1ul per min for 1 hr. Excess avidin-HRP was then washed off by flowing through a solution of 1x phi29 and sybr green at .1ul per min for 1 hr.

Quantification of Avidin-HRP Activity. Activity of avidin-HRP was quantified in-situ using quantaRed substrate solution. QuantaRed produces a red fluorescent product following catalyzation using HRP which allows for direct observation and localization of HRP activity using a fluorescent microscope. The QuantaRed substrate solution was used as is by loading into a syringe and flowing through a DASH bound avidin-HRP device at .1ul per min for 100 minutes. The solution was collected in order to quantify the red fluorescence on a fluorescent plate reader. A second method of verifying the activity of DASH bound avidin-HRP was used using One-Step Ultra TMB-ELISA substrate solution as a substrate. TMB substrate was flowed through a device as is at .1ul per min for 1 hr. The product of the TMB was found to directly stain DASH fibers due to the electrostatic interaction of negatively charged DNA and the positively charged TMB product.

6.1.6 DASH-based Protein Expression

Oligonucliotides and reagents. RepliPHI™ Phi29 DNA Polymerase, 10x Phi29 buffer (400mM Tris-HCl (pH 7.5), 500mM KCl, 100mM MgCl, 50mM $(NH_4)_sSO_4$ and 40mM DTT) and

deoxynucleotides (dNTPs) were obtained from Epicenter. NEBuffer 3.1 (1M NaCl, 500mM Tris-HCl, 100mM $MgCl_2$, 1mg/ml bovine syrum albumin (pH 7.9)), Nb.BsmI, Exonuclease I and III were obtained from New England Biolabs. Oligonucliotides were obtained from Integrated DNA Technologies (IDT) and purified using standard desalting. Polydimethylsiloxane (PDMS) was obtained from Sylgard/Elast kits which were manufactured by Krayden and purchased from Fisher. GelRed and Nuclease free water were obtained from VWR. Hoechst 33342 was obtained from ThermoFisher. Cell-free protein expression was conducted using the S30 T7 High-Yield Protein Expression System from Promega. 30k Amicon Ultra Centrifugal Filter Units were purchased from EMD Millipore.

Sequences. Amplification primer: caaaaaacccctcaagaccc, Protein expression primer: taatacgactcactataggg, Green fluorescent protein expression template:

agatcaaaggatcttcttgagatccttttttttctgcgcgtaatctgctgcttgcaaacaaaaaaaccaccgctaccagcggtggtttgtttgc

cggatcaagagctaccaactctttttccgaaggtaactggcttcagcagagcgcagataccaaatactgttcttctagtgtagccgtagtt

aggccaccacttcaagaactctgtagcaccgcctacatacctcgctctgctaatcctgttaccagtggctgctgccagtggcgataagtcg

tgtcttaccgggttggactcaagacgatagttaccggataaggcgcagcggtcgggctgaacgggggttcgtgcacacagcccagctt

ggagcgaacgacctacaccgaactgagatacctacagcgtgagctatgagaaagcgccacgcttcccgaagggagaaaggcggacag

gtatccggtaagcggcagggtcggaacaggagagcgcacgagggagcttccagggggaaacgcctggtatctttatagtcctgtcgggt

ttcgccacctctgacttgagcgtcgatttttgtgatgctcgtcaggggggcggagcctatggaaaaacgccagcaacgcgatcccgcgaa

attaatacgactcactatagggagaccacaacggtttccctctagaaataattttgtttaactttaagaaggagatatacatatgagcaaa

ggtgaagaactgtttaccggcgttgtgccgattctggtggaactggatggcgatgtgaacggtcacaaattcagcgtgcgtggtgaaggt

gaaggcgatgccacgattggcaaactgacgctgaaatttatctgcaccaccggcaaactgccggtgccgtggccgacgctggtgaccac

cctgacctatggcgttcagtgttttagtcgctatccggatcacatgaaacgtcacgatttctttaaatctgcaatgccggaaggctatgtgc

aggaacgtacgattagctttaaagatgatggcaaatataaaacgcgcgccgttgtgaaatttgaaggcgataccctggtgaaccgcattg

aactgaaaggcacggattttaaagaagatggcaatatcctgggccataaactggaatacaactttaatagccataatgtttatattacgg

cggataaacagaaaaatggcatcaaagcgaattttaccgttcgccataacgttgaagatggcagtgtgcagctggcagatcattatcag

cagaataccccgattggtgatggtccggtgctgctgccggataatcattatctgagcacgcagaccgttctgtctaaagatccgaacgaa

aaaggcacgcgggaccacatggttctgcacgaatatgtgaatgcggcaggtattacgctaggtgcggccgcagaacaaaaactcatctc

agaagaggatctgaatggggccgcactcgagggtggcgatcagaacgcgaccggcggtcatcaccatcatcaccattaagtcgaccgg

ctgctaacaaagcccgaaaggaagctgagttggctgctgccaccgctgagcaataactagcataaccccttggggcctctaaacgggtc

ttgaggggttttttgctgaaagccaattctgattagaaaaactcatcggcatcaaatgaaactgcaatttattcatatcaggattatcaata

ccatatttttgaaaaagccgtttctgtaatgaaggagaaaactcaccgaggcagttccataggatggcaagatcctggtatcggtctgcg

attccgactcgtccaacatcaatacaacctattaatttcccctcgtcaaaaataaggttatcaagtgagaaatcaccatgagtgacgactg

aatccggtgagaatggcaaaagcttatgcatttctttccagacttgttcaacaggccagccattacgctcgtcatcaaaatcactcgcatc

aaccaaaccgttattcattcgtgattgcgcctgagcgagacgaaatacgcgatcgctgttaaaaggacaattacaaacaggaatcgaat

gcaaccggcgcaggaacactgccagcgcatcaacaatattttcacctgaatcaggatattcttctaatacctggaatgctgttttcccggg

gatcgcagtggtgagtaaccatgcatcatcaggagtacggataaaatgcttgatggtcggaagaggcataaattccgtcagccagtttag

tctgaccatctcatctgtaacatcattggcaacgctacctttgccatgtttcagaaacaactctggcgcatcgggcttcccatacaatcgat

agattgtcgcacctgattgcccgacattatcgcgagcccatttatacccatataaatcagcatccatgttggaatttaatcgcggcttcgag

caagacgtttcccgttgaatatggctcataacacccttgtattactgtttatgtaagcagacagttttattgttcatgatgatatattttatc

ttgtgcaatgtaacatcagagattttgagacacaacgtg

DASH device fabrication. See 6.1.1: DASH Device Fabrication.

Device casting. See 6.1.1: Device Casting.

Template preparation. The expression template was prepared using a solution of 1x NEBuffer containing 100ng of double stranded expression plasmid per ul of solution and .25 units of Nb.BsmI per ul of solution. The solution was incubated at 65°C for 5 hours followed by an enzyme inactivation step at 80°C for 20 minutes and cooling to room temperature at 1°C per minute. .2 units of Exonuclease I per ul of solution and 1 unit of Exonuclease III per ul of solution were then added and the reaction incubated at 37°C for 5 hours. Exonuclease was inactivated at 80C for 20 minutes and the solution allowed to cool at 1°C per minute. The solution containing single stranded circular plasmid template was buffer exchanged using a 30k Amicon Ultra Spin Filter by placing the solution in the filter, adding 8ul of nuclease free water per ul of reaction solution and centrifugation at 10,000 Gs. The addition of water followed by centrifugation was repeated twice before collecting the template. In order to prepare the single stranded plasmid template for amplification, primer was annealed to the template in a 1:1 molar ratio. This was done by heating the solution to 95°C and cooling at 1°C per minute.

Amplification to form DASH. Following template preparation, 15 nM of the template was added to a solution containing an 8mM mix of deoxynucleotides, 4 units of Phi29 DNA polymerase per ul of solution, xxxx Hoechest, and enough 10x Phi29 buffer to make the final solution 1x. The solution was then placed in a syringe and injected into a microfluidic device at .1ul per minute until DASH formed. While injecting the solution, the device was imaged using fluorescent microscopy with a 4x objective and an exposure of 100ms for the bright field and 2000ms for the green fluorescent channel.

Cell-free protein expression.

After forming DASH using the expression template, a protein expression primer was flowed through the device at .1ul per minute for 60 minutes. This primer bound to any single stranded T7 promoters present on DASH in order to enable protein expression. Nuclease free water, NEB S30 Premix Plus and T7 S30 Extract were then mixed in a 2.4:4:3.6 ratio and infected into the microfluidic device at .1ul per min. In order to increase protein expression yields, the pump was programmed to pause every 20 minutes so that residence time could be increased. This allowed for higher yields so that green fluorescence from GFP could be observed in the microfluidic device.

Quantifying protein expression.

Green fluorescent protein was quantified by collecting all solution flowed through DASH and placing the solution in a Greiner Bio-one 96 well half volume plate. The solution was then measured at xxxxnm and xxxxnm using a xxxx fluorescent plate reader.

Equipment. Thermocycler: BioRad C1000 Touch, Fluorescent Microscope: Olympus BX61, xxxx fluorescent plate reader, 96 Well Half Volume Plates: Greiner Bio-One.

Provide a scheme for template preparation.

6.2 Chapter 3: DASH detection methods

6.2.1 DASH-based Detection

Oligonucliotides and reagents. RepliPHI™ Phi29 DNA Polymerase, 10x Phi29 buffer (400mM Tris-HCl (pH 7.5), 500mM KCl, 100mM MgCl, 50mM $(NH_4)_sSO_4$ and 40mM DTT) and deoxynucleotides (dNTPs) were obtained from Epicenter. DNA ligase and Exonuclease I and III were obtained from New England Biolabs. Oligonucliotides were obtained from Integrated DNA

Technologies (IDT) and purified using standard desalting. Polydimethylsiloxane (PDMS) was obtained from Sylgard/Elast kits which were manufactured by Krayden and purchased from Fisher. GelRed and Nuclease free water were obtained from VWR. SYBR Green I, 40% Acrylamide/Bis (19:1), ammonium persulfate and tetramethylethylene diamine (TEMED) were obtained from ThermoFisher.

Sequences. Synthetic CMV target sequence: CTGAGTGTGACCTAGGCCGGCATCATTGGATGC, Synthetic one base pair mismatched CMV non target: CTGAGTGTGACCTAGGCAGGCATCATTGGATGC, Synthetic two base pair mismatched non target sequence: CTGAGTGTGACCTAGGAAGGCATCATTGGATGC, CMV detection Template sequence: /5Phos/GCCTAGGTCACACTCAGTTTTTTTTCGGTGCGAGTTTACGCTCTACTTTTTTTTGCATCCAATGATGCCG, Amplification Primer sequence: GTAGAGCGTAAACTCGCACCG, mtDNA target sequence: ATTCTTCTTAGTAGCTATTACCTTCTTATTAT, mtDNA one base pair mismatched non target: ATTCTTCTTAGTAGCCATTACCTTCTTATTAT, mtDNA two base pair mismatched non target: ATTCTTCTTAGTAGCCTTTACCTTCTTATTAT, mtDNA detection template sequence: /5Phos/AGCTACTAAGAAGAATTTTTTTTTACGGTCCACAGAGCTGCCAACTTTTTTTTATAATAAGAAGGTAAT

DASH Device Fabrication. See 6.1.1: DASH Device Fabrication.

Device casting. See 6.1.1: Device Casting.

Target-dependent ligation. In order to detect cucumber mosaic virus (CMV) or mitochondrial DNA (mtDNA), synthetic CMV target or a two base pair mismatched non-target was added to a solution of detection template and amplification primer containing 1x phi29 buffer. Assembly of

the template, primer and synthetic target/non-target then occurred by heating the solution to 95C and then allowing to cool at 1°C per minute. 10 units of T4 DNA Ligase per ul of solution was then added along with 1.19mM ATP and the reaction left at 4°C overnight.

Ligation-dependent amplification (DASH). Following ligation, 4mM of a mix of deoxynucleotides was added to the reaction along with a known concentration of ligated detection template, 5.7 units of Phi29 DNA polymerase per ul of solution and enough 100x Sybr Green 1 and Phi29 buffer for the solution to have a 1x concentration. The solution was then placed into a syringe and injected into a microfluidic device for DASH at .1ul per min for 4 hours. While this occurred, the device was imaged using fluorescent microscopy with a 4x objective and an exposure of 100ms for bright field and 2000ms for the green fluorescent channel.

Determining ligation efficiency. Ligation efficiency was determined by taking the solution of synthetic target/non-target, amplification primer and ligated template and adding .5 units of Exonuclease I and 2.3 units of Exonuclease III per ul of solution. The solution was then incubated at 37°C for 2 hours followed by inactivation of Exonuclease by heating at 80°C for 20 minutes. The ligation efficiency was then evaluated by running the solution out on a gel using polyacrylamide gel electrophoresis and imaged with a Syngene gel imager. Band analysis of the sample versus a known standard was then used to calculate ligation efficiency by taking a rolling average of the gel background, subtracting the value from both bands and integrating the pixel intensity over the area of each band.

Polyacrylamide gel electrophoresis (PAGE). PAGE was conducted by loading samples on to a 10% gel of Acrylamide/Bis in a Biorad gel electrophoresis chamber. 50 volts was then applied for 70 minutes and the result gel post-stained for 30 minutes in a GelRed in an orbital shaker.

Equipment. Thermocycler: BioRad C1000 Touch, Fluorescent Microscope: Olympus BX61, Gel Imager: Syngene G:Box.

DASH Staining. DASH DNA fibers were either chemically stained with a solution of TMB diamine or with gold nanoparticles. For chemical staining, TMB diamine was prepared from a TMB HRP substrate kit by introducing HRP to the stock solution. The solution was then flowed through a DASH device containing DASH fibers. For nanoparticle staining, a suspension of 40nm fold nanoparticles was created in 1x PHI29 buffer. The solution was then flowed through a DASH device containing DASF Fibers at .1ul/min for 45 minutes or until stained.

6.3 Chapter 4: Metagel detection methods

6.3.1 Macroscale DNA formation using the metagel platform

Oligonucliotides and reagents. RepliPHI™ Phi29 DNA Polymerase, 10x Phi29 buffer (400mM Tris-HCl (pH 7.5), 500mM KCl, 100mM MgCl, 50mM $(NH_4)_sSO_4$ and 40mM DTT) and deoxynucleotides (dNTPs) were obtained from Epicenter. DNA ligase and Exonuclease I and III were obtained from New England Biolabs. Oligonucliotides were obtained from Integrated DNA Technologies (IDT) and purified using standard desalting. Polydimethylsiloxane (PDMS) was obtained from Sylgard/Elast kits which were manufactured by Krayden and purchased from Fisher. GelRed and Nuclease free water were obtained from VWR. SYBR Green I, 40%

Acrylamide/Bis (19:1), ammonium persulfate and tetramethylethylene diamine (TEMED) were obtained from ThermoFisher.

Sequences. Synthetic CMV target sequence: CTGAGTGTGACCTAGGCCGGCATCATTGGATGC, Synthetic two base pair mismatched non target sequence: CTGAGTGTGACCTAGGAAGGCATCATTGGATGC, CMV detection Template sequence: GCCTAGGTCACACTCAGTTTTTTTTCGGTGCGAGTTTACGCTCTACTTTTTTTTGCATCCAATGATGCCG, Amplification Primer sequence: GTAGAGCGTAAACTCGCACCG. , mtDNA target sequence: ATTCTTCTTAGTAGCTATTACCTTCTTATTAT, mtDNA two base pair mismatched non target: ATTCTTCTTAGTAGCCTTTACCTTCTTATTAT, mtDNA detection template sequence: /5Phos/AGCTACTAAGAAGAATTTTTTTTTACGGTCCACAGAGCTGCCAACTTTTTTTTATAATAAGAAGG TAAT

Target-dependent ligation. In order to detect cucumber mosaic virus (CMV) or mitochondrial DNA (mtDNA), synthetic CMV target or a two base pair mismatched non-target was added to a solution of detection template and amplification primer containing 1x phi29 buffer. Assembly of the template, primer and synthetic target/non-target then occurred by heating the solution to 95C and then allowing to cool at 1°C per minute. 10 units of T4 DNA Ligase per ul of solution was then added along with 1.19mM ATP and the reaction left at 4°C overnight.

Ligation-dependent amplification (metagel). Following ligation, 4mM of a mix of deoxynucleotides was added to the reaction along with a known concentration of ligated detection template, 5.7 units of Phi29 DNA polymerase per ul of solution and enough 100x Sybr

Green 1 and Phi29 buffer for the solution to have a 1x concentration. The solution was then placed into a tube and allowed to incubate at 30C for 24 hours at 900 RPM.

Determining ligation efficiency. Ligation efficiency was determined by taking the solution of synthetic target/non-target, amplification primer and ligated template and adding .5 units of Exonuclease I and 2.3 units of Exonuclease III per ul of solution. The solution was then incubated at 37°C for 2 hours followed by inactivation of Exonuclease by heating at 80°C for 20 minutes. The ligation efficiency was then evaluated by running the solution out on a gel using polyacrylamide gel electrophoresis and imaged with a Syngene gel imager. Band analysis of the sample versus a known standard was then used to calculate ligation efficiency by taking a rolling average of the gel background, subtracting the value from both bands and integrating the pixel intensity over the area of each band.

Polyacrylamide gel electrophoresis (PAGE). PAGE was conducted by loading samples on to a 10% gel of Acrylamide/Bis in a Biorad gel electrophoresis chamber. 50 volts was then applied for 70 minutes and the result gel post-stained for 30 minutes in a GelRed in an orbital shaker.

Equipment. Thermocycler: BioRad C1000 Touch, Fluorescent Microscope: Olympus BX61, Gel Imager: Syngene G:Box.

6.3.2 Rheology

.Viscoelasticity of RCA-based DNA hydrogels were characterized by oscillatory shear measurements using TA Instruments Discovery DHR-3. RCA gels with a template concentration of 100nM were tested after 48hr of growth time. Total 200µL of gel were applied to the sample

holder with sandblasted plate and 25mm 2 deg. cone-shaft, and oscillated using logarithmic sweep with 0.75% strain from 0.1 to 10 rad/s (10 points per decade).

6.3.3 Microaspiration

Non-hydrated true target gels, off target controls, and water controls were placed at the bottom of a 0.5mL tube. A glass capillary micropipette (ID 0.75 mm) was placed on the sample surface. Hydrated true target gels were tested in a 60mm dish in 1x reliphi buffer. Pressure was incrementally applied via silicone tubing and calibrated by manometer. The pressure source was a 20 mL pipetter calibrated with a custom manometer. Previous The tubing was filled with reliphi buffer and an air gap was present to prevent hydration of samples. The lowest pressure that ensured stable contact with the micropipette was taken as zero pressure. Pressure loads were incremented uniformly, and aspirated length was observed at each increment using a Zeiss Discovery v20 stereo microscope (Spectra Services, Inc.) at 7.5x magnification. The aspirated length was measured using calibrated images in NIH ImageJ. An experimental stretch ratio, k 5 (L 1 rp)/rp was defined by normalizing the aspirated length to the pipette radius as previously described [80].

7 REFERENCES

1. Crick, F., *Central Dogma of Molecular Biology.* Nature, 1970. **227**(5258): p. 561-563.
2. Meyer, M., et al., *A mitochondrial genome sequence of a hominin from Sima de los Huesos.* Nature, 2014. **505**(7483): p. 403-406.
3. Peng, S.M., et al., *From cells to DNA materials.* Mater. Today, 2012. **15**: p. 190.

4. Roh, Y.H., et al., *Engineering DNA-based functional materials.* Chemical Society Reviews, 2011. **40**(12): p. 5730-5744.

5. Luo, D., *The road from biology to materials.* Mater. Today, 2003. **6**: p. 38.

6. Roberts, R.J., et al., *REBASE--enzymes and genes for DNA restriction and modification.* Nucleic Acids Res, 2007. **35**(Database issue): p. D269-70.

7. Roberts, R.J., et al., *REBASE--a database for DNA restriction and modification: enzymes, genes and genomes.* Nucleic Acids Res, 2015. **43**(Database issue): p. D298-9.

8. Caruthers, M.H., *Gene synthesis machines: DNA chemistry and its uses.* Science, 1985. **230**(4723): p. 281-5.

9. Kosuri, S. and G.M. Church, *Large-scale de novo DNA synthesis: technologies and applications.* Nat Meth, 2014. **11**(5): p. 499-507.

10. Dormitzer, P.R., et al., *Synthetic generation of influenza vaccine viruses for rapid response to pandemics.* Sci Transl Med, 2013. **5**(185): p. 185ra68.

11. Sano, T., C.L. Smith, and C.R. Cantor, *Immuno-PCR: very sensitive antigen detection by means of specific antibody-DNA conjugates.* Science, 1992. **258**(5079): p. 120-2.

12. Niemeyer, C.M. and R. Wacker, *Combination of DNA-directed immobilization and immuno-PCR: very sensitive antigen detection by means of self-assembled DNA–protein conjugates.* 2003. **31**(16): p. e90.

13. Wilner, O.I., et al., *Enzyme cascades activated on topologically programmed DNA scaffolds.* Nat Nano, 2009. **4**(4): p. 249-254.

14. Bailey, R.C., et al., *DNA-Encoded Antibody Libraries: A Unified Platform for Multiplexed Cell Sorting and Detection of Genes and Proteins.* Journal of the American Chemical Society, 2007. **129**(7): p. 1959-1967.

15. Niemeyer, C.M., *The developments of semisynthetic DNA-protein conjugates.* Trends Biotechnol, 2002. **20**(9): p. 395-401.

16. Niemeyer, C.M., *Functional devices from DNA and proteins.* Nano Today, 2007. **2**(2): p. 42-52.

17. Niemeyer, C.M., *Semisynthetic DNA-protein conjugates for biosensing and nanofabrication.* Angew Chem Int Ed Engl, 2010. **49**(7): p. 1200-16.

18. Kwong, G.A., et al., *Modular Nucleic Acid Assembled p/MHC Microarrays for Multiplexed Sorting of Antigen-Specific T Cells.* Journal of the American Chemical Society, 2009. **131**(28): p. 9695-9703.

19. Cheng, W.L., et al., *Nanopatterning self-assembled nanoparticle superlattices by moulding microdroplets.* Nat. Nanotechnol., 2008. **3**: p. 682.

20. Cheng, W.L., et al., *Free-standing nanoparticle superlattice sheets controlled by DNA.* Nat. Mater., 2009. **8**: p. 519.

21. Tan, S.J., et al., *Building plasmonic nanostructures with DNA.* Nat Nano, 2011. **6**(5): p. 268-276.

22. Mirkin, C.A., et al., *A DNA-based method for rationally assembling nanoparticles into macroscopic materials.* Nature, 1996. **382**(6592): p. 607-609.

23. Alivisatos, A.P., et al., *Organization of 'nanocrystal molecules' using DNA.* Nature, 1996. **382**(6592): p. 609-611.

24. Park, S.Y., et al., *DNA-programmable nanoparticle crystallization.* Nature, 2008. **451**(7178): p. 553-556.

25. Elghanian, R., et al., *Selective Colorimetric Detection of Polynucleotides Based on the Distance-Dependent Optical Properties of Gold Nanoparticles.* Science, 1997. **277**(5329): p. 1078-1081.

26. Nykypanchuk, D., et al., *DNA-guided crystallization of colloidal nanoparticles.* Nature, 2008. **451**(7178): p. 549-552.

27. Alemdaroglu, F.E., et al., *Enzymatic Control of the Size of DNA Block Copolymer Nanoparticles.* Angewandte Chemie International Edition, 2008. **47**(5): p. 974-976.

28. Gibbs, J.M., et al., *Polymer–DNA Hybrids as Electrochemical Probes for the Detection of DNA.* Journal of the American Chemical Society, 2005. **127**(4): p. 1170-1178.

29. Immoos, C.E., S.J. Lee, and M.W. Grinstaff, *DNA-PEG-DNA Triblock Macromolecules for Reagentless DNA Detection.* Journal of the American Chemical Society, 2004. **126**(35): p. 10814-10815.

30. Kwak, M. and A. Herrmann, *Nucleic Acid/Organic Polymer Hybrid Materials: Synthesis, Superstructures, and Applications.* Angewandte Chemie International Edition, 2010. **49**(46): p. 8574-8587.

31. Safak, M., et al., *Polymerase Chain Reaction as an Efficient Tool for the Preparation of Block Copolymers.* Advanced Materials, 2007. **19**(11): p. 1499-1505.

32. Watson, K.J., et al., *DNA−Block Copolymer Conjugates.* Journal of the American Chemical Society, 2001. **123**(23): p. 5592-5593.

33. Annaluru, N., et al., *Total Synthesis of a Functional Designer Eukaryotic Chromosome.* Science, 2014. **344**(6179): p. 55.

34. Human Genome Sequencing, C., *Finishing the euchromatic sequence of the human genome.* Nature, 2004. **431**(7011): p. 931-945.

35. Huggett, J., C. Green, and A. Zumla, *Nucleic acid detection and quantification in the developing world.* Biochem Soc Trans, 2009. **37**(Pt 2): p. 419-23.

36. O'Connor, L. and B. Glynn, *Recent advances in the development of nucleic acid diagnostics.* Expert Rev Med Devices, 2010. **7**(4): p. 529-39.

37. Weile, J. and C. Knabbe, *Current applications and future trends of molecular diagnostics in clinical bacteriology.* Anal Bioanal Chem, 2009. **394**(3): p. 731-42.

38. Muldrew, K.L., *Molecular diagnostics of infectious diseases.* Curr Opin Pediatr, 2009. **21**(1): p. 102-11.

39. Stramer, S.L., et al., *Nucleic acid testing to detect HBV infection in blood donors.* N Engl J Med, 2011. **364**(3): p. 236-47.

40. Peng, S., *Synthesis and Chracterization of a Physically Entangled DNA Hydrogel and its Applications.* 2014.

41. Wikipedia. *"DNA --- Wikipedia{,} The Free Encyclopedia"*. 2017 [cited 2017 28-March-2017]; Available from: https://en.wikipedia.org/w/index.php?title=DNA&oldid=771879492.

42. Abdul-Ghani, R., A.M. Al-Mekhlafi, and P. Karanis, *Loop-mediated isothermal amplification (LAMP) for malarial parasites of humans: would it come to clinical reality as a point-of-care test?* Acta Trop, 2012. **122**(3): p. 233-40.

43. Lucchi, N.W., et al., *Real-time fluorescence loop mediated isothermal amplification for the diagnosis of malaria.* PLoS One, 2010. **5**(10): p. e13733.

44. Sun, B., et al., *Mechanistic Evaluation of the Pros and Cons of Digital RT-LAMP for HIV-1 Viral Load Quantification on a Microfluidic Device and Improved Efficiency via a Two-Step Digital Protocol.* Analytical Chemistry, 2013. **85**(3): p. 1540-1546.

45. Zhao, X. and T. Dong, *Multifunctional Sample Preparation Kit and On-Chip Quantitative Nucleic Acid Sequence-Based Amplification Tests for Microbial Detection.* Analytical Chemistry, 2012. **84**(20): p. 8541-8548.

46. Schmidt, T.L., et al., *Scalable amplification of strand subsets from chip-synthesized oligonucleotide libraries.* Nature Communications, 2015. **6**: p. 8634.

47. Blanco, L., et al., *Highly efficient DNA synthesis by the phage phi 29 DNA polymerase. Symmetrical mode of DNA replication.* Journal of Biological Chemistry, 1989. **264**(15): p. 8935-8940.

48. *Molecular Facts and Figures.* 2011: p. 9.

49. Hollis, F. *How Small Can the Naked Eye See*. 2016 [cited 2017 5/2/2017]; Available from: http://www.sciencefocus.com/qa/how-small-can-naked-eye-see.

50. Lee, J.B., et al., *A mechanical metamaterial made from a DNA hydrogel.* Nat Nano, 2012. **7**(12): p. 816-820.

51. Um, S.H., et al., *Enzyme-catalysed assembly of DNA hydrogel.* Nat Mater, 2006. **5**(10): p. 797-801.

52. Cheng, E., et al., *A pH-Triggered, Fast-Responding DNA Hydrogel.* Angewandte Chemie, 2009. **121**(41): p. 7796-7799.

53. Roh, Y.H., et al., *DNAsomes: Multifunctional DNA-based nanocarriers.* Small, 2011. **7**: p. 74.

54. Um, S.H., et al., *Enzyme-catalysed assembly of DNA hydrogel.* Nat. Mater., 2006. **5**: p. 797.

55. Park, N., et al., *A cell-free protein-producing gel.* Nat Mater, 2009. **8**(5): p. 432-437.

56. Park, N., et al., *High-yield cell-free protein production from P-gel.* Nat. Protoc., 2009. **4**: p. 1759.

57. Hur, J., et al., *DNA hydrogel-based supercapacitors operating in physiological fluids.* Sci. Rep., 2013. **3**: p. 1282.

58. Xing, Y.Z., et al., *Self-assembled DNA hydrogels with designable thermal and enzymatic responsiveness.* Adv. Mater., 2011. **23**: p. 1117.

59. Liedl, T., et al., *Controlled Trapping and Release of Quantum Dots in a DNA-Switchable Hydrogel.* Small, 2007. **3**(10): p. 1688-1693.

60. Lee, J.B., et al., *A mechanical metamaterial made from a DNA hydrogel.* Nat. Nanotechnol., 2012. **7**: p. 816.

61. Urdea, M., et al., *Requirements for high impact diagnostics in the developing world.* Nature, 2006. **444 Suppl 1**: p. 73-9.

62. Yager, P., et al., *Microfluidic diagnostic technologies for global public health.* Nature, 2006. **442**(7101): p. 412-8.

63. Kulinsky, L., Z. Noroozi, and M. Madou, *Present technology and future trends in point-of-care microfluidic diagnostics.* Methods Mol Biol, 2013. **949**: p. 3-23.

64. Hartman, M.R., et al., *Point-of-care nucleic acid detection using nanotechnology.* Nanoscale, 2013. **5**(21): p. 10141-10154.

65. Lee, T., *Over-the-Counter Biosensors: Past, Present, and Future.* Sensors, 2008. **8**(9): p. 5535.

66. Lee-Lewandrowski, E. and K. Lewandrowski, *Perspectives on Cost and Outcomes for Point-of-Care Testing.* Clinics in Laboratory Medicine, 2009. **29**(3): p. 479-489.

67. Chin, C.D., V. Linder, and S.K. Sia, *Commercialization of microfluidic point-of-care diagnostic devices.* Lab Chip, 2012. **12**(12): p. 2118-34.

68. Ngom, B., et al., *Development and application of lateral flow test strip technology for detection of infectious agents and chemical contaminants: a review.* Anal Bioanal Chem, 2010. **397**(3): p. 1113-35.

69. Gubala, V., et al., *Point of care diagnostics: status and future.* Anal Chem, 2012. **84**(2): p. 487-515.

70. Lohman, Gregory J.S., et al., *A high-throughput assay for the comprehensive profiling of DNA ligase fidelity.* Nucleic Acids Research, 2016. **44**(2): p. e14-e14.

71. Craw, P. and W. Balachandran, *Isothermal nucleic acid amplification technologies for point-of-care diagnostics: a critical review.* Lab Chip, 2012. **12**(14): p. 2469-86.

72. Chang, C.-C., et al., *Diagnostic Devices for Isothermal Nucleic Acid Amplification.* Sensors, 2012. **12**(6): p. 8319.

73. Asiello, P.J. and A.J. Baeumner, *Miniaturized isothermal nucleic acid amplification, a review.* Lab Chip, 2011. **11**(8): p. 1420-30.

74. Hur, J., et al., *DNA hydrogel-based supercapacitors operating in physiological fluids.* Scientific Reports, 2013. **3**: p. 1282.

75. Nishikawa, M., et al., *Biodegradable CpG DNA hydrogels for sustained delivery of doxorubicin and immunostimulatory signals in tumor-bearing mice.* Biomaterials, 2011. **32**: p. 488.

76. Xing, Y., et al., *Self-Assembled DNA Hydrogels with Designable Thermal and Enzymatic Responsiveness.* Advanced Materials, 2011. **23**(9): p. 1117-1121.

77. Xiao, Z., et al., *A lateral flow biosensor for detection of single nucleotide polymorphism by circular strand displacement reaction.* Chem Commun (Camb), 2012. **48**(68): p. 8547-9.

78. Bi, S., Y. Cui, and L. Li, *Dumbbell probe-mediated cascade isothermal amplification: A novel strategy for label-free detection of microRNAs and its application to real sample assay.* Analytica Chimica Acta, 2013. **760**: p. 69-74.

79. Lee, H.Y., et al., *DhITACT: DNA Hydrogel Formation by Isothermal Amplification of Complementary Target in Fluidic Channels.* Adv Mater, 2015. **27**(23): p. 3513-7.

80. Buskohl, P.R., R.A. Gould, and J.T. Butcher, *Quantification of embryonic atrioventricular valve biomechanics during morphogenesis.* J Biomech, 2012. **45**(5): p. 895-902.